

**Stability Assessment of Homogeneous Slopes Loaded with Mobile
Tracked Cranes –
An Artificial Neural Network Approach**

Xin Ai

A Thesis
in
The Department
of
Building, Civil and Environmental Engineering

Presented in Partial Fulfillment of the Requirements
for the Degree of Master of Applied Science (Civil Engineering) at
Concordia University
Montreal, Quebec, Canada

February 2016

© Xin Ai, 2016

CONCORDIA UNIVERSITY
School of Graduate Studies

This is to certify that the thesis prepared

By: Xin Ai

Entitled: Stability Assessment of Slopes Loaded with Mobile Tracked Cranes – An
Artificial Neural Network Approach

and submitted in partial fulfillment of the requirements for the degree of

Master of Applied Science (Civil Engineering)

complies with the regulations of the University and meets the accepted standards with respect to originality and quality.

Signed by the final examining committee:

_____	Dr. A. M. Hanna	Chair, Examiner
_____	Dr. A. Hammad	External
_____	Dr. Z. Zhu	Examiner
_____	Dr. A. M. Hanna	Examiner
_____	Dr. A. M. Zsaki	Supervisor

Approved by

Chair of Department or Graduate Program Director

Dean of Faculty

ABSTRACT

Stability Assessment of Homogeneous Slopes Loaded with Mobile Tracked Cranes – An Artificial Neural Network Approach

Xin Ai

The assessment of stability of homogeneous slopes found as part of embankments, approach ramps, in bridge construction or flood protection levees could be a complex task. Either during construction or at a point in the operating life of the earth structure it can be subjected to loads from the equipment operating on it. Mobile tracked cranes used in heavy lifting or dredging operations can apply loads due to their substantial self-weight combined with the load carried by them. It is important to be able to determine the minimum factor of safety for such slopes. However due to the combination of soil parameters, slope geometry and the variable nature of loading imposed, a substantial number (measured perhaps in hundreds of combinations) slope stability analyses would be required to find the minimum factor of safety. One approach to reduce the number of analyses needed is to develop an Artificial Neural Network, train it using a representative dataset of stability analyses, and rely on its predicting capabilities to determine the minimum factor of safety for the slope for any combination of model parameters. Artificial Neural Networks can simulate the central nervous system of a human brain, by training them using the input data and target data one can build a neural network and use them for the factor of safety prediction. Since this thesis considers the case of homogeneous constructed slopes, thus the slope stability analysis was performed using Bishop Simplified Method, and the load distribution due to mobile tracked cranes was represented by an equivalent triangular distribution acting on the slope surface. The slope stability analysis was performed using Slide (from roscience Inc.) to obtain the training dataset and MATLAB was used to develop and train the artificial neural network. A detailed investigation to assess and improve the network accuracy was carried out, and it was established that by increasing the neuron numbers and hidden layers, the ultimate average error in predicting the factor of safety for an independent test data set was 0.677%. This error, considering the inherent uncertainty of soil properties, instils confidence in using the Artificial Neural Network for predicting the factor of safety of homogeneous slopes loaded by mobile cranes.

ACKNOWLEDGEMENTS

I would like to express my sincere gratitude to my supervisor Dr. A.M. Zsaki for his full support and continuous patience during the period of my graduate studies.

Thanks are also owed to professors for imparting their knowledge through graduate courses which I took. The knowledge learned greatly assisted my thesis research.

I am deeply impressed by the help from my colleague Pengfei Zhao, who generously provided me effective information and guidance.

Especially, I am desirous to be grateful of my parent for their funding my academic career, encouragement and love in the period of my stay at Concordia University.

TABLE of CONTENTS

List of Figures.....	vii
List of Tables.....	x
Chapter 1 - Introduction.....	1
1.1 Motivation.....	1
1.2 Objectives, Methodology and Approach	1
1.3 Outcomes.....	2
Chapter 2 – Literature Review	3
2.1 Review of Slope Stability.....	3
2.1.1 History and Introduction.....	3
2.1.2 Slope Stability Assessment Based on Limit Equilibrium Analysis	6
2.1.4 Shear Strength Reduction Finite Element Method.....	18
2.2 Review of Crawler Crane Stability.....	21
2.2.1 Definition and Introduction	21
2.2.2 Track Pressure and Equipment Stability Calculations for Crawler Cranes	22
2.3 Artificial Neural Networks (ANN).....	27
2.3.1 ANN History and Development.....	27
2.3.2 Artificial Neural Networks – Basics, Structure and Training.....	27
2.3.3 The Backpropagation Algorithm.....	28
2.3.4 Basic Equations and Theory of the Backpropagation Algorithm	30
Chapter 3 – Slope Stability Analysis	33
3.1 Research Process Brief Summary.....	33
3.2 Slope Stability Analysis Using Slide - Introduction.....	33
3.3 Determination of Surface Loading Due to a Crawler Crane	34

3.3.1 Contact Pressure between the Equipment and the Crest of the Slope.....	34
3.4 Credible Ranges of Key Model Parameters	41
3.4.1 Credible Range Relative Documents Collection	41
3.4.2 Unit weight	41
3.4.3 Cohesion	42
3.4.4 Angle of Internal Friction	42
3.4.5 Slope Angle and Slope Height	43
3.4.6 Crawler Crane Parameters	45
3.4.7 Credible Ranges Summarization.....	46
3.5 Monte Carlo Data Sampling and Slide Model Building	47
3.5.1 Monte Carlo Data Sampling	47
3.5.2 Building of Slide Models for Slope Stability Analysis	49
3.6 Stability Analysis Results - Discussion	53
3.7 The Effect of Having No Crane on the Slope	63
Chapter 4 – Development, Training and Verification of the Artificial Neural Network.....	66
4.1 Training a Neural Network	66
4.2 Brief Introduction to ANN using MATLAB.....	66
4.2 Data filtering.....	70
4.3 MATLAB Script for the ANN	73
4.4 FeedForwardnet Network Introduction.....	76
4.5 Training and Testing	77
4.6 Interpretation of ANN Predictions Using an Average Error Value.....	79
Chapter 5 – Summary and Conclusions	81
5.1 General Remarks	81
5.2 Limitation.....	82

5.2.1 Limitation of Thesis	82
5.2.2 Limitation of Applicability of ANN.....	82
References.....	84

LIST of FIGURES

Figure 1 Governing parameters of a slope model loaded with a crawler crane	4
Figure 2 basic elements of slope.....	6
Figure 3 Setup of slope for total stress analysis of homogeneous cohesive soils	7
Figure 4 Setup of slope and slices for the Swedish method of slices	8
Figure 5 Setup of slope and slices for Bishop’s simplified method.....	10
Figure 6 Bishop simplified method hand calculation example	11
Figure 7 Setup of slope and slices for Janbu’s rigorous method	14
Figure 8 Forces acting on a slice – Janbu’s rigorous method	15
Figure 9 Slip surface computed with finite element shear strength reduction method.....	19
Figure 10 Deformed mesh.....	20
Figure 11 Dimensions of a typical crawler crane.....	21
Figure 12 Force diagram for crawler crane stability calculations.....	23
Figure 13 Force diagram of wind loads acting on a crawler crane.....	25
Figure 14 the force diagram of crane extension.....	26
Figure 15 Structure of a typical ANN	27
Figure 16 A schematic of a simple artificial neural network.....	28
Figure 17 Basic structure of the backpropagation algorithm.....	30
Figure 18 Sigmoidal function.....	31
Figure 19 Slope stability analysis using Slide	34
Figure 20 Contact pressure due to a vertical eccentric load - forces.....	35

Figure 21 Contact pressure due to a vertical eccentric load – moments and force.....	36
Figure 22 Load applied on X-X axis.....	36
Figure 23 Load distribution – with tensile forces	37
Figure 24 Load distribution – without tensile forces	37
Figure 25 Slope stability analysis model setup	38
Figure 26 Maximum pressure (Pmax) formula derivation - sketch 1.....	39
Figure 27 Maximum pressure (Pmax) formula derivation - sketch 2.....	40
Figure 28 Calculation of Pmax for various loading scenarios	40
Figure 29 Natural and engineered slopes in China.....	45
Figure 30 Crawler crane specifications	45
Figure 31 Parameter sampling using random numbers	48
Figure 32 Slide model input data summary.....	48
Figure 33 Project Setting.....	49
Figure 34 Defining external boundary for the slope.....	50
Figure 35 Defining material properties in Slide.....	51
Figure 36 External loading and material properties display in Slide.....	51
Figure 37 Automatic search grid for the minimum FS – in Slide.....	52
Figure 38 Typical analysis results from Slide.....	53
Figure 39 Comparison of FS as a function of cohesion.....	53
Figure 40 26 independent slide models.....	63
Figure 41 26 independent slide models, (continued).....	63
Figure 42 Table Difference between FS (with the load) and FS (without the load).....	64
Figure 43 MATLAB - neural network toolbox.....	67
Figure 44 Neural network structure in MATLAB.....	68
Figure 45 Selection on the training algorithm in MATLAB.....	68

Figure 46 Regression.....	69
Figure 47 Error histogram in MATLAB.....	70
Figure 48 An example data sample that resulted in an inappropriate failure surface	71
Figure 49 An example data sample that resulted in an inappropriate failure surface	71
Figure 50 ANN predicting capabilities before replacement of outlier sample datasets.....	72
Figure 51 ANN predicting capabilities after replacement of outlier sample datasets.....	73
Figure 52 ANN training and error (difference in outputdata and outputdata_net).....	75
Figure 53 ANN structure.....	77
Figure 54 MATLAB ANN regression results.....	79
Figure 55 Errors between Slide results and ANN prediction for the 20 independent test cases...80	

LIST of TABLES

Table 1 Bishop simplified method hand calculation.....	12
Table 2 Bishop simplified method hand calculation, (continued).....	13
Table 3 Unit weight of soils.....	41
Table 4 Cohesion of soils.....	42
Table 5 Angle of internal friction for soils.....	43
Table 6 Slope angle and slope height.....	44
Table 7 Credible ranges of crawler crane parameters.....	46
Table 8 Credible ranges – soil properties	46
Table 9 Credible range – slope geometry and crawler crane parameters	47
Table 10 Key parameters for 150 slide models.....	54
Table 11 Key parameters for 150 slide models, (continued).....	55
Table 12 Key parameters for 150 slide models, (continued).....	56
Table 13 Key parameters for 150 slide models, (continued).....	57
Table 14 Key parameters for 150 slide models, (continued).....	58
Table 15 FS, x, y, R for global minimum slip surface.....	58
Table 16 FS, x, y, R for global minimum slip surface, (continued).....	59
Table 17 FS, x, y, R for global minimum slip surface, (continued).....	60
Table 18 FS, x, y, R for global minimum slip surface, (continued).....	61
Table 19 FS, x, y, R for global minimum slip surface, (continued).....	62
Table 20 Difference statistics in percent.....	65

Chapter 1 - Introduction

1.1 Motivation

Geotechnical engineering has developed into an established field of civil engineering, and slope stability analysis within it became an important sub-field. When a concrete-faced rockfill dam is built across a river, a hydraulic engineer is concerned whether the slopes comprising it will fail or not. Or when a new highway is designed near a steep mountain, a road designer should consider the minimum Factor of Safety (FS) of nearby slopes, excavations and fills. Quite a few geotechnical engineering projects will encounter a slope stability issue. Among them, a mobile tracked crane operating on the top slope surface is a common phenomenon. These crawler cranes will carry out several construction duties; excavations or fills on the slope, or dredging operations on levees, to name a few examples. The crane will apply a certain magnitude of load on the slope, which might cause slope failure or other kinds of soil slides. Consequently, the prediction of minimum FS of slopes and the control and mitigation of related natural or man-made disasters are important assignments for geotechnical engineers.

However, current methods of using various slope stability analyses cannot meet the requirements that geotechnical engineers need to deal with a large number of potential combinations of parameters; slope geometry, soil properties, crane location, load being lifted, etc. In the field of computer science, artificial neural networks (ANN) were developed to predict the behaviour of a complex system, without the need to evaluate every possible combination of parameters. The essence of ANN is *machine learning*, which can not only be used into engineering fields, but also in others, such as; intelligent robotics, computer numerical control, pattern recognition, economy estimation, neural biology and so on.

1.2 Objectives, Methodology and Approach

The first objective of this thesis is to review fundamental knowledge and principal theory of different slope stability analysis methods. The second objective of this thesis is to determine the credible range of key parameters, such as slope geometry, soil properties, and pressure

distribution due to crawler crane, based on reliable references. The third objective is to successfully train a neural network and achieve the final goal of minimizing the prediction error of the ANN. In this thesis, a Monte Carlo simulation was adopted as the methodology to sample the key parameters of the system and to discover the dataset size. Two primary software were used; Slide (Rocscience, Inc., 2015) for slope stability analysis and MATLAB (Mathworks, 2015), for neural network training.

To clarify the basic assumptions in the research, it is necessary to define what types of engineering problems and slopes can be solved;

- Artificial or constructed homogeneous slope. that can be designed as homogenous single layer in the engineering projects. Slope height cannot exceed 30m.
- No groundwater.
- No weak layers or seams.
- Bishop Simplified Method used for analysis (appropriate for homogeneous slopes).
- Load applied on the slope surface due to a crawler crane. A typical crawler crane used was a SCX500 hydraulic crawler crane, from HITACHI..
- The distance between the slope edge and the crawler crane should be within 30m.

1.3 Outcomes

In this thesis, as a result of analysis and ANN development, the predicting capabilities of the ANN were such that the final average error of FS in an independent test dataset was 0.677 percent with the maximum error of 1.6 percent, which is quite acceptable in the geotechnical field due to the general data-limited nature of problems, where quantities, such as soil properties, are seldom known within an accuracy of 20-30 percent. Thus, the precision of the ANN is sufficiently high that the network can be competent in predicting FS of slopes loaded with mobile cranes. In this research, the advantage of ANN is more distinctive than traditional slope stability analysis software due to its convenience, simple operation and working efficiency. An ANN can deal with a large amount of slopes with different key parameters with a fast processing speed.

Chapter 2 – Literature Review

2.1 Review of Slope Stability

A slope must be stable enough to avoid landslides or other failures, which will be hazardous to the infrastructure and people living near the slope. In addition to its self-weight, the slope needs to support the external pressure applied to it, which can come from the structures constructed or equipment operated on the top surface of the slope. Thus, it is necessary to review the fundamental mechanisms of slope stability and in particular, the pressure distribution generated by the crawler cranes. In this chapter, a review of slope stability and of crawler crane stability will be discussed.

2.1.1 History and Introduction

The stability assessment of slopes loaded by equipment is determined by the soil properties and strength of the slope in addition to external loads. In practice, many construction sites already encountered such engineering problems when crawler cranes, operating on the top surface of the slope, resulted in slope failures. The most important factor to represent the stability of a slope is the FS in which the resisting shear strength should exceed failure-causing shear stress. Generally, a slope is considered as safe if the factor of safety is at least 1.0.

A large number of studies had been conducted from 1950s to 1990s in which a few key slope stability methods were developed. In 1954, Janbu attempted to assess the stability of a slope with loads imposed on the top surface of the slope. He developed the Janbu Simplified Method to analyze a slope and assumed external surcharge as uniform loads (Shields et al., 1990). Meyerhof (1957) modified the analysis by considering the slope angle, the distance from the slope edge and the shearing resistance angle. Later, Shields et al. in 1990 had a similar research done about the bearing capacity of foundations, representing the external load, on the top surface of the slope (Shields et al., 1990). The main concept of their paper was to find an equivalent to the bearing capacity of footings or strips of load on slopes to the percentage of the bearing

capacity of a footing on a level ground. Recently, Abdalla et al. in 2012 have utilized an ANN to predict the FS of slopes (Abdalla et al., 2012).

The use of heavy equipment or construction equipment, which can be dated back to 3000 years ago had emerged when Chinese lifted stones to build the Great Wall. Such equipment is versatile and applicable in mining, building, excavation and highway construction. From the late 18th century, the beginning of the Industrial Revolution, and the invention of steam engine, steam provided the power for earthmoving equipment (Haycraft, 2011). In the 20th century, Benjamin Holt was the first one to assemble an internal combustion engine and add it into an excavator, and thus created the crawler-mounted style. After that, cable-operated shovels occupied a dominating position during the post-World War II period, and currently hydraulic technology came out as the mainstream means of operation in conjunction with internal combustion engines (Haycraft, 2011).

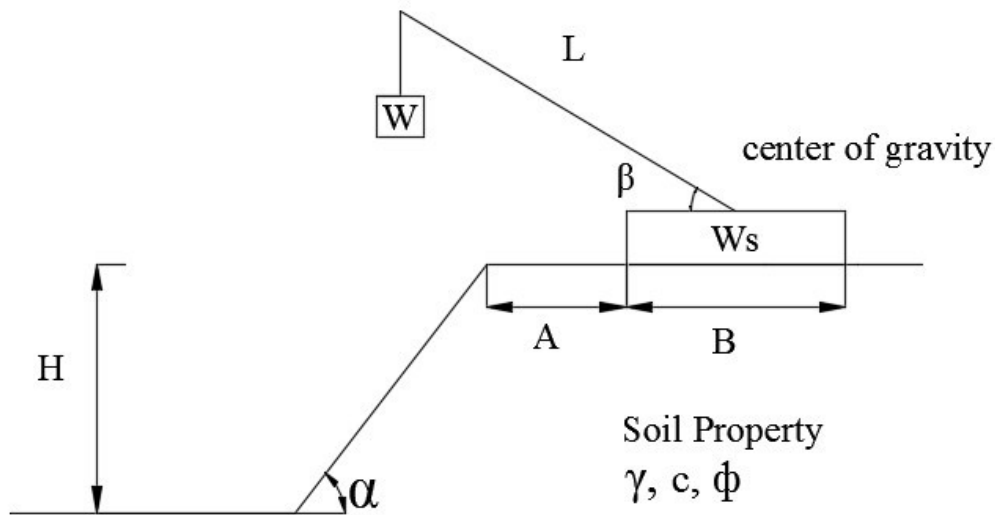


Figure 1 Governing parameters of a slope model loaded with a crawler crane

In this thesis, the following input parameters, as illustrated in the *Figure 1*, represent the model of a homogeneous slope loaded with a crawler crane. In this model, γ, c, ϕ are the basic parameters to describe the soil properties, namely the unit weight, soil cohesion, the angle of shearing resistance (or internal friction); H is the slope height and α is the slope angle; A is the distance from the edge of the slope to the crawler crane, and B is the width of the operating

equipment; W_s is the self-weight of the equipment and W is the weight lifted by the equipment; L is the arm length and β is the lift angle.

By definition, a slope is an inclined boundary surface between air and earth. A slope can be found on an embankment dam, expressway cut or a fill. The basic elements of a slope are shown in *Figure 2*. Generally, slopes can be classified into two main categories; natural slopes formed by geological processes and artificial slopes, generated by human activity. On the other hand, based on the material comprising the slope, it can either be a rock slope or a soil slope. Due to the gravity acting on the soil mass and the external forces applied, the slope has an inherent tendency to degrade and move toward a flat, horizontal state. In general, a shear failure will take place in the slope when the induced shear stresses exceed the shear strength of the material.

The stability of slopes depends on five influencing factors: (a) type of soil particles or rocks which comprise the slope; (b) geometric configuration of the cross section of the slope; (c) load distribution including gravity, externally applied loads, pore water pressure, and other surcharges; (d) groundwater table variation and increase of moisture content in soil particles; (f) any other factors reducing the effective stress of the soil mass, such as the vibrations and earthquakes (Lu, 2005).

At failure, the slopes in different soil materials form diverse failure surfaces. The slip circle for slopes in homogeneous cohesive soils is overall a continuous curve, which has a smaller radius of curvature on the top surface of the slope, and much gentler at the bottom. Based on empirical evidence, scholars have assumed this curve to be a circular arc in stability calculations (Lu, 2005). However, a plane translational slip surface often occurred in homogeneous cohesionless soil slopes. For heterogeneous soil slopes with several strata or slopes with soft soil layer at the base, the movement of the rupture surface usually occurs along the soft soil layer, and the compound slip surface is the combination of a curve and a straight line.

Practically, the stability analysis of soil slopes is based on limit equilibrium conditions. In such a setting, it is postulated that failure takes place along an assumed or known sliding surface. Also, it is presumed that a Mohr-Coulomb failure criterion is valid and satisfied along the entire rupture surface at the point of limiting equilibrium.

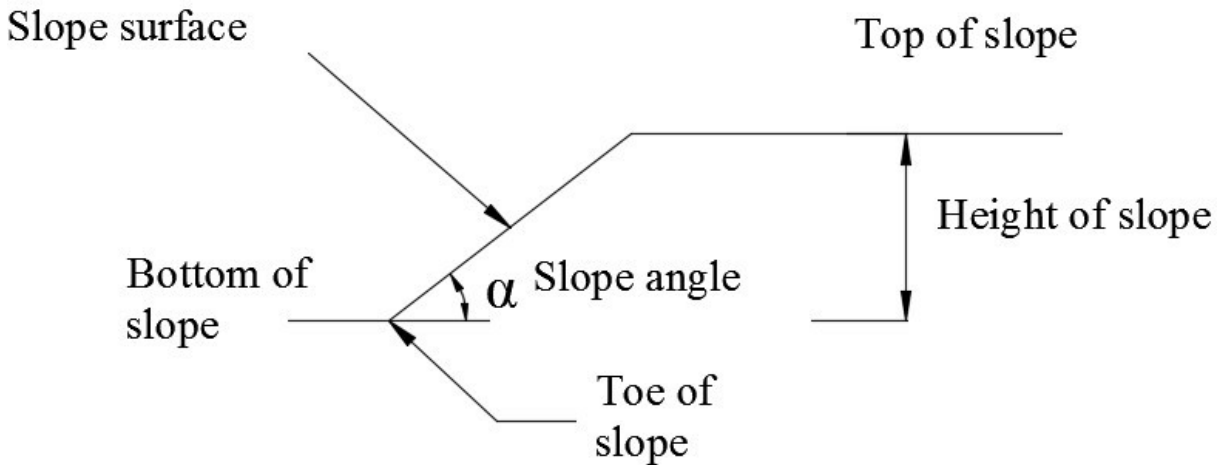


Figure 2 Basic elements of a slope

2.1.2 Slope Stability Assessment Based on Limit Equilibrium Analysis

2.1.2.1 Total Stress Analysis of Slopes in Cohesive Soils

The most common method of performing slope stability analysis in cohesive soils is the total stress analysis, which is based on the principle of limiting equilibrium (Lu, 2005). Due to cohesion existing among the soil particles, the entire soil mass moves downward when failure occurs. So, the stable condition of each element in the soil mass cannot represent the stability of the whole slope. It is usually necessary to consider the slope as rigid body, and analyze the forces and moments acting on this free-body under limit equilibrium condition (Lu, 2005). For homogeneous, cohesive soil slopes, the actual slip circle (or failure surface) approximates a cylindrical shape, and has always been assumed as a cross-sectional form of a circular arc in the calculations (Lu, 2005). Therefore, the factor of safety can be presented as the following equation:

$$FS = \frac{M_f}{M} = \frac{\tau_f * L * R}{\tau * L * R} \quad (2-1)$$

Where τ_f is the shear resistance (kPa), τ is the mobilized shear strength (kPa), M_f is the shear resistance moment (N*m), M is the disturbing moment (N*m), R is radius of the slip circular arc (m) and L is the length of the circular arc AC (in m) as shown in *Figure 3*.

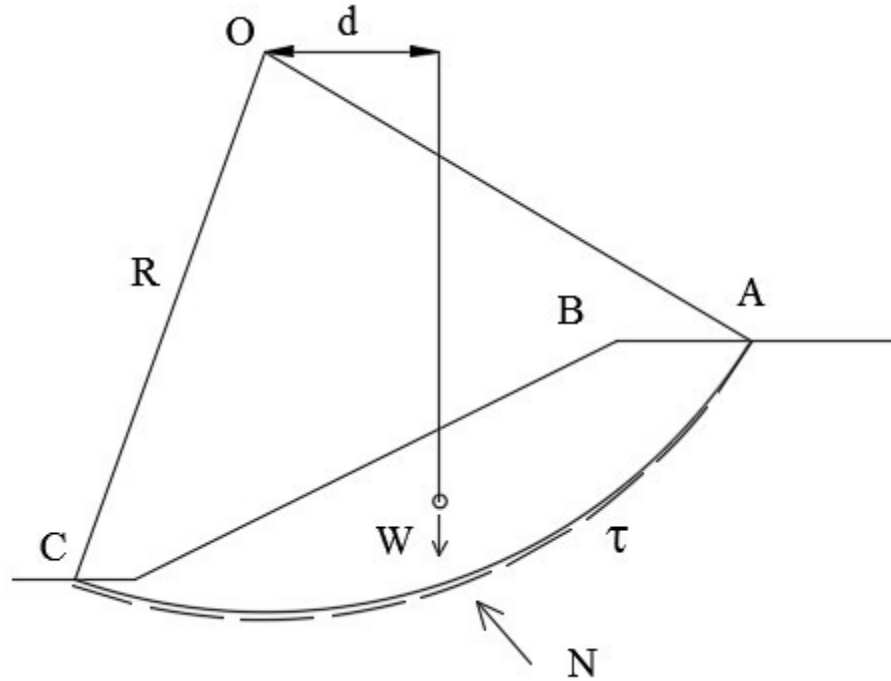


Figure 3 Setup of slope for total stress analysis of homogeneous cohesive soils

The above figure illustrates the cross-section of a slope together with a trial slip circle. Instability tends to be caused due to the moment of the self-gravity of the sliding body (Lu, 2005). When the sliding body is in the state of the moment equilibrium, the following equation holds

$$\tau * L * R = W * d \quad (2-2)$$

Thus, the factor of safety is defined as

$$FS = \frac{\tau_f LR}{Wd} \quad (2-3)$$

The FS result obtained in the above equation is one discrete value given for a single potential failure surface. However, the ultimate objective is to search for the location of the critical failure surface and the corresponding minimum FS value. For this purpose, geotechnical engineers usually hypothesize several potential failure surfaces and conduct tentative calculations repeated many times for all potential slip surface locations (Lu, 2005). In summary, the steps are as follows;

- (1) Determine the range of the center O of probable slip circles.

- (2) Calculate a set of probable radii corresponding to each center by using above-mentioned formulas to repeat the procedure, and find the minimum value as the FS for this center.
- (3) Compare all the FS values, and search for the minimum value of the FS for this slope, then corresponding slip circle is the critical failure surface.

2.1.2.2 Swedish Method of Slices

The Swedish Method assumes the sliding surface to be a circular arc, and ignores the internal (interslice) forces within the soil mass (Lu, 2005). Because of the early extensive research and application of the method of slices made by Swedish engineers, this method is often defined as the Swedish method of slices. For an arbitrary soil slice, the forces acting on the i th slice of unit length can be schematically shown as follows: soil self-weight $W_i = \gamma_i b_i h_i$, the normal reaction force N_i , the shear force T_i and the pore water pressure u (Lu, 2005).

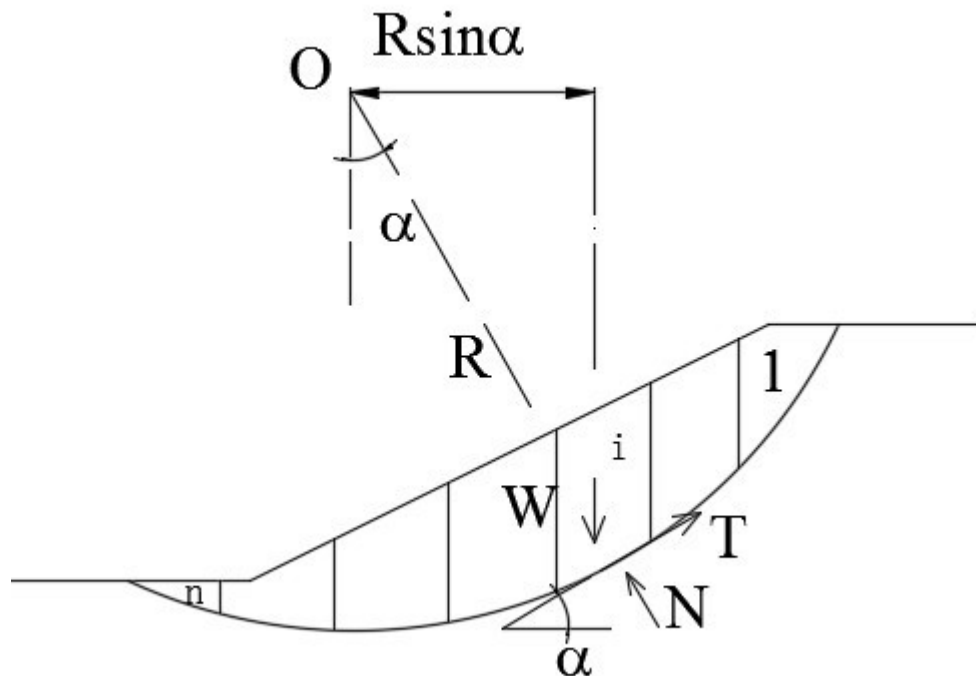


Figure 4 Setup of slope and slices for the Swedish method of slices

In reference to *Figure 4*, according to the conditions of static equilibrium on the i th slice, the weight W_i can be resolved into two components:

$$N_i = W_i \cos \alpha_i, T_i = W_i \sin \alpha_i \quad (2-4)$$

Designating the factor of safety as FS :

$$FS = \frac{\tau_{fi}}{\tau_i} \quad (2-5)$$

$$\tau_{fi} = c' + (\sigma_i - u_i) \tan \varphi' \quad (2-6)$$

$$N_i = \sigma_i * l_i, T_i = \tau_i * l_i \quad (2-7)$$

For overall moment equilibrium about the origin O :

$$\sum T_i R = \sum W_i R \sin \alpha_i \quad (2-8)$$

Thus, the factor of safety FS can be defined as

$$F_s = \frac{R * \sum \tau_{fi} * l_i}{R * \sum W_i \sin \alpha_i} = \frac{\sum c' l_i + \sum (W_i \cos \alpha_i - u_i l_i) \tan \varphi'}{\sum W_i \sin \alpha_i} \quad (2-9)$$

Where α represents the angle between the base of a slice and a horizontal line, T_{fi} represents the shear resistance; l_i is the length of the slice base; and the soil properties are c, γ, φ , as seen on Figure 3.

2.1.2.3 Bishop's Simplified Method

Bishop has proposed Bishop's Simplified method in 1955 (Eberhardt, 2003). He postulated that the FS in each slice is equal to the FS of the overall failure surface. In this case, the slip surface is also regarded as a circular arc, and the stability analysis considers the horizontal inter-slice forces. For the i th slice, the force diagram, as seen in *Figure 5*, is presented as follows:

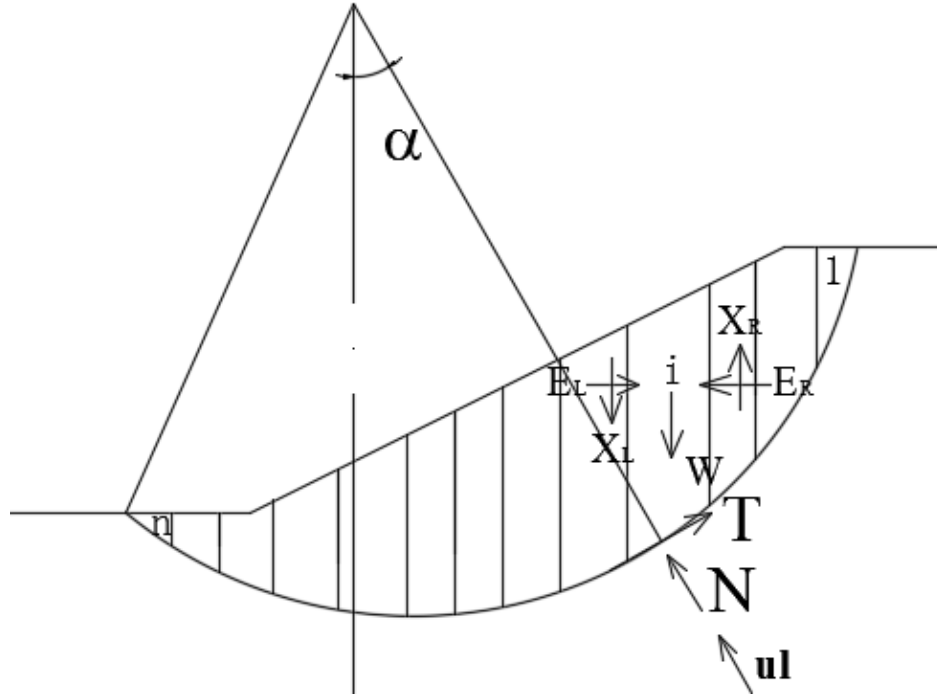


Figure 5 Setup of slope and slices for Bishop's Simplified method

For equilibrium along the vertical direction of the slice

$$W_i + \Delta X_i - T_i \sin \alpha_i - N_i \cos \alpha_i = 0, \Delta X_i = 0 \quad (2-10)$$

$$N_i = \sigma_i * l_i \quad (2-11)$$

Hence:

$$N_i = \frac{W_i - c' l_i \sin \alpha_i / F_s - u_i b_i}{m_i} \quad (2-12)$$

$$m_i = \frac{\tan \varphi'}{F_s} \sin \alpha_i + \cos \alpha_i \quad (2-13)$$

According to the definition of FS:

$$FS = \frac{\tau_{fi}}{\tau_i} \quad (2-14)$$

$$\tau_{fi} = c' + (\sigma_i - u_i) \tan \varphi' \quad (2-15)$$

$$T_i = \tau_i * l_i = \frac{1}{F_s} [c' l_i + (\sigma_i l_i - u_i l_i) \tan \varphi'] \quad (2-16)$$

For the overall moment equilibrium about the center O:

$$\sum W_i R \sin \alpha_i = \sum T_i R \quad (2-17)$$

Hence

$$FS = \frac{\sum [c' l_i + (N_i - u_i l_i) \tan \phi']}{\sum W_i \sin \alpha_i} \quad (2-18)$$

Substituting equation (2-12) into equation (2-18):

$$F_s = \frac{\sum \frac{1}{m_i} [c' b_i + (W_i - u_i b_i) \tan \phi']}{\sum W_i \sin \alpha_i} \quad (2-19)$$

Since N_i is the function of FS , the method demands an iterative calculation. The procedure is commenced by assuming a trial value for FS and then repeating the iterative process to eventually converge to the true value of FS for a given trial FS (Lu, 2005).

2.1.2.4 Bishop's Simplified Method Hand Calculation Example

Bishop simplified method is the analysis method used in this research to establish Slide models. So, it is necessary to describe the whole hand calculation process of Bishop's Simplified method. One practical engineering example (Lu, 2005) from China was used, as shown the below in *Figure 6*.

Example: A slope of an embankment with a height of 15m is inclined at 1:2. The properties of a clayey soil are $c' = 10\text{kPa}$, $\phi' = 36^\circ$ and unit weight $\gamma = 19.5\text{kN/m}^3$. Pore water Pressure coefficient B was 0.6.

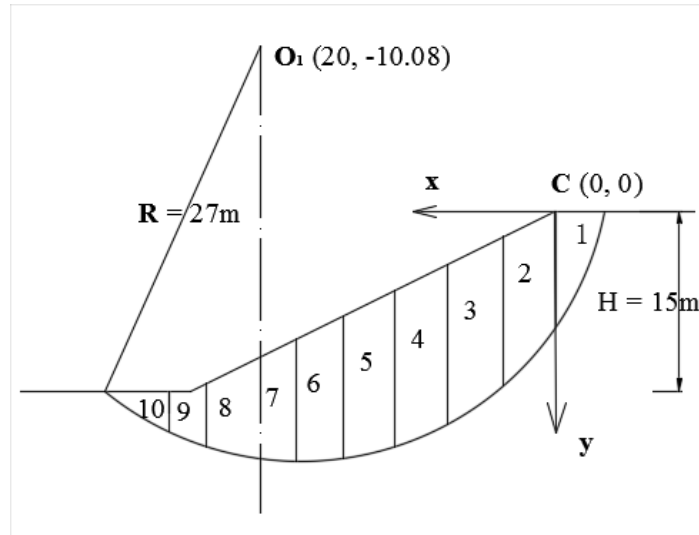


Figure 6 Bishop simplified method hand calculation example

For calculation, pore water pressure coefficient B is designated to replace pore water pressure, namely $B = \frac{u_i b_i}{W_i}$.

Hence equation (2-19):

$$F_s = \frac{\sum \frac{1}{m_i} [c' b_i + (1-B) W_i \tan \varphi']}{\sum W_i \sin \alpha_i} = \frac{\sum A_i}{\sum W_i \sin \alpha_i} \quad (2-20)$$

Where: $m_i = \frac{\tan \varphi'}{F_s} \sin \alpha_i + \cos \alpha_i$, $B = \frac{u_i b_i}{W_i}$, $A_i = \frac{1}{m_i} [c' b_i + (1 - B) W_i \tan \varphi']$.

Solution (Lu, 2005):

Step 1: Select a center of slip circle O_1 (20m,-10.08m). Draw the radius and assume it as 27m. Then draw the slip surface and take this circle as the first trial slip circle.

Step 2: Divide the sliding body into 10 slices and number them. The number of each slice is labeled in *Figure 6*.

Step 3: Find the height of each slice (through the slice center) h_i , the width of each slice (through the slice center) b_i and the slice circular arc length l_i . Calculate items of $\sin \alpha_i$, $\cos \alpha_i$ and W_i in the *Table 1*. And calculate corresponding Factor of Safety.

Series number of slices	h_i (m)	b_i (m)	l_i (m)	$\sin \alpha_i$	$\cos \alpha_i$	W_i (kN/m)	first trial FS=1.0	
							m_i	A_i
1	2.42	2.55	5.47	0.8806	0.4739	120.33	1.1137	67.34
2	6.45	2.5	4.08	0.787	0.6169	314.44	1.1887	138.33
3	8.865	4	5.39	0.6667	0.7454	691.47	1.2297	296.29
4	9.39	4	4.69	0.5185	0.8551	732.42	1.2318	311.44
5	9.91	4	4.31	0.3704	0.9289	772.98	1.198	317.01
6	9.165	4	4.1	0.2222	0.975	714.87	1.1364	281.54
7	7.77	4	4.01	0.0741	0.9973	606.06	1.0512	227.16
8	6.085	3	3	-0.0556	0.9984	355.97	0.9581	127.85
9	4.245	3	3.04	-0.1667	0.986	248.33	0.8649	88.36
10	1.62	4	4.18	-0.2963	0.9551	126.36	0.7399	56.76

Table 1 Bishop simplified method hand calculation

Series number of slices	second trial FS=1.206		third trial FS=1.162		fourth trial FS=1.170		note
	m_i	A_i	m_i	A_i	m_i	A_i	
1	1.0044	67.73	1.0245	61.95	1.0207	61.72	first trial FS=1.0
2	1.091	126.97	1.109	129.06	1.1056	128.66	first calculate FS=1.206
3	1.147	276.35	1.1622	280.02	1.1593	279.33	second trial FS=1.206
4	1.1674	295.18	1.1793	298.17	1.177	297.61	second calculate FS=1.162
5	1.152	304.85	1.1605	307.09	1.1589	306.67	third trial FS=1.162
6	1.1089	274.71	1.114	275.97	1.113	275.73	third calculate FS=1.170
7	1.0419	225.17	1.0436	225.54	1.0433	225.47	fourth trial FS=1.170
8	0.965	128.17	0.9637	128.6	0.9639	128.63	fourth calculate FS=1.169
9	0.8856	90.48	0.8818	90.09	0.8825	90.16	final result FS=1.17
10	0.7766	59.58	0.7699	59.06	0.7711	59.16	

Table 2 Bishop simplified method hand calculation, (continued)

Take 1st slice in the first trial (first trial FS=1.0) as an example:

$$\sin \alpha_1 = \frac{b_7 + b_6 + b_5 + b_4 + b_3 + b_2 + 0.5b_1}{R} = \frac{23.775}{27} = 0.8806 \quad (2-21)$$

$$\cos \alpha_1 = \sqrt{1 - \sin^2 \alpha_1} = 0.4739 \quad (2-22)$$

$$W_1 = \gamma b_1 h_1 = 19.5 * 2.55 * 2.42 = 120.33 \text{ kN/m} \quad (2-23)$$

$$m_1 = \frac{\tan \phi'}{F_s} \sin \alpha_1 + \cos \alpha_1 = \frac{\tan 36^\circ}{1.0} * 0.8806 + 0.4739 = 1.1137 \quad (2-24)$$

$$A_1 = \frac{1}{m_1} [c \cdot b_1 + (1 - B) W_1 \tan \phi'] \quad (2-25)$$

$$= \frac{1}{1.1137} [10 * 2.55 + (1 - 0.6) * 120.33 * \tan 36^\circ] = 67.34$$

$$FS = \frac{\sum A_1 + A_2 + \dots + A_{10}}{\sum W_1 * \sin \alpha_1 + W_2 * \sin \alpha_2 + \dots + W_{10} * \sin \alpha_{10}} = 1.206 \quad (2-26)$$

Step 4: Reselect a different radius for circle center O_1 . Obtain the minimum Factor of Safety for O_1 .

Step 5: Reselect other circle center O_2, O_3 and so on. Repeat above steps in order to obtain the minimum Factor of Safety for the slope (Lu, 2005).

Therefore, the idea of this calculation can be summarized below:

- Obtain the Factor of Safety for a specific circle center and slip surface (or radius).
- Obtain the minimum Factor of Safety for a specific circle center and different radii.

- Obtain the minimum Factor of Safety for the slope and different circle centers.

2.1.2.4 Janbu's Rigorous Method

The failure surfaces of cohesionless soil slopes are usually planar, while for homogeneous cohesive soil slopes the failure surfaces are circular arcs, thus applying Swedish Method or Bishop's Simplified method leads to the solution (Lu, 2005). For a practical engineering project, designers adopt the circular arc analysis for calculating the stability of the compacted earth dams and rockfill dams. However, when the slope contains obvious soft soil layers, such as the sliding along the core surface inside the core wall dam, or soft soil layer lain on the foundation of the embankment slope, or the excavation problem on a rock mass with joints or old landslides, the circular arc analysis is invalid (Lu, 2005). The sliding, which will occur along the soft layers is considerably different from a cylindrical shape. Therefore, these cases will non-circular methods to solve for slope stability. Note that, in general, non-circular methods could converge to circular arcs if the critical failure surface is such (Zsaki, 2014).

For Janbu's rigorous method, the failure surface profile can be of arbitrary shape, as shown schematically in *Figure 7*. Janbu hypothesized the position of a line, which consists of the points of application of all inter-slice forces. Based on the empirical evidence, most scholars assume the line is located 1 / 3 height of the slice above the base (Lu, 2005). Additionally, the method must satisfy both the overall moment equilibrium and the overall force equilibrium in the calculations.

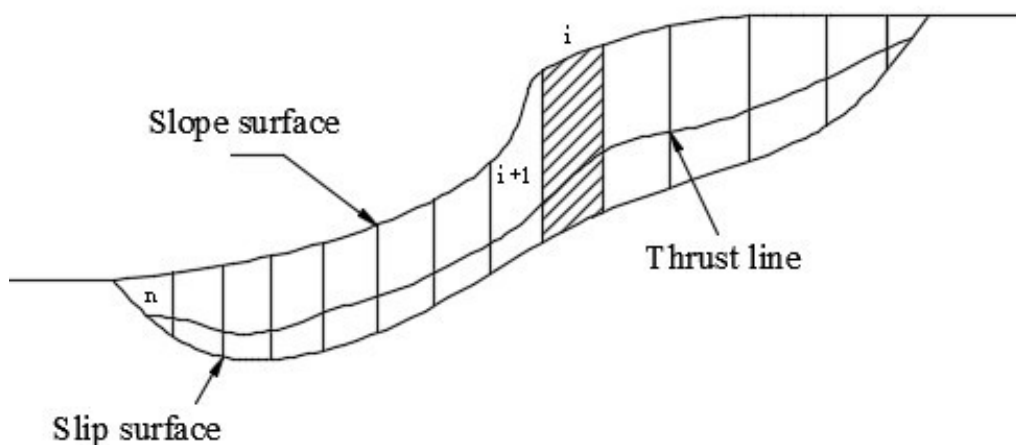


Figure 7 Setup of slope and slices for Janbu's rigorous method

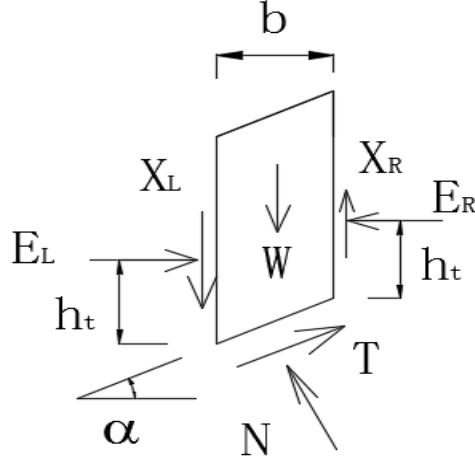


Figure 8 Forces acting on a slice – Janbu's rigorous method

In reference to *Figure 8*, the Mohr-Coulomb Failure Criterion at the base of a slice can be written

$$\tau_{f_i} = c' + (\sigma_i - u_i) \tan \varphi', FS = \frac{\tau_{f_i}}{\tau_i} \quad (2-27)$$

$$N_i = \sigma_i * l_i, T_i = \tau_i * l_i \quad (2-28)$$

$$T_i = \frac{1}{FS} [c'l_i + (\sigma_i l_i - u_i l_i) \tan \varphi'] \quad (2-29)$$

Resolving vertically:

$$W_i - (X_R - X_L) = T_i \sin \alpha_i + N_i \cos \alpha_i \quad (2-30)$$

So that

$$N_i = \frac{W_i - (X_R - X_L) - (c'l_i \sin \alpha_i - u_i l_i \sin \alpha_i \tan \varphi') / FS}{m_i} \quad (2-31)$$

$$m_i = \frac{\tan \varphi'}{FS} \sin \alpha_i + \cos \alpha_i \quad (2-32)$$

Resolving parallel to the base of the *ith* slice:

$$T_i + (E_R - E_L) \cos \alpha_i = [W_i - (X_R - X_L)] \sin \alpha \quad (2-33)$$

So

$$E_R - E_L = [W_i - (X_R - X_L)] \tan \alpha_i - T_i \sec \alpha_i \quad (2-34)$$

Substituting in T_i

$$E_R - E_L = [W_i - (X_R - X_L)] \tan \alpha_i - \frac{1}{FS} [c'l_i + (N_i - u_i l_i) \tan \varphi'] \sec \alpha_i \quad (2-35)$$

Taking moments about the center O of the slice at the base

$$E_R b_i \tan \alpha_{ti} - X_R b_i - (E_R - E_L) h_{ti} = 0 \quad (2-36)$$

Hence

$$X_R = E_R \tan \alpha_{ti} - (E_R - E_L)h_{ti} / b_i \quad (2-37)$$

Overall Force equilibrium (in the absence of surface loading)

$$\sum(E_R - E_L) = 0 \quad (2-38)$$

$$\sum(X_R - X_L) = 0 \quad (2-39)$$

Solving Equation (2-35) and Equation (2-38) simultaneously leads to

$$\sum[W_i - (X_R - X_L)] \tan \alpha_i = \frac{1}{FS_{(f)}} \sum [c'l_i + (N_i - u_i l_i) \tan \varphi'] \sec \alpha_i \quad (2-40)$$

Hence

$$FS_{(f)} = \frac{\sum [c'l_i + (N_i - u_i l_i) \tan \varphi'] \sec \alpha_i}{\sum [W_i - (X_R - X_L)] \tan \alpha_i} \quad (2-41)$$

2.1.3 Other Slope Stability Analysis Methods

All the methods summarized above are based on the concept of limit equilibrium. On the basis of mechanical principle of a sliding body, the methods can analyze diverse slope failure models, stress states, and the relationship between shear resistance and mobilized shear strength to estimate the slope stability. All the above-introduced methods, plus methods like the Morgenstern-Price method, Spencer's method and Sarma's method are two-dimensional. Additionally, Hovland's method and Leshchinsky's method can be adopted to solve the three-dimensional limit equilibrium analysis problems (Lei, 2014).

In addition to methods based on limit equilibrium, there are other methods for slope stability analysis. Most of these are numerical methods of analysis, and some of the will be summarized briefly

- The finite element method (FEM) dates back to 1967 when it is applied the first time. It is one of the most popular numerical analyses applied in the engineering field. However, it cannot solve the discontinuous deformation problems and large strain (or called large deformation, or finite strain) problems. Furthermore, its solutions for stress concentration and infinite domain are not ideal (Lei, 2014).

- The Boundary element method (BEM) is somewhat similar to the FEM. But it only discretizes the boundaries of the problem, so the amount of input data is relatively less. This method specializes in solving infinite domain problems and semi-infinite domain problems. However FEM is more suitable, than the BEM, dealing with non-linear and heterogeneous materials behaviour, and simulating excavation process. Finally, both BEM and FEM can have difficulties solve the large strain problems (Lei, 2014).
- Discontinuous Deformation Analysis (DDA) is a novel numerical methodology established by Shi in 1988 (Lei, 2014). The element grid in DDA is accordance with the physical joint network in the rock mass. It can model the continuous and discontinuous parts in the rock body. The consideration of discontinuous deformation and time factor and introducing the inertia force, the advantages that make DDA applicable into calculating static force problems or dynamic force problems, small displacement before failure or large displacement after failure.
- The Numerical Manifold Method (NMM), which is one of the most appropriate methods to simulate deformations and stabilities of rock masses. The NMM is based on the topological manifold and differentiable manifold concepts. It is a combination of FEM and DDA created by Shi (1991). The overlapping and intersecting mathematical covers are established with the physical covers in the domain. Then this method creates the independent displacement functions on each physical cover. Finally, it forms a general displacement function by weighting and summing independent displacement functions on all the covers, and can obtain the solutions of other geotechnical problems (Lei H. , 2011).
- The Fast Lagrangian Analysis of Continua (FLAC) overcomes the disadvantages of FEM that it cannot solve large strain problem for problems in geotechnical engineering. Scholars proposed the FLAC based on the theory of the explicit finite difference method. FLAC considers the discontinuous characteristics and large strain of soil mass and rock mass more comprehensively than FEM, and the processing speed of FLAC running in the computer is also faster. But the same disadvantage with FEM is the difficulties in boundary discretization and mesh generation (Lei, 2014).
- The Discrete Element Method (DEM) is first proposed and applied by Cundall in 1971 to the stability analysis of soil and rock (Farhang and Frédéric, 2011). It is a dynamic method capable of simulating heterogeneous and discontinuous properties and large

strains of rock masses in a slope. Based on the Newton's Second Law, this method is innovative in such that it divides the rock slope into several rigid bodies, and use various constitutive relations to analyze the motion and the stress state of the blocks, and the variation of block motion as changing with time.

- Block Theory (BT) has been put forward by Goodman in 1985 (Lei, 2014). It utilizes stereographic projection and analytic methods to analyze the slope stability of three-dimensional discontinuous rock masses, based on the rules of topology and group theory. According to the dip angle and orientation of realistic discontinuous faces in the rock body, and the intersections among the blocks, users can find out the amount and position of critical blocks, which have a tendency to move. So, it is also called Key Block theory (KB). This method usually considers the shear strength on the discontinuous faces, but neglects their deformations and the moment effect. Whereas, all these prerequisites cannot conform to the practical construction situation.

2.1.4 Shear Strength Reduction Finite Element Method

Rapid developments in computer technology and civil engineering have pushed the finite element method (FEM) and other numerical methods forward, since it was first applied to geotechnical engineering in 1966. Finite element Shear Strength Reduction (SSR) method in *Figure 9* has been widely applied in engineering projects and academic research in last years, which proved it is feasible and superior mainly in tunnel engineering. The application in slope stability analysis can be one of the most significant applications of finite element Shear Strength Reduction method. This method is particularly useful when several different modes of failure are possible, because it automatically finds the critical mechanism. The outstanding advantage of finite element strength reduction method is that it can be used in some finite element software like ANSYS and ABQUS to obtain solutions. Without assuming the failure mode and location of the slip surface, the safe Factor of Safety and the failure of the slopes can be obtained. It is important to select the appropriate yield criterion to solve different problems. In the future, the application scope of finite element SSR method will continue to be expand and the selection of yield criterion will be more accurate (Hammah, 2007).

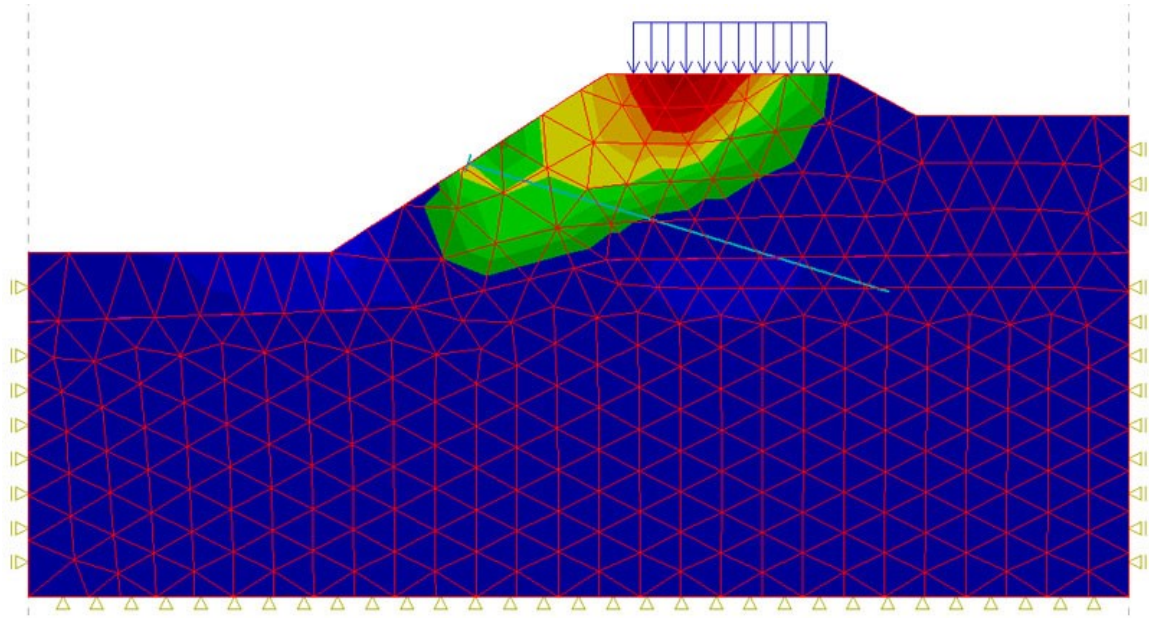


Figure 9 Slip surface computed with finite element shear strength reduction method (Zheng and Zhao, 2004)

For the limit equilibrium slope stability analysis, the basic assumption is that failure surface (a soil mass or a rock block) will slide along the assumed slip surface. The popularity of limit equilibrium method is mainly due to its simplicity in assessing slope stability and involving different key parameters (Zheng and Zhao, 2004). The Factor of Safety value obtained by limit equilibrium method can help engineers to prevent against the uncertainties. So, the recommended Factor of Safety values for slopes can usually ensure that failures are controlled within acceptable range. In spite of all the advantages, limit equilibrium method has some obvious defects. Firstly, it ignores stress-strain behavior of soils and rocks. Then, various assumptions have been postulated to meet static determinacy. Finally, it has some limitation for slope stability analysis, such as the failure of cantilever and retaining walls, where slip surface involves deformed wedges (Zheng and Zhao, 2004).

In finite element SSR method, shear strength reduced by a FS for Mohr-Coulomb material can be determined from the equation (Zsaki, 2014):

$$\frac{\tau}{FS} = \frac{c'}{FS} + \frac{\sigma \tan \phi'}{FS} \quad (2-42)$$

This equation can be rewritten as:

$$\frac{\tau}{FS} = c^* + \sigma \tan \varphi^* \quad (2-43)$$

Where: $c^* = \frac{c'}{FS}$, $\varphi^* = \arctan \frac{\tan \varphi'}{FS}$.

The advantages of FEM-SSR for analyzing the slope stability can be listed below, comparing traditional limit equilibrium method (Zheng and Zhao, 2004):

- FEM-SSR can analyze the slopes located within complicated geological structures and topography.
- FEM-SSR can consider nonlinear elasto-plastic relationship and stress-strain behaviors of soils and rocks.
- FEM-SSR can model the failure process (displacement) and three-dimensional shape of slip surface as shown in *Figure 10*.
- FEM-SSR can model the interactive effect of soils and supports.
- FEM-SSR does not need to assume the shape of the slip surface and slice the sliding body when calculating Factor of Safety. That is the most distinctive criterion to distinguish FEM-SSR in comparison to limit equilibrium methods.

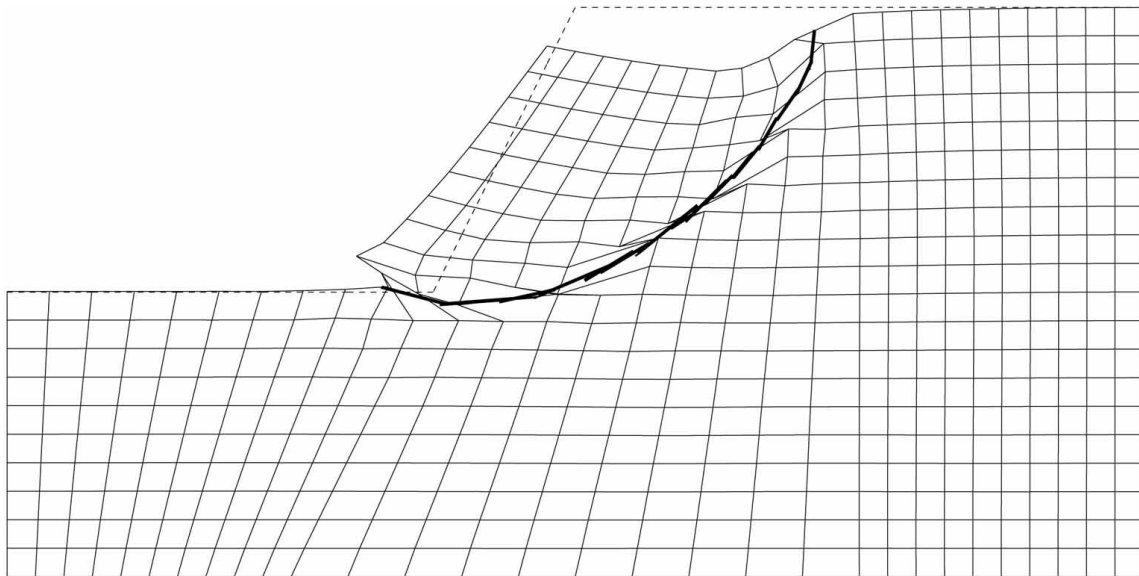


Figure 10 Deformed mesh (Hammah, 2007)

2.2 Review of Crawler Crane Stability

2.2.1 Definition and Introduction

A crawler crane is a crane mounted on an undercarriage with a set of caterpillar tracks (also called crawlers) that have the ability to move (Haycraft, 2011). It takes a dominant position in the construction industry because of its mobility and simple operation. Crawler cranes are one of four main mobile cranes, and extensively used in the hoisting, excavation and fill jobs. The crawler crane consist of five components; an engine device, operating mechanism, hoist, turntable and an underpan. Its typical dimension on lateral view and front view are shown in *Figure 11*. Crawler cranes have both advantages and disadvantages. The main advantage is that they can move around on the jobsite and perform the lift quite conveniently, since the crane is stably operated on the crawlers without outriggers. In spite of that, its disadvantage is still evident that the contractors incur a large amount of expense for moving the crawler crane from one construction site to another, because of its heavy weight. Finally, the lifting capacity of the crawler crane is from about 40 to 3,500 short tons (Hao, 2015).

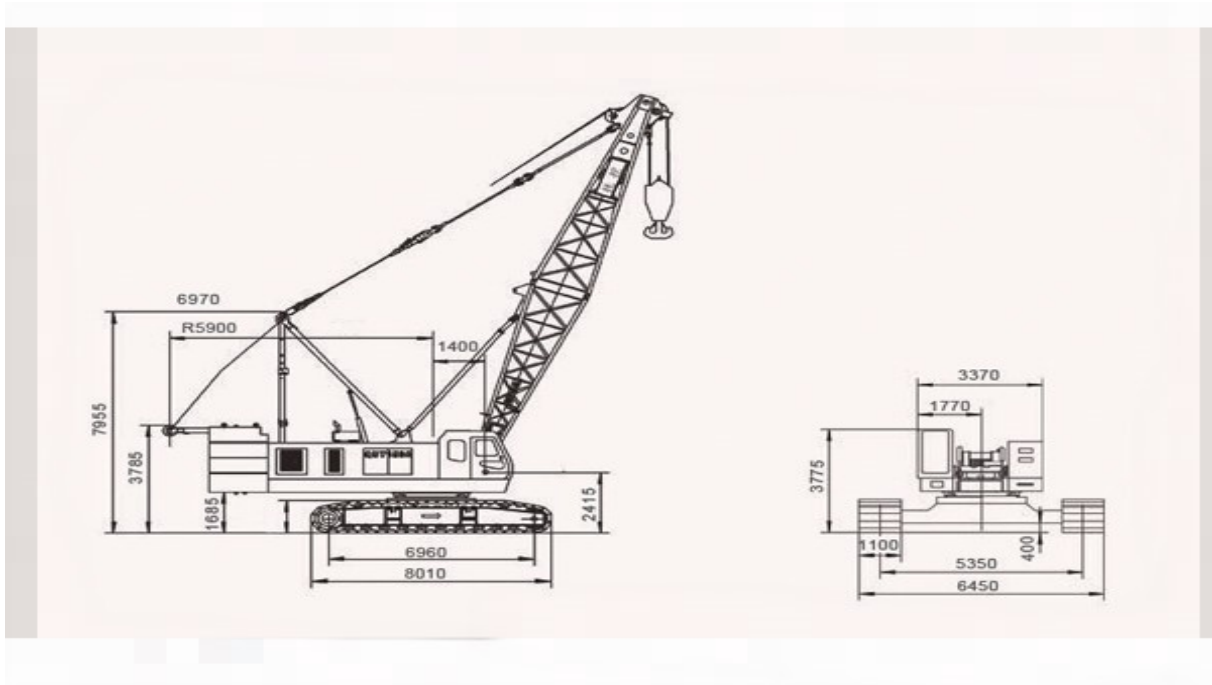


Figure 11 Dimensions of a typical crawler crane (QY150A, Xuzhou Construction Machinery Group Co., Ltd., 2012)

2.2.2 Track Pressure and Equipment Stability Calculations for Crawler Cranes

2.2.2.1 Background

For crane stability, all the moments acting on the base of the crane must be in the state of equilibrium in order that the crane does not overturn, which means the sum of moments should be approximately zero. According to the American Society of Mechanical Engineers in the volume ASME B30.5-2014 Mobile and Locomotive Cranes (Hao, 2015), the magnitude of allowable weight (termed as the “rated load” in the US standards) lifted by the hook of the crane should be less than the value, which induces the crane to tip. For crawler cranes, the stability-limit rated load is 75 percent of the tipping load. But for mobile cranes supported on outriggers, it is 85 percent of the tipping load. Furthermore, the regulations for cranes mounted on vessels or offshore platforms are much stricter due to the dynamic load acting on the crane (Teng, 2005).

2.2.2.2 Stability Calculations for Crawler Cranes

To guarantee avoiding the overturning accident in the hoisting and the stable state of the crawler crane, it requires that the stability calculations be done for the overall equipment. If the equipment cannot satisfy the requirement after checks, the staff will take several measurements to increase the bob-weight and reinforce the equipment.

On such condition, presented in *Figure 12*, when the driving direction is perpendicular to the operation direction, the stability of crawler crane is the lowest. To check the stability, the method considers point *A* in the figure, or the center of the track, as the critical overturning center.

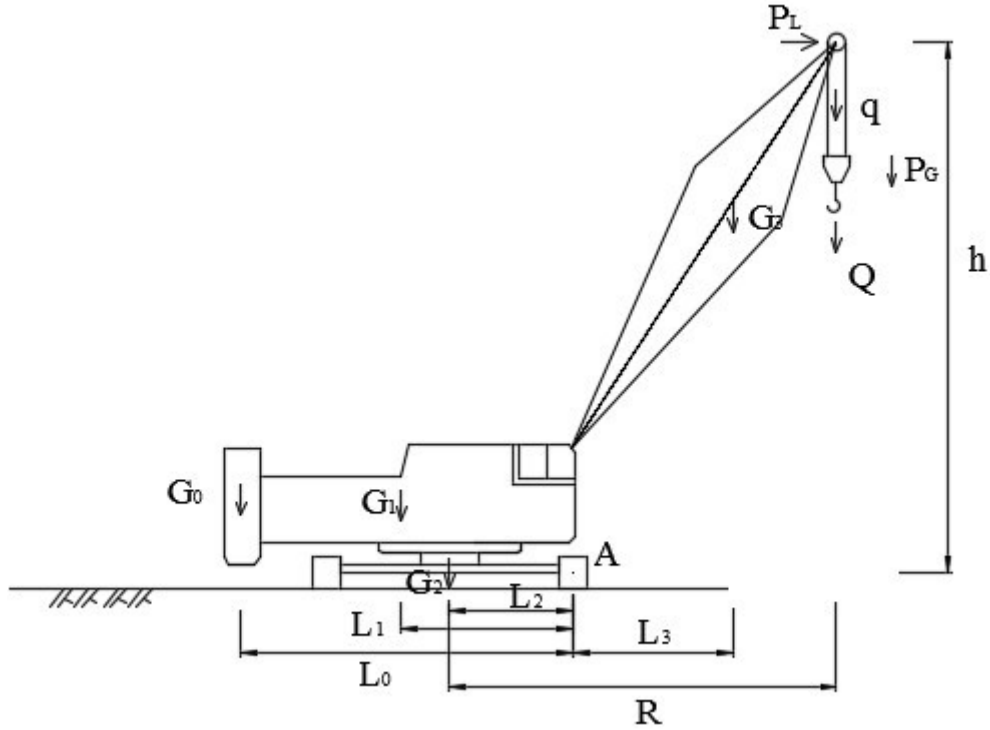


Figure 12 Force diagram for crawler crane stability calculations

When considering both hoisting load ($Q + q$) and additional load (Teng, 2005):

$$K_1 = \frac{M_{stable}}{M_{overturn}} \geq 1.15 \quad (2-44)$$

$$K_1 = \frac{G_1 l_1 + G_2 l_2 + G_0 l_0 - (G_1 h_1 + G_2 h_2 + G_0 h_0 + G_3 h_3) \sin \beta - G_3 l_3 - M_F - M_G - M_L}{(Q+q)(R-l_2)} \quad (2-45)$$

When only considering hoisting load and ignoring the additional load:

$$K_2 = \frac{M_{stable}}{M_{overturn}} \geq 1.4 \quad (2-46)$$

$$K_2 = \frac{G_1 l_1 + G_2 l_2 + G_0 l_0 - G_3 l_3}{(Q+q)(R-l_2)} \quad (2-47)$$

Where G_0 represents the bob-weight, G_1 represents the weight of the rotatable crane, G_2 represents the weight of the unrotatable crawler, G_3 represents the boom weight, Q represents the lifting capacity, q represents the weight of pulley and hook, l_1 represents the distance between G_1 and point A, l_2 represents the distance between G_2 and point A (ignoring the ground inclination effect), l_3 represents the distance between G_3 and point A, l_0 represents the distance

between G_0 and point A , h_1 represents the distance between G_1 and the ground, h_2 represents the distance between G_2 and the ground, h_3 represents the distance between G_3 and the ground, h_0 represents the distance between G_0 and the ground, β represents the dip angle of the inclined ground surface, and R represents the lifting radius. K_1 and K_2 are the factors of safety in these two formulas. To simplify the calculation, the overturning moment is only generated by the hoisting load, and the stable moment is the difference between the sum of all the stable moments and other overturning moments except the hoisting load. On a construction site during operation, it always ensured to use K_2 to check the calculation.

M_F is the overturning moment induced by the wind load. Usually the crawler crane cannot perform the work on an at least intensity 6 wind. Additionally, the M_F can be neglected on a maximum intensity 6 wind when the length of the boom is shorter than 25 meters. M_F can be calculated as :

$$M_F = W_1 h_1 + W_2 h_2 + W_3 h_3 \quad (2-48)$$

Where: W_1, W_2, W_3 are the wind loads acting on the corresponding position shown in *Figure 13*.

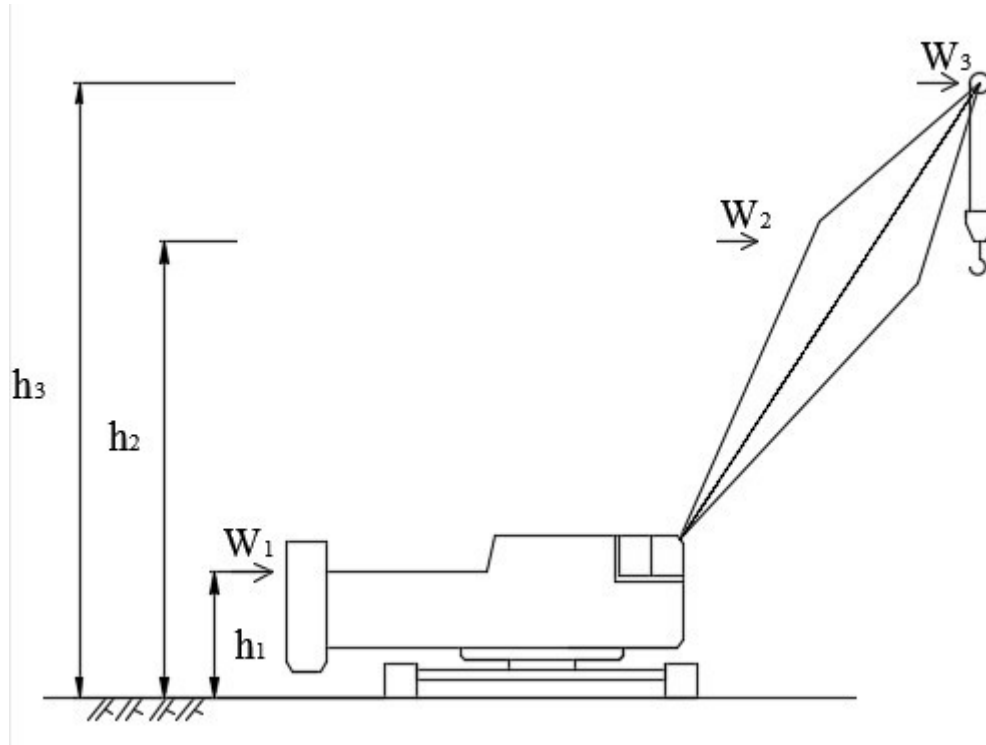


Figure 13 Force diagram of wind loads acting on a crawler crane

M_G is the overturning moment induced by the braking force when the weight Q is falling down.

$$M_G = P_G(R - L_2) = \frac{(Q+q)*v*(R-L_2)}{g*t} \quad (2-49)$$

Where: P_G is the braking force; v is the falling speed of the hook, taken as 1.5 times as the lifting speed of the hook (m/s); g is gravity acceleration taken as $9.8 m/s^2$; t is the braking time when changing with the speed of the hook from v to 0.

M_L is the overturning moment due to the centrifugal force by the turntable rotation.

$$M_L = P_L h_3 = \frac{(Q+q)Rn^2 h_3}{900-n^2 h} \quad (2-50)$$

Where P_L is the centrifugal force; n represents the rotation speed of the crane taken as $1 r/min$; h represents the distance from the center of the pulley to the gravity center of the weight Q when the hook has reached the lowest position; h_3 represents the distance from the pulley center to the ground.

The special calculation about the extended boom on the crawler crane. Sometimes, the staff will extend the boom length of the crawler crane due to a surcharged hoisting or meeting the construction requirements. When the lifting height and working radius cannot meet building requirements, and the boom strength can be guaranteed, the construction staff can take some actions to lengthen the boom as shown on *Figure 14*. According to the theorem that the moment is the same as before, during and after the extension, it can be concluded that $\sum M_A = 0$.

$$Q' \left(R' - \frac{M}{2} \right) + G' \left(\frac{R'+R}{2} - \frac{M}{2} \right) = Q \left(R - \frac{M}{2} \right) \quad (2-51)$$

Simplified

$$Q' = \frac{1}{2R'-M} [Q(2R - M) - G'(R + R' - M)] \quad (2-52)$$

Where R and R' are the original working radius and the after-extension working radius separately, Q and Q' are the original lifting capacity and the after-extension lifting capacity separately, G' is the weight of the extended part on the boom, M is the spacing between the edges of two tracks as shown in the figure.

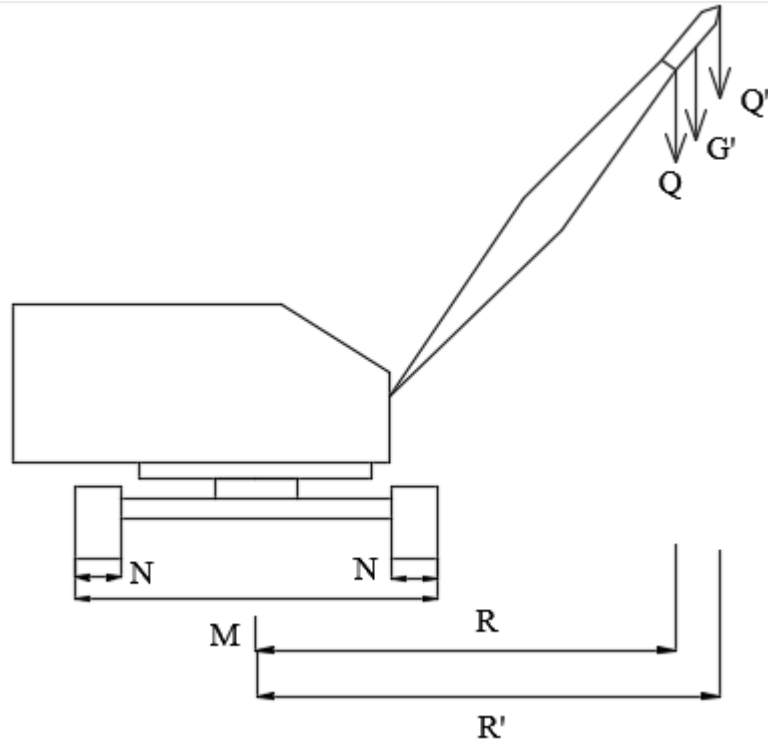


Figure 14 Force diagram of crane extension

2.3 Artificial Neural Networks (ANN)

2.3.1 ANN History and Development

In computer science, artificial neural networks are a class of statistical models analogically educated by the model of a central nervous system in human brain, which is designated as a biological neural network (Gurney, 1997). An ANN uses a large amount of input data to approximate functions, and its internal structure is comprised of interconnected nodes, like the neurons in the brain, where they can transmit the information and communicate interactively. For instance, one neural network is attempted to recognize handwriting sourced from paper documents, photographs, touch-screens or other devices (Abdalla et al., 2012). It is defined as a set of input nodes, which can be activated by the pixels of an input image. Following, by being processed and translated in the function, which is pre-defined by the network's designer, the activated nodes are passed on to stimulate other nodes repeatedly until an output node is activated.

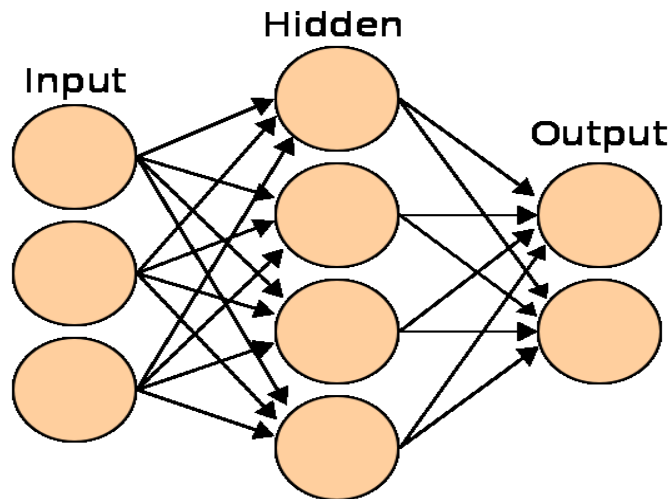


Figure 15 Structure of a typical ANN

2.3.2 Artificial Neural Networks – Basics, Structure and Training

A complicated system can be divided into a number of simple elements to aid its comprehension. The main framework of an ANN is comprised of by a set of nodes and connections between nodes, as shown in *Figure 15*. These nodes can be regarded as “artificial neurons”. Some nodes whose function is to receive inputs from the network are called “input neurons”. Similarly, other

nodes, which process inputs to obtain the outputs are named “output neurons”. The whole data process is similar to the transmission of signals to the natural neurons in the brain. Firstly, the sum of the inputs multiplied by their respective weights should be computed in a mathematical Activation Function as following *Figure 16*, which determines the activation of the neurons (Abdalla et al., 2012). Then, in another function, which might be the identity function, calculates the result as the outputs. It is obvious that the output depends on the activation, and the activation depends on the input and weights. We can obtain the desired output through adjusting the weights of this artificial neural network for the given inputs. However, generally, hundreds and thousands of neurons can exist in one network and it is a difficult and complex way to adjust the weights by hand. So, researchers found algorithms to obtain the output they wanted. This process of adjusting the weights is called “*learning or training*”. In recent studies, the implementation of the algorithm is performed by two methods. One is to utilize software engineering to develop a software program, and the other one is to use mathematical assistant applications, such as MATLAB or Mathematica. The ANN has been widely used in various fields including modeling real neural networks or studying biochemistry characteristics and behaviors of humans and animals in biological sciences. In addition, ANN is also applied in engineering fields, like pattern recognition, predicting the behavior of complex and dynamic system and stability analysis (Abdalla et al., 2012).

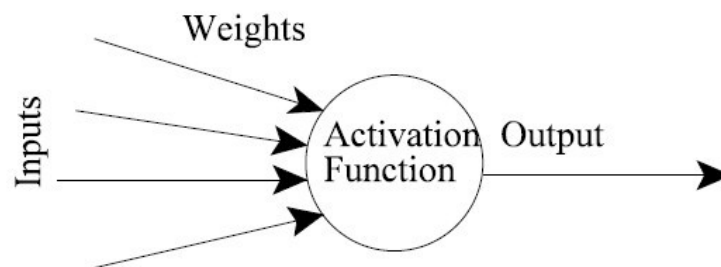


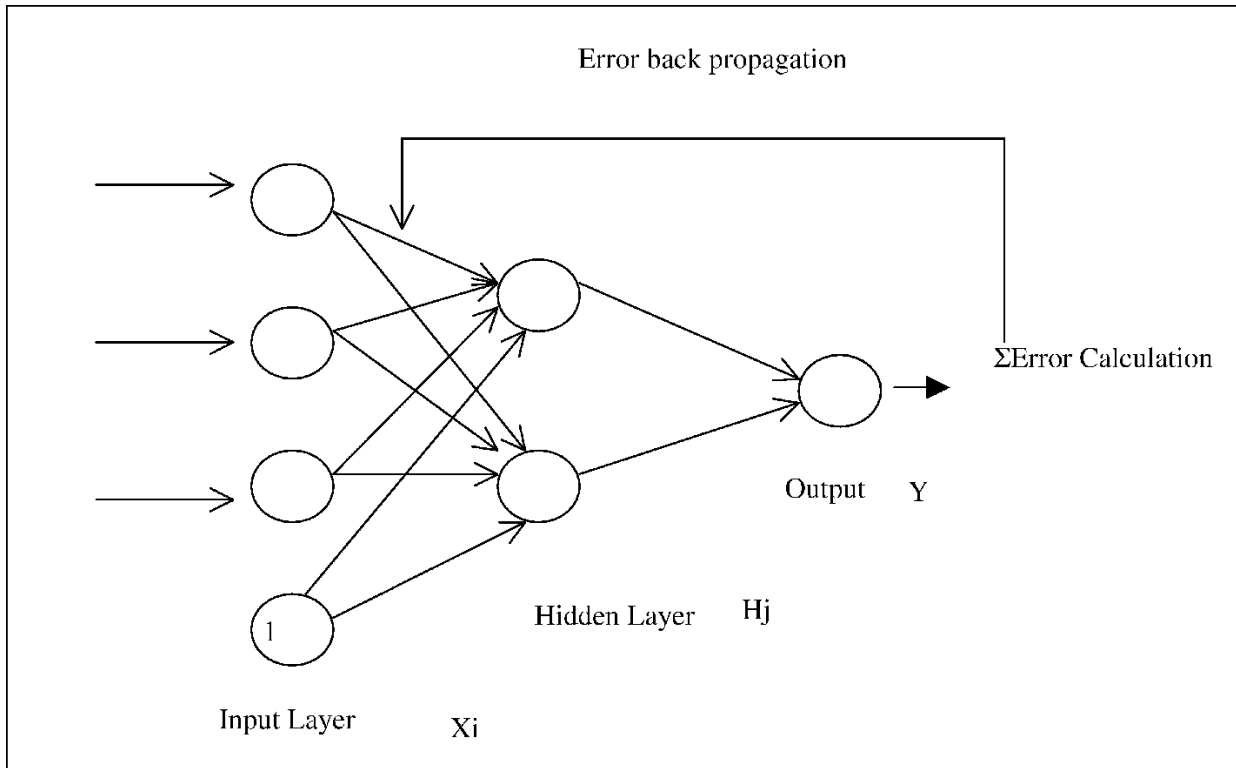
Figure 16 A schematic of a simple artificial neural network

2.3.3 The Backpropagation Algorithm

There have been a number of implementations of an ANN developed since the first model was created by McCulloch and Pitts (1943). The important differences between these ANN

implementations are their functions, the input data, topological structure and the learning algorithms. But, in this thesis, we will adopt the backpropagation algorithm established by Rumelhart and McClelland in 1986, and it is the most commonly and widely used algorithm. The status of the backpropagation algorithm in training for the ANN model is analogical to the status of Ordinary Method of Slices in the slope stability methodology. It is the basis and any other training algorithm is derived from the backpropagation algorithm. And another reason why adopting the backpropagation algorithm is that it's easily understandable to learn for the beginners. Only researchers have already mastered the basic backpropagation algorithm, and they can study more advanced algorithm, which includes Evolutionary Methods, Gene Expression Programming, Simulated Annealing, Expectation-Maximization, Non-parametric Methods and Particle Swarm Optimization (Abdalla et al., 2012).

The backpropagation algorithm is a classical multilayered feed-forward type algorithm. Its essentials are illustrated in *Figure 17*. The essence of this method is the process that, the artificial neurons are arranged in different layers and send signals forward, after that the “errors” (the differences between actual results and expected outputs) are send and fed back. In the structure of the backpropagation algorithm, the network has been divided into three main parts, comprised of the input layer, output layer and one or more intermediate hidden layers between the input layer and output layer. The operation of the backpropagation algorithm is called supervised learning (Mehryar et al., 2012). The user supplies examples with sample input and output data that the users wants a network to compute using the algorithm, and then the error is calculated and fed back to the user. Therefore, users only need to adjust the weights assigned in the network in order that the error becomes zero (or suitably small) and the final outputs are in accordance with the expectation. When the error achieves the minimal value, it is manifested that the ANN has learned the training data.



Notes: The weight connecting node i in the input layer to node j in the hidden layer is denoted by W_{ji} , and the weight connecting node j to the output node is represented by V_j

Figure 17 Basic structure of the back-propagation algorithm

2.3.4 Basic Equations and Theory of the Backpropagation Algorithm

The activation function of ANN is executed by the sum of the inputs x_i multiplied by their respective weights w_i (Saxe, 2012):

$$A_j(\bar{x}, \bar{w}) = \sum_{i=0}^n x_i w_{ji} \quad (2-53)$$

When the output function is the same as the activation function, it would be called linear, which nevertheless has several restrictions. The most prevailing output function is the sigmoidal function as following formula and *Figure 18*:

$$O_j(\bar{x}, \bar{w}) = \frac{1}{1+e^{-A_j(\bar{x}, \bar{w})}} \quad (2-54)$$

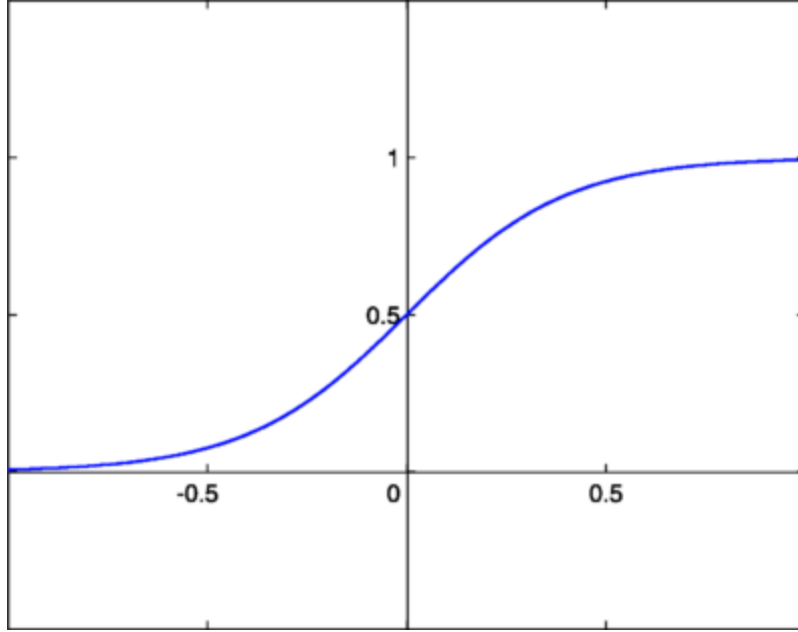


Figure 18 Sigmoidal function (<http://www.saedsayad.com>)

Since the objective of the training process is to obtain a desired output calculated by a given input, it is necessary to adjust the weights to reduce the error. So, the error function can be defined as follows:

$$E_j(\bar{x}, \bar{w}, d) = [O_j(\bar{x}, \bar{w}) - d_j]^2 \quad (2-55)$$

The above formula is for the error of each neuron, and thus error of the overall network must sum the errors of all the neurons in the output layers.

$$E(\bar{x}, \bar{w}, d) = \sum_j [O_j(\bar{x}, \bar{w}) - d_j]^2 \quad (2-56)$$

Adopting the square of the difference has two primary reasons; one is because the error can be always positive, while the other is that the error will be greater when the difference is large, and less when the difference is small.

The backpropagation method utilizes the *gradient descent method* to adjust the weights as follows:

$$\Delta W_{ji} = -\eta \frac{\partial E}{\partial W_{ji}} \quad (2-57)$$

In which, η is a constant; $\frac{\partial E}{\partial W_{ji}}$ is the derivative of E in respect to W_{ji} ; ΔW_{ji} is the adjustment for a specific weight W_{ji} .

Formula (2-57) is used until an appropriate weight is found, in which the error should be the minimum value. There are two ways to use this formula; using derivatives directly and by replacing them with algebraic expressions. For the sake of clarity, it can be demonstrated how to replace and solve by the basic algebraic equation in formal mathematical method as follows:

At first, the derivative of E with respect to O_j should be calculated, according to equation (2-55):

$$\frac{\partial E}{\partial O_j} = 2(O_j - d_j) \quad (2-58)$$

And then, another derivative can be obtained from equations (2-54) and (2-55):

$$\frac{\partial O_j}{\partial W_{ji}} = \frac{\partial O_j}{\partial A_j} \frac{\partial A_j}{\partial W_{ji}} = O_j(1 - O_j)x_i \quad (2-59)$$

Also it can be concluded from by substituting equation (2-58) and equation (2-59):

$$\frac{\partial E}{\partial W_{ji}} = \frac{\partial E}{\partial O_j} \frac{\partial O_j}{\partial W_{ji}} = 2(O_j - d_j)O_j(1 - O_j)x_i \quad (2-60)$$

Finally, the adjustment to each weight can be converted into algebraic expression based on equation (2-57) and (2-60):

$$\Delta W_{ji} = -\eta \frac{\partial E}{\partial W_{ji}} = -2\eta(O_j - d_j)O_j(1 - O_j)x_i \quad (2-61)$$

Then equations (2-57) and (2-61) can be used for training an ANN which only have two layers. Several changes and modification should be considered if training for the network with at least three layers. Practically speaking, less layers the network has, simpler the backpropagation algorithm will be, and faster the processing speed will become.

Chapter 3 – Slope Stability Analysis

3.1 Research Process Brief Summary

The entire research process used two key software implementations; MATLAB and Slide by rocscience Inc. At first, Slide software was used to develop a model of a slope, and establish key parameters in dataset format. Then, the slope stability analyses generated the FS, which depends on the slope stability analysis model. After that, the dataset of parameters and FS was entered as the input data in MATLAB. Finally, MATLAB can learn the algorithm and train the whole neural network and generate the desired FS for a given set of new parameters. Therefore, there are two main parts in this thesis research; slope stability analysis and neural network development and training. The first part, the slope stability analysis will be addressed in this chapter.

3.2 Slope Stability Analysis Using Slide - Introduction

Slide is a product created by the Rocscience Inc. (Rocscience, Inc., 2015), a company specializing in geomechanics research and development. Slide is a 2D limit equilibrium slope stability analysis application. In this thesis the slope stability analysis will be applied to establish a generic geometric model of a slope, use Monte Carlo Sampling to sample the key input parameters from their credible ranges, and apply the additional loading (generated by the crawler crane) and obtain the output FS, as shown for example in *Figure 19*. Thus, this chapter is comprised of four main parts; determination of surface loading, establishing the credible range of key input parameters, Monte Carlo sampling of data and Slide model development.

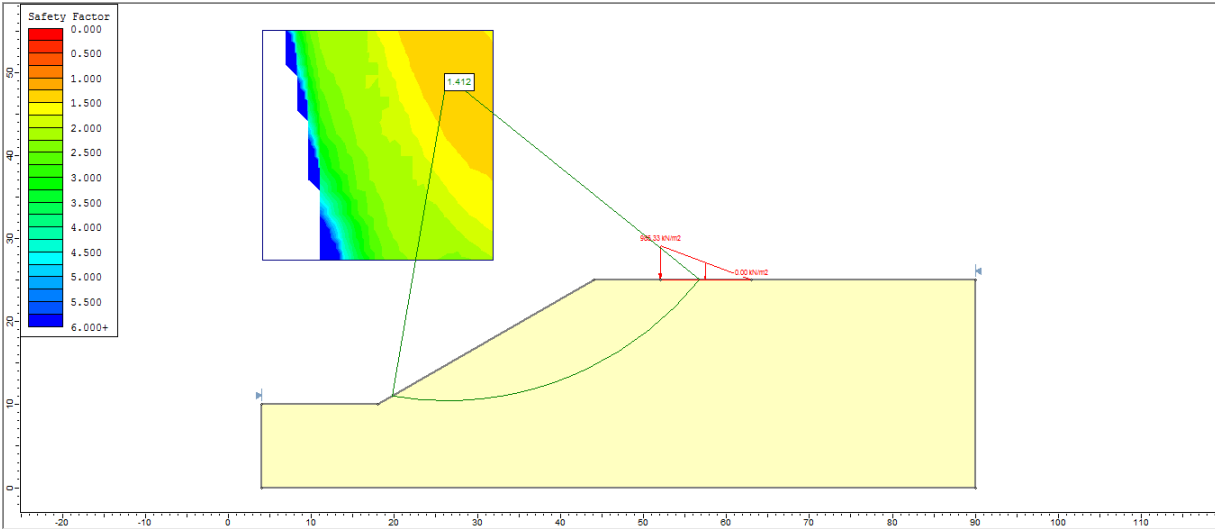


Figure 19 Slope stability analysis using Slide

3.3 Determination of Surface Loading Due to a Crawler Crane

3.3.1 Contact Pressure between the Equipment and the Crest of the Slope

Contact pressure is the intensity of loading transmitted from the superstructure loads and the self-weight of a foundation to the ground soil, acting on the underside of the foundation. In this thesis, the contact pressure is the total force of crawler crane self-weight and hoisting loads divided by the contact area between the caterpillar tracks and the ground. The magnitude and the distribution pattern of the contact pressure have an important impact on the stress increase induced. The magnitude and the distribution pattern of the contact pressure depend on many factors such as the crawler crane type and its manufacturer, the hoisting load, the boom length, and the boom angle, etc.

3.3.1.1 Contact Pressure Due to a Vertical Eccentric Load

The relevant problem can be classified into two main categories; contact pressure due to central load and contact pressure due to an eccentric load. Since the hoisting load is not collinear, the offset between the hoisting load and the crane's center of gravity cannot be ignored in the model simulation, and the research method should consider this eccentricity.

When an eccentric load is applied to a rectangular area, as shown in *Figure 20*, the contact pressure at any arbitrary point can be calculated using the formula of eccentric compression from mechanics of materials, as given by:

$$P(x, y) = \frac{P}{A} + \frac{M_x}{I_x} y + \frac{M_y}{I_y} x \quad (3-1)$$

$$M_x = P e_y \quad (3-2)$$

$$M_y = P e_x \quad (3-3)$$

$$I_x = b l^3 / 12 \quad (3-4)$$

$$I_y = l b^3 / 12 \quad (3-5)$$

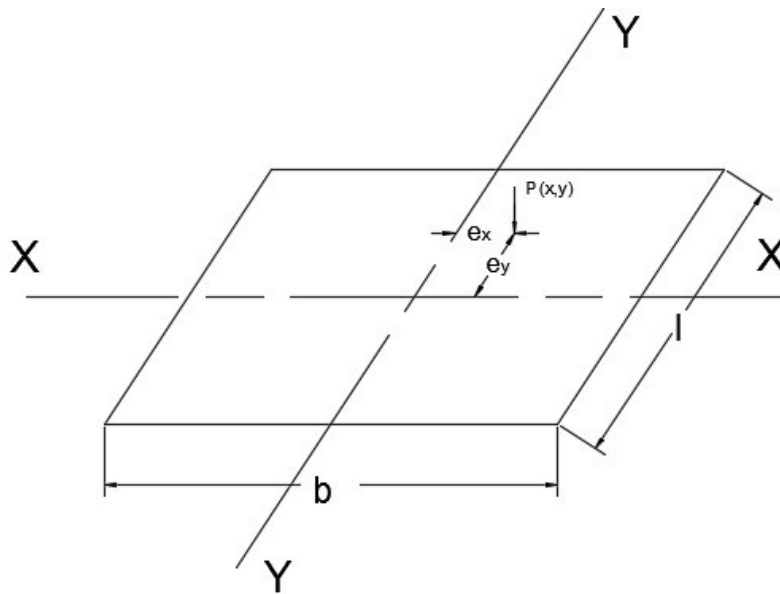


Figure 20 Contact pressure due to a vertical eccentric load - forces

Where $P(x, y)$ represents the contact pressure at arbitrary point (coordinate x, y); M_x represents the moment of the eccentric load about the X-X axis; e_y is the offset of the eccentric load line to the Y-Y axis; I_x represents the moment of inertia of the rectangular area about the X-X axis; M_y represents the moment of the eccentric load about the Y-Y axis; e_x is the offset of the eccentric load line to the X-X axis; I_y represents the moment of inertia of the rectangular area about the Y-Y axis, as summarized in *Figure 21*.

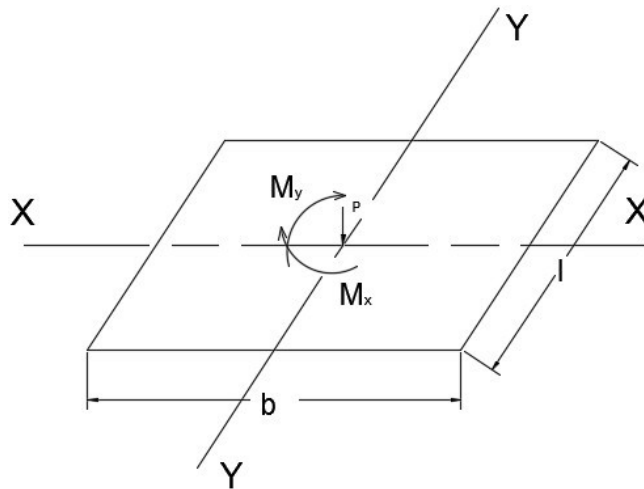


Figure 21 Contact pressure due to a vertical eccentric load – moments and force

3.3.2.2 Contact Pressure for a Two-Dimensional Plane Problem and Model Simulation

The contact pressure problem about the eccentricity on both x and y direction is for three-dimensional spatial problem. But in our model simulation, it is two-dimensional plane problem that the load is applied on one major axis, such as X-X axis (Figure 22). Then e_y equals zero, and hence M_x equals zero, and let the resultant offset equal e . Substituting $I_y = lb^3/12$ and $x = \pm b/2$ into Eq. (3-1), it will give the formula of the maximum and minimum contact pressures on both sides of the rectangular area under a vertical eccentric loading (Figure 23), as given by:

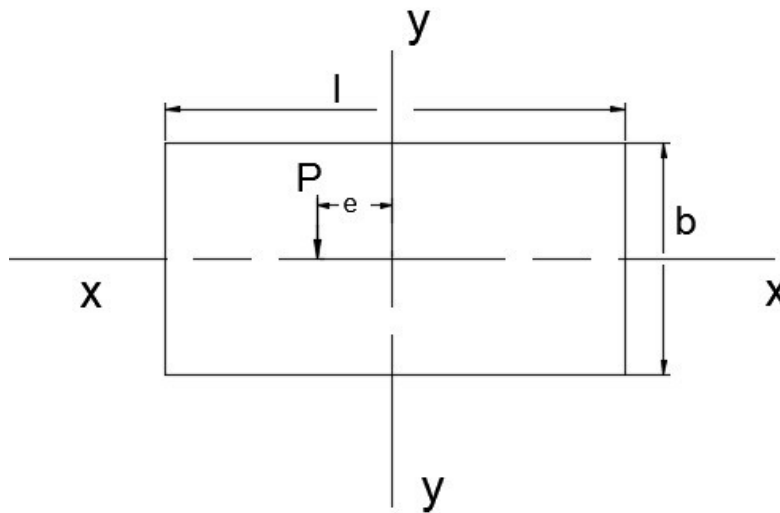


Figure 22 Load applied on X-X axis

$$P_{min}^{max} = \frac{P}{A} \pm \frac{M_y}{I_y} x \quad (3-6)$$

$$P_{min}^{max} = \frac{P}{l*b} \pm \frac{M}{S}, \quad S = \frac{bl^2}{6}, \quad e = \frac{M}{P} \quad (3-7)$$

$$P_{min}^{max} = \frac{P}{l*b} (1 \pm \frac{6e}{l}) \quad (3-8)$$

Where: S means section modulus of the rectangular area.

As $e < l/6$ in sketch (a), the pressure distribution shape is trapezoidal; $e = l/6$ in sketch (b), the distribution is triangular; $e > l/6$ in sketch (c), tensile force occurs.

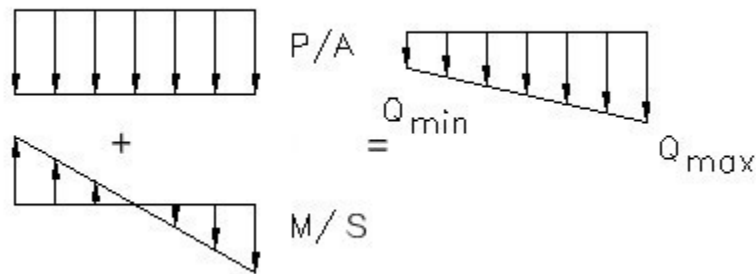


Figure 23 Load distribution – with tensile forces

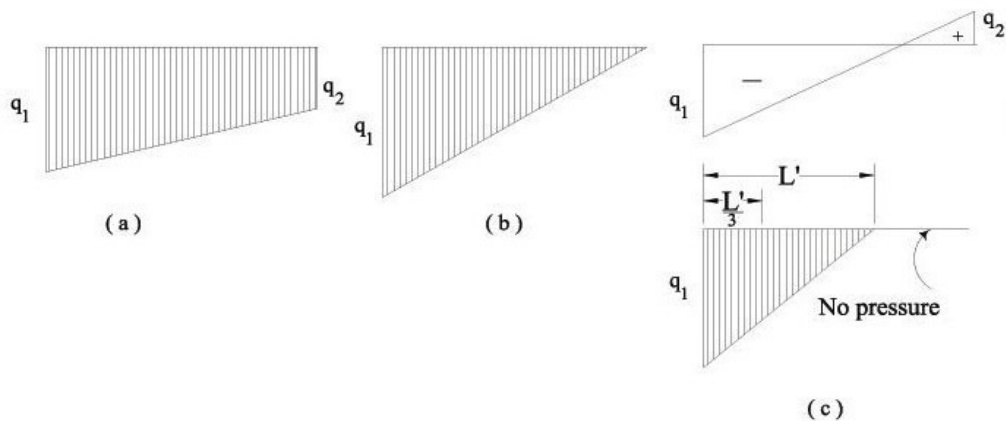


Figure 24 Load distribution – without tensile forces

Generally speaking, for soils the tensile force on a rectangular area is not allowed in the engineering practice, because soils are inherently incapable of reacting to tensile forces (*Figure 24*). Therefore, in Slide, a triangular load will be chosen to be applied on the top surface of the slope as shown in the following sketch (*Figure 25*).

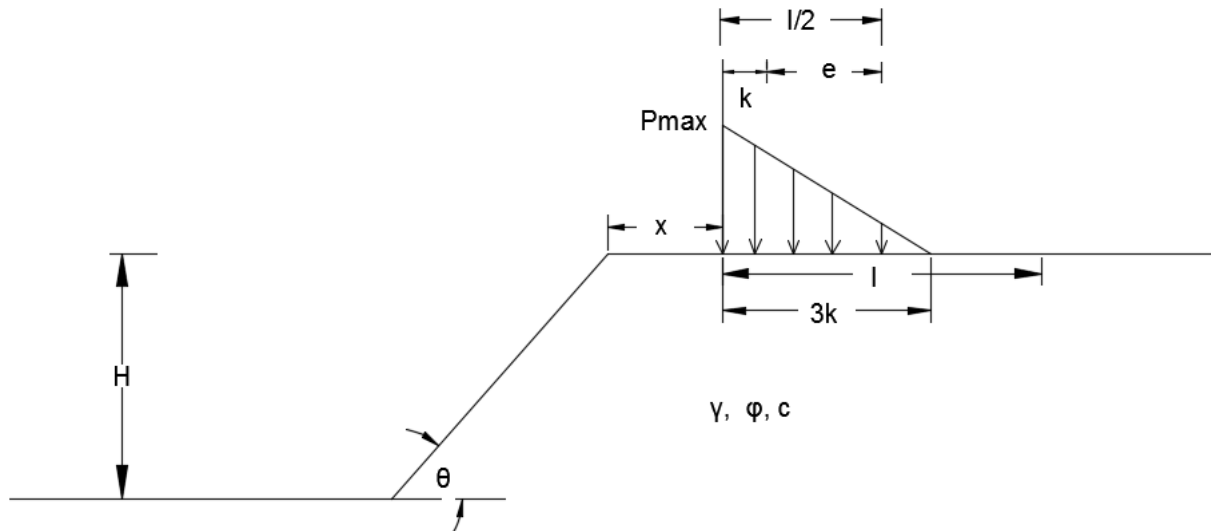


Figure 25 Slope stability analysis model setup

3.3.2.3 Maximum Pressure (P_{max}) Formula Derivation in the Model Simulation

First of all, based on the Force Translation Theorem in the theoretical mechanics, the hoisting load W lifted by the crawler crane should be translated from point C to point B, flush with the center of gravity on point A in the following sketch. Simultaneously, one additional moment M_1 should be added on the whole rectangular area. Then, another addition moment M_2 should be added by translating the hoisting load from point B to point A. Therefore, the entire concept of this calculation is collinear of the crawler crane's center of gravity and hoisting load. In this calculation, M_1 and M_2 are in the same rotation direction, since the situation in the model is assumed as the 2D plane problem that has only one eccentricity (*Figure 26*).

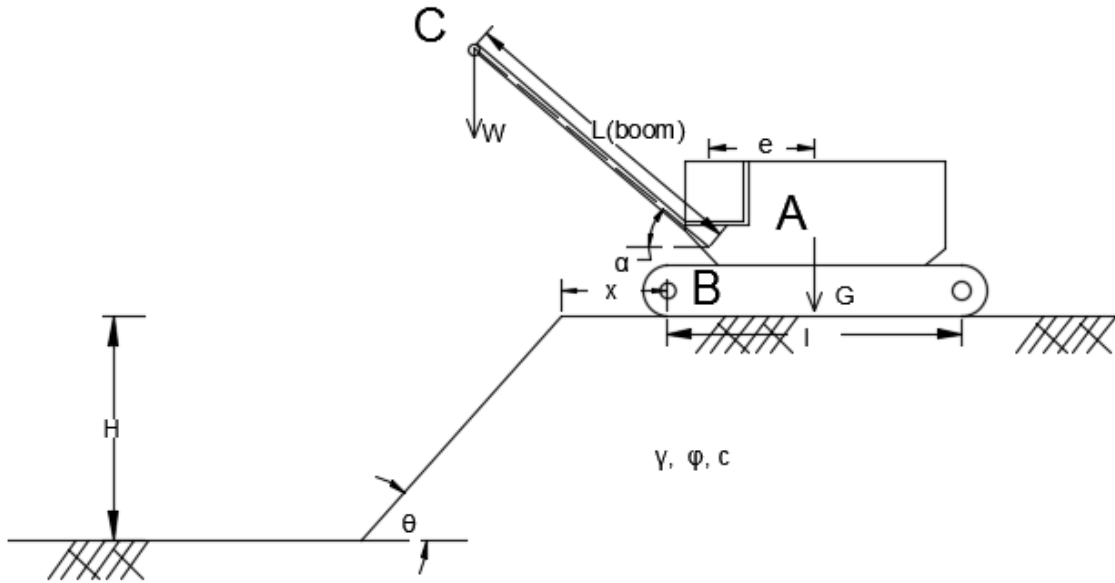


Figure 26 Maximum pressure (P_{max}) formula derivation - sketch 1

$$P_{min}^{max} = \frac{W+G}{l*b} \pm \frac{M_1+M_2}{S} \quad (3-9)$$

$$M_1 = W * L(\text{boom}) \cos \alpha \quad (3-10)$$

$$M_2 = W * e \quad (3-11)$$

$$S = \frac{bl^2}{6} \quad (3-12)$$

$$P_{min}^{max} = \frac{W+G}{l*b} \pm \frac{W*L(\text{boom})\cos\alpha+W*e}{\frac{bl^2}{6}} \quad (3-13)$$

$$P_{min}^{max} = (W + G) \frac{1}{l*b} \pm \left[\frac{6W}{bl} \left(\frac{L(\text{boom})\cos\alpha}{l} + \frac{e}{l} \right) \right] \quad (3-14)$$

$$P_{min}^{max} = \frac{1}{l*b} [(W + G) \pm 6W * \left(\frac{L(\text{boom})\cos\alpha+e}{l} \right)] \quad (3-15)$$

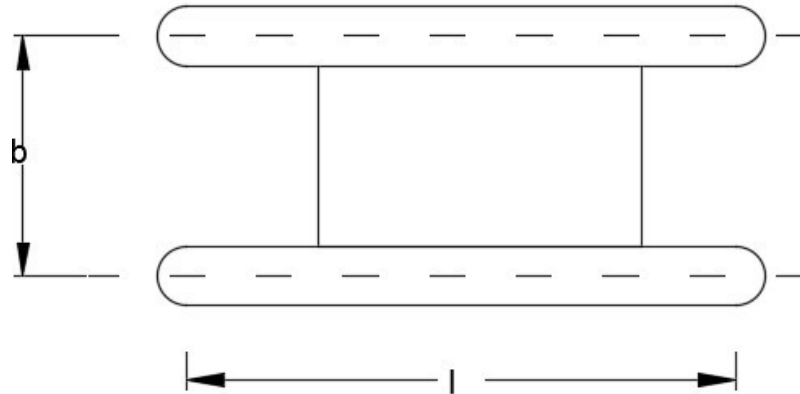


Figure 27 Maximum pressure (P_{max}) formula derivation - sketch 2

Computation in Slide is 2D, so $b = 1$. As the tension force cannot be transmitted to soils in engineering practice, the contact pressure distribution only consider the P_{max} , as given by:

$$P_{Max} = \frac{1}{l} [(W + G) + 6W * \left(\frac{L(\text{boom}) \cos \alpha + e}{l} \right)] \quad (3-16)$$

By using the above equation, an Excel sheet (Figure 28) was developed to collect a credible range of boom length data, boom angle data and hoisting load data, which will be used to calculate the final P_{Max} .

Model No.	Pmax Determination Crawler Crane Model: SCX500 Manufacturer: HITACHI Unit:m											
	Pmax determination (Enter the input data, you can obtain the output data)											
	Input data			constant parameter				angle → radian		output data		
L(boom)	α(angle)	W (kN)	e	l	b	G	α(radian)	cosα	Pmax(kPa)	A	B	
Model61	11.63	50.25	461.1	1	4.71	1	423.556	0.877028	0.639439	1239.97081	884.656	1.791226
Model62	6.41	71.37	377.52	1	4.71	1	423.556	1.245641	0.319456	481.267958	801.076	0.647072
Model63	10.43	71.04	392.19	1	4.71	1	423.556	1.239882	0.324908	638.727804	815.746	0.931803
Model64	8.52	60.25	457.35	1	4.71	1	423.556	1.051561	0.496217	833.686114	880.906	1.109929
Model65	11.28	49.35	382.59	1	4.71	1	423.556	0.86132	0.651437	1035.00186	806.146	1.772443
Model66	10.51	35.72	464.13	1	4.71	1	423.556	0.623432	0.81188	1385.13211	887.686	2.023961
Model67	10.2	50.76	463.11	1	4.71	1	423.556	0.885929	0.63257	1121.6759	886.666	1.582211
Model68	9.69	51.38	437.31	1	4.71	1	423.556	0.89675	0.624152	1016.3919	860.866	1.496398
Model69	7.47	66.44	384.75	1	4.71	1	423.556	1.159597	0.399709	586.384142	808.306	0.846248
Model70	9.09	35.06	479.5	1	4.71	1	423.556	0.611912	0.818551	1286.37541	903.056	1.792065

Figure 28 Calculation of P_{max} for various loading scenarios

3.4 Credible Ranges of Key Model Parameters

3.4.1 Credible Range Relative Documents Collection

In this thesis, five key parameters were identified that describe a homogeneous soil slope; the unit weight of the soil, the cohesion, the angle of internal friction, the slope height, and the slope angle. In addition, parameters for the crawler crane are listed as well. The following sections present each parameter separately. The credible ranges of parameters were collected from books, engineering handbooks, journal articles, and national design codes. The compiled references can be found in the Appendix.

3.4.2 Unit weight

For many soils this parameter is typically about 15 kN/m³ but can vary between 11kN/m³ for a loose dry soil to 22 kN/m³ for dense wet soils. The following *Table 3* summarizes a range of typically recorded values.

Soil Type	SPT Penetration N-Value (blows/ foot)	Unit weight (kN/m³)
Very loose sand	0 - 4	11.53 - 16.48
Loose sand	4 to 10	14.83 - 18.95
Medium sand	10 to 30	18.12 - 21.42
Dense sand	30 to 50	18.12 - 23.07
Very dense sand	>50	21.42 - 24.72
Very Soft clay	0 - 2	15.00 – 16.00
Soft clay	2 to 4	16.00 – 17.00
Medium clay	4 to 8	17.00 – 18.00
Stiff clay	8 to 16	18.00 – 19.00
Very Stiff clay	16 - 32	19.00 – 20.00
Hard clay	>32	20.00 – 22.00

Table 3 Unit weight of soils (collected from references – see Appendix)

Note: The original unit of the sand unit weight was lb/ft³. In this thesis, the conversion formula used was 1lb/ft³=0.16475kN/m³.

3.4.3 Cohesion

This is almost zero for dry loose sandy soils and can rise to maximum 100kN/m² for hard dry clayey soils. Friable (moist) loam type soils are typically in the range of 5 to 15 kN/m² and moist plastic clayey soils are from 10 to 40kN/m².

Soil Type	SPT Penetration (blows/ foot)	c (kPa)
Very Soft clay	0 - 2	0 - 0.25
Soft clay	2 to 4	0.25 - 0.5
Medium clay	4 to 8	0.5-1.0
Stiff clay	8 to 16	1.0-2.0
Very Stiff clay	16 - 32	2.0-4.0
Hard clay	>32	>4
Sand		0

Table 4 Cohesion of soils (collected from references – see Appendix)

3.4.4 Angle of Internal Friction

Theoretically, pure clay would have a value of zero degrees and from there the internal friction angle would rise with increasing sand content and density to approximately 40 degrees for a compact sandy loam soil. Loose sands range between 25 degrees to 30 degrees. As pure clays are rarely found in top soils, the typical value for a ‘clay’ soil would be in the range 5 to 10 degrees.

Soil Type	SPT Penetration, N-value(blows/foot)	ϕ (degrees)
Very loose sand	<4	<29
Loose sand	4 to 10	29-30
Medium sand	10 to 30	30-36
Dense sand	30 to 50	36-41
Very dense sand	>50	>41
Very Soft clay	0 – 2	<3
Soft clay	2 to 4	3 to 5
Medium clay	4 to 8	4 to 9
Stiff clay	8 to 16	8 to 16
Very Stiff clay	16 – 32	15 to 25
Hard clay	>32	>25

Table 5 Angle of internal friction for soils (collected from references – see Appendix)

3.4.5 Slope Angle and Slope Height

According to the Geological Engineering Manual (2006), a slope can be classified into extra high slope, high slope, medium slope and low slope, four categories based on the slope height. Slopes can be also categorized into steep slope, medium slope and gentle slope based on the slope angle as illustrated in the following table.

1. Slope height	
Slope type	Slope height (m)
Extra High slope	>100
High slope	30 to 100
Medium slope	10 to 30
Low slope	<10
2. Slope angle	
Slope type	Slope angle (degrees)
Steep slope	60-90
Medium slope	30-60
Gentle slope	0-30

Table 6 Slope angle and slope height (collected from references – see Appendix)

One resource, Rock Slope Engineering 4th Ed. (Wyllie and Mah, 2005), shows that numerous slope angles converge into the range from 10 to 80 degree, and natural or man-made slopes almost distribute between 50m and 300m as shown in the *Figure 29* below.

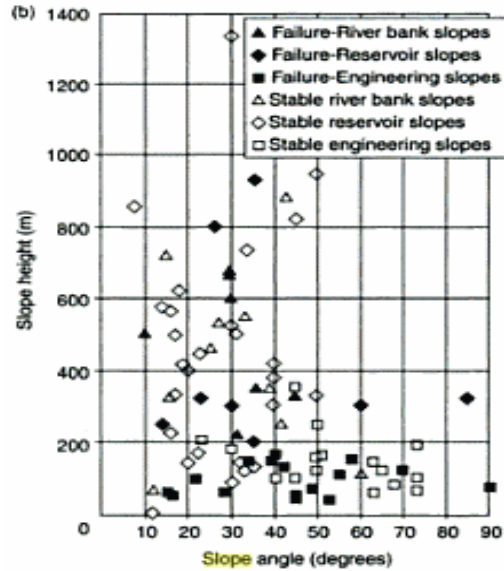


Figure 29 Natural and engineered slopes in China, data from Chen (1995a, b) (Wyllie and Mah, 2005),

3.4.6 Crawler Crane Parameters

In this thesis, a crawler crane is represented by a typical example, a HITACHI product, SCX500. The detailed specifications for this crawler crane model are summarized as follows:

■ Specifications		(1 t = 1 000 kg)	
Maximum rated load × Working radius	t × m	50 × 3.8	
Basic boom length	m	10	
Maximum boom length	m	52	
Winch			
Maximum line pull	t	15.6	
Maximum rated line pull	t	6.5	
Line speeds	Main hoist drum	m/min	*110/74/37
	Auxiliary hoist drum	m/min	*110/74/37
	Boom hoist drum	m/min	*60
Swing speed	min ⁻¹ (rpm)	3.7 (3.7)	
Travel speed	km/h	2.0/1.5	
Gradeability	% (°)	40 (22)	
Diesel Engine			
Rated horsepower	kw/min ⁻¹ (PS/rpm)	147/2 100 (200/2 100)	
Ground pressure	kPa (kgf/cm ²)	68.6 (0.70)	
Operating weight	t	50.1 (including 10 m boom and 50 t capacity hook)	

Notes : 1. Data is expressed in SI units, followed by conventional units in ().
2. *Line speeds marked will vary with the load.

Figure 30 Crawler crane specifications (SCX500 Specification, HITACHI, 2015)

Crawler Crane Parameters	Credibile range
L (boom)	6-12 m
A (angle)	35-75 degrees
W (weight)	350-490 kN

Table 7 credible ranges of crawler crane parameters (SCX500 Specification, HITACHI, 2015)

Thus, the range of parameters is summarized in *Table 7* based on:

1. For the boom length, the actual range is 6-52m. The basic unextended boom length is 10m. The maximum boom length is 52m, and the minimum boom insert is 6m. However, the overturning rate increases largely when the crawler crane operates with the maximum boom length of 52m. Therefore, conservatively, a reasonable boom length range was assumed to be 6-12m.
2. Theoretically for the hoisting load W, the minimum value can be zero, but it makes no sense. And even though the hoisting load is too small, the cost of the crawler crane is quite expensive in the project budget.

3.4.7 Credible Ranges Summarization

By filtering the maximum number and the minimum number in each table, the credible ranges for each key parameter can be concluded as:

Soil Properties Credible Range							
Unit weight (kN/m³)		φ (degree)		c (kPa)		x (m)	
Min	Max	Min	Max	Min	Max	Min	Max
11.53	24.72	0	41	0	60	0	30

Table 8 Credible ranges – soil properties

Slope Properties and Crawler Crane Parameters			
Item		Credible Range	
		Min	Max
Slope Properties	Slope Height (m)	3	30
	Slope Angle (°)	10	70
Crawler Crane Parameters	L(boom) (m)	6	12
	α (angle) (°)	35	75
	W (kN)	350	490

Table 9 Credible range – slope geometry and crawler crane parameters

3.5 Monte Carlo Data Sampling and Slide Model Building

3.5.1 Monte Carlo Data Sampling

After the determination of credible ranges of key parameters, these ranges need to be sampled. A simple Monte Carlo technique was adopted using a random function in Excel. It was used to generate the sampled data within the range of credible range. Using the random function can ensure randomness and applicability in the research and practical engineering field. The following figures show an Excel table and how key parameters were sampled.

Figure 31 shows the use of a random function to generate a random sample between the maximum values and minimum values for the key parameters for two typical models. While the second figure (*Figure 32*) shows input data summary for the Slide model using the sampled parameters.

Model 1				
	min	max		Random Number
Unit weight	11.53	24.72		17.05
ϕ	0	41		22.08
c	0	60		50.04
Slope Height	3	30		23.06
Slope Angle	10	70		57.23
L(boom)	6	12		7.70
α	35	75		64.67
W	350	490		428.36
x	0	30		0.22

Model 2				
	min	max		Random Number
Unit weight	11.53	24.72		24.55
ϕ	0	41		28.00
c	0	60		45.95
Slope Height	3	30		6.64
Slope Angle	10	70		22.46
L(boom)	6	12		10.47
α	35	75		59.66
W	350	490		375.50
x	0	30		11.87

Figure 31 Parameter sampling using random numbers

Bishop Simplified Method (Slide Software)									
Crawler Crane Model: SCX500 Manufacturer: HITACHI Unit:m									
Model No.	Input data							Output data	
	Slope and Soil Properties				Triangular Load			x	Fs
Slope Height H	Slope Angle θ (angle)	Angle of Internal Friction ϕ (angle)	unit weight γ (kN/m ³)	Cohesion c (kPa)	Magnitude (Pmax)	length (3k)			
Model 51	16.51	50.58	31.63	19.02	57.53	468.65	4.065	21.03	2.072
Model 52	21.12	16.92	8.32	15.47	23.45	834.46	4.065	24.54	1.091
Model 53	19.42	54.73	33.82	17.86	3.15	930.93	4.065	19.58	0.723
Model 54	28.36	4485	15.79	21.46	45.94	568.29	4.065	24.67	0.978
Model 55	23.82	46.59	0.47	21.37	11.64	674.33	4.065	15.42	0.125
Model 56	11.24	36.62	38.15	19.32	49.92	600.84	4.065	5.14	2.25
Model 57	23.58	42.66	21.99	24.45	53.47	915.41	4.065	21.26	1.337
Model 58	21.35	29.89	11.33	19.03	8.67	940.14	4.065	14.75	0.455
Model 59	27.71	18.7	27.66	16.82	32.51	744.40	4.065	14.9	2.372
Model 60	12.25	3390	23.68	22.8	11.23	875.62	4.065	26.13	1.196

Figure 32 Slide model input data summary

3.5.2 Building of Slide Models for Slope Stability Analysis

Model building is an important part for slope stability analysis using Slide. The three main common features of more than 150 models generated will be; homogeneous slope material, no ground water table and circular slip surface analysis (with grid search). Since the slope is homogeneous, Bishop simplified method is adopted as the slope stability analysis method. The general slope settings in Slide, in the 'Project Settings' tab, are illustrated in *Figure 33*. The slopes were defined from right to left.

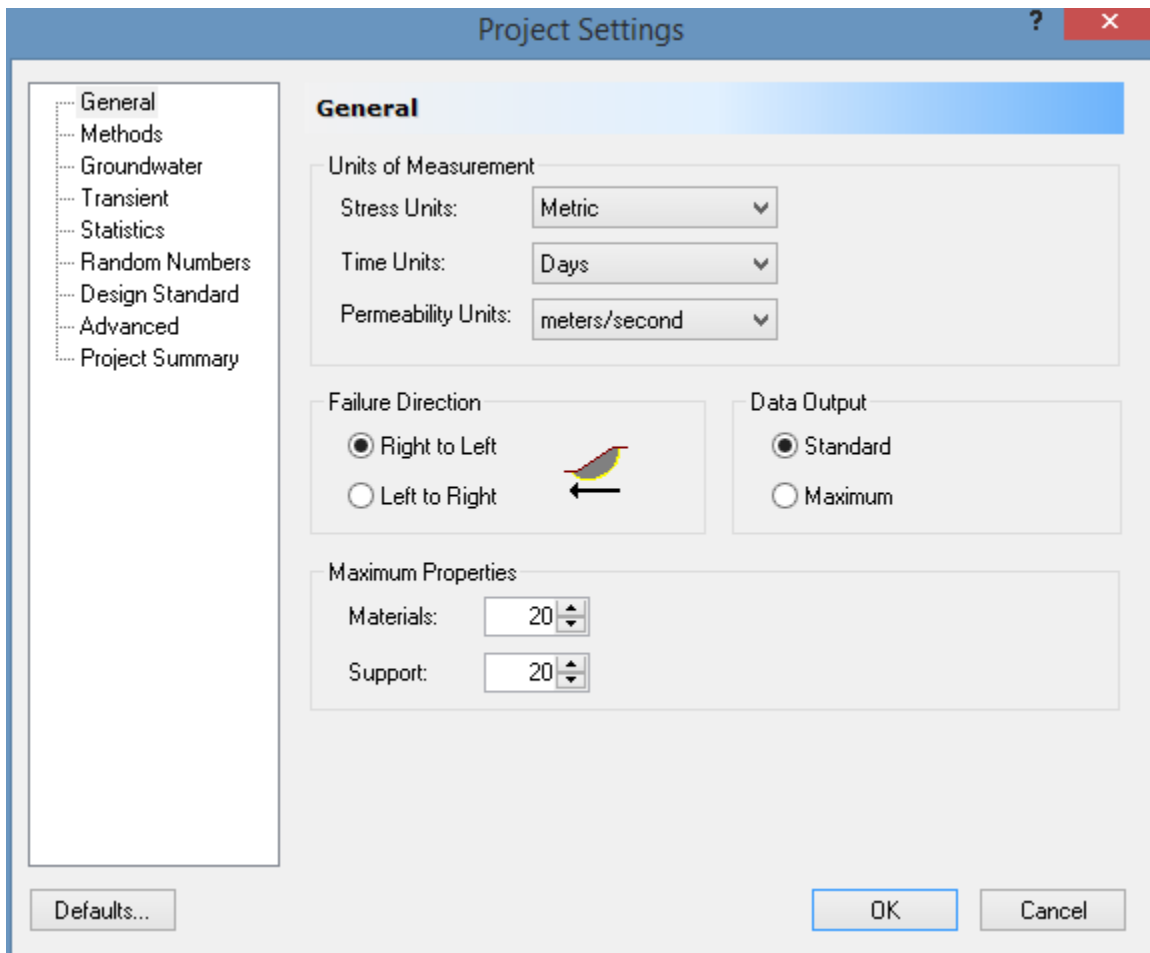


Figure 33 Project Setting

Once the project settings are defined, the external boundary should be created to delineate the extent of slope and material encompassed by the model. In essence, the external boundary is a closed polyline, and it encloses the soil area, which will be analyzed. Moreover, the upper portion of the external boundary displays the slope crest surface where the loading will be

applied. The left, right and lower limits of the external boundary were defined such that a sizeable search area is possible for the critical failure surface search, where no external boundary will limit the search zone. Guidelines in Slide documentation were used to establish this zone.

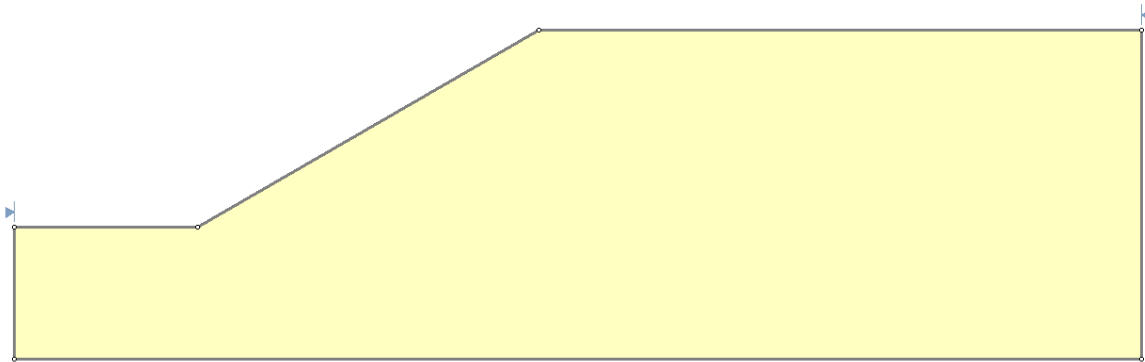


Figure 34 Defining external boundary for the slope

Lastly, the slope material data from the Montel Carlo sampling should be entered, as shown in *Figure 35*. In Slide, external loads can be categorized as either concentrated loads or distributed loads. For this thesis research, the distribution of loading on the crest of a slope applied by the crawler crane is of triangular type (*Figure 36*), as discussed in the previous chapter. The magnitude of the loading is determined by the equation (3-16), as mentioned previously. After adding an external load, slip center grids should be set up, as seen in *Figure 37*. Each slip surface in the model will be analyzed individually by the Slide engine, and a critical surface search will be used to find the global minimum FS and the corresponding failure surface.

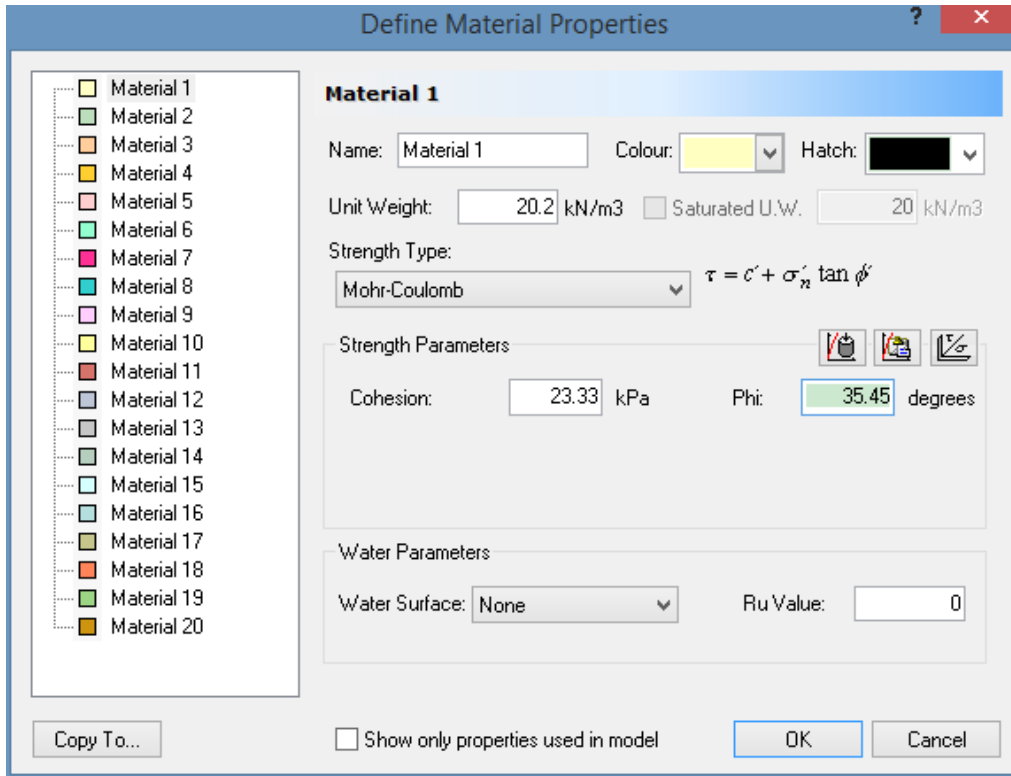


Figure 35 Defining material properties in Slide

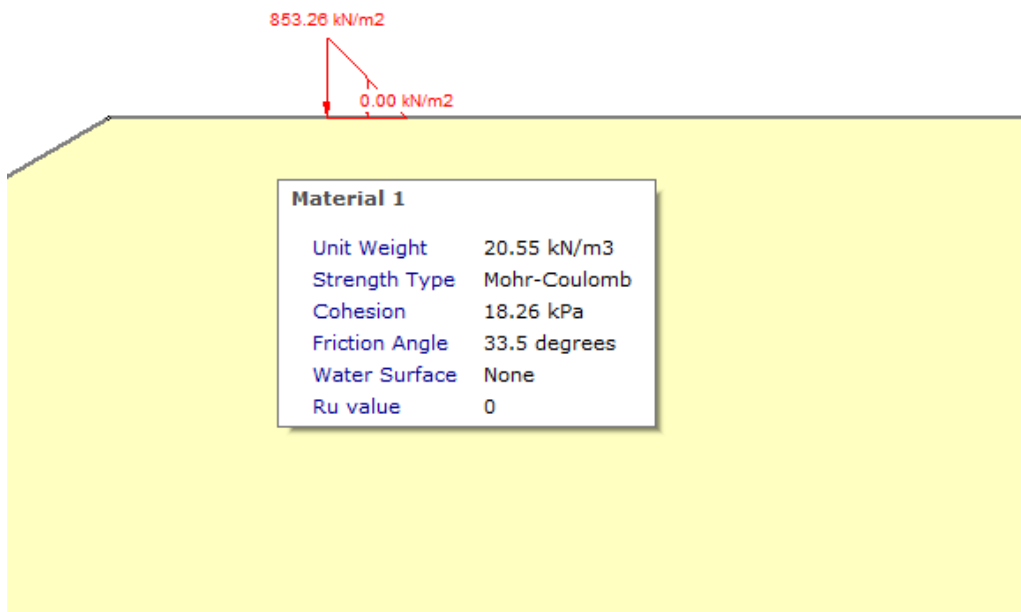


Figure 36 External loading and material properties display in Slide

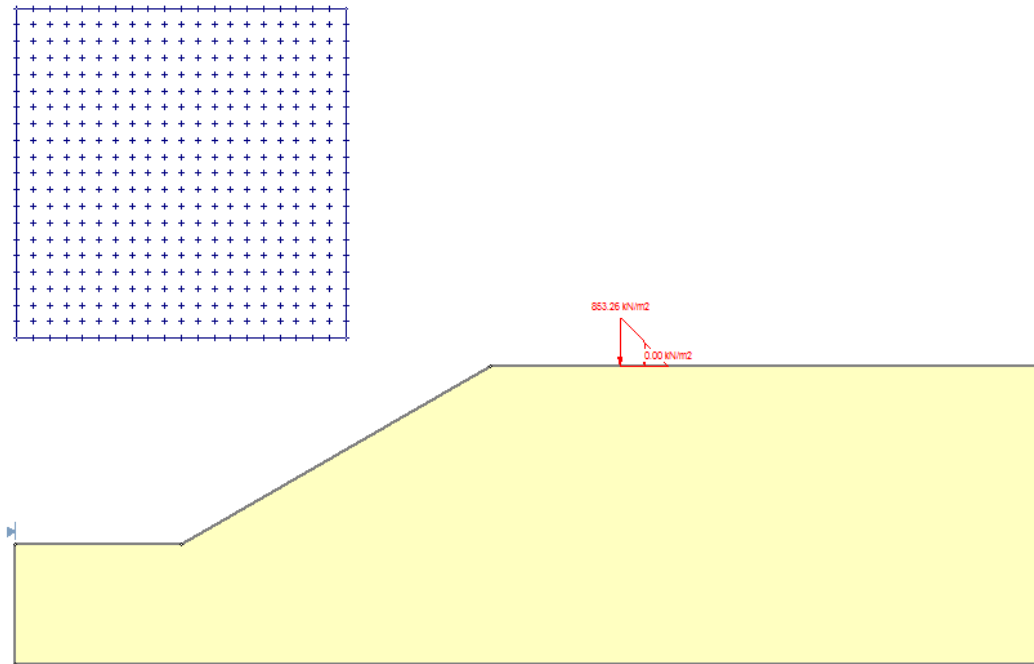


Figure 37 Automatic search grid for the minimum FS – in Slide

Finally, the ultimate step is to run the analysis and view the results. By computing and interpreting, the lowest FS of the global minimum slip surface in the Slide model can be observed directly. The slip center radius and x, y coordinates can be also checked and recorded. Additionally, the contours of each slip surface in the slip center grid can be examined. The color legend of the FS can be used to estimate if the slip surface is dangerous or safe. Darker the color will be, higher the value of FS will be and safer the slip surface will be.

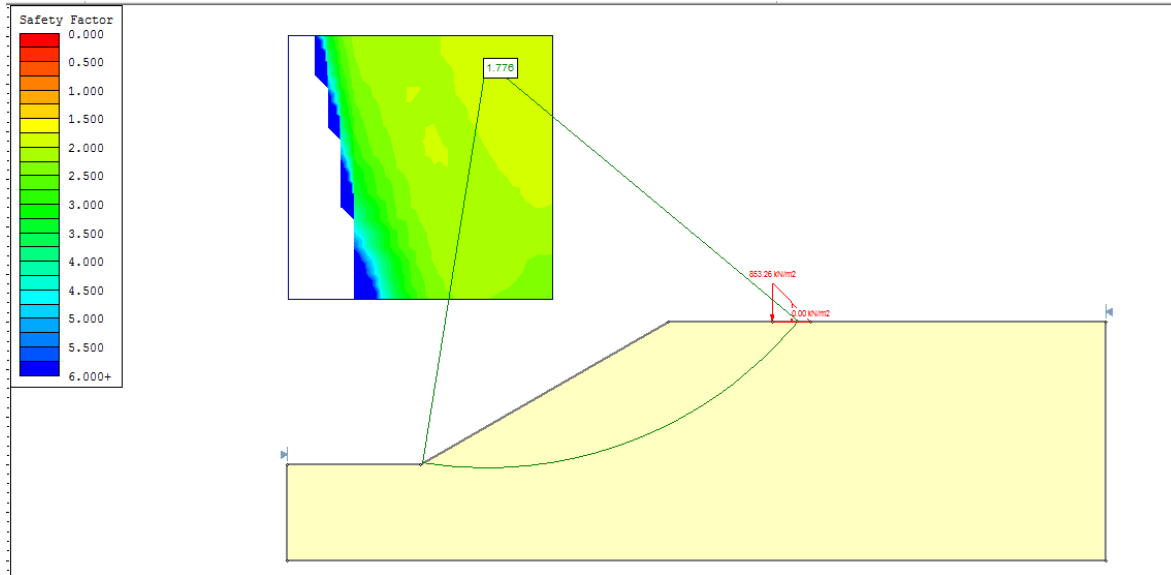


Figure 38 Typical analysis results from Slide

3.6 Stability Analysis Results - Discussion

First of all, the most important assumption of Bishop simplified method is the circular stability analysis for slip surface. This method considers the horizontal interslice forces, and assumes the local FS for each slice is equal to the global FS for the whole slope. For slope condition setting, it is homogenous, no ground water and no weak layer.

Secondly, the reason of causing the slope failure was also explored. The slope failure is controlled by multiple interacting factors. For example, even though the strengths of unit weight and cohesion in the slope material are sufficient strong, the low-value internal friction angle can also cause the slope failure. An experiment was conducted to prove this perspective. As seen in Figure 39, no any other key parameter changes except cohesion.

Change before	Model 1	Model 2	Model 3	Model 4	Model 5	Model 6	Model 7	Model 8	Model 9	Model 10
Cohesion	1.03	1.38	3.88	0.82	0.8	3.44	5.71	6.55	1.84	4.1
FS	0.862	0.388	0.889	0.091	0.598	0.155	1.16	0.208	0.023	0.968
Unit weight	18.17	12.82	20.98	19.43	21.87	13.93	22.92	15.8	18.18	14.96
Internal friction angle	35.52	18.33	25.41	3.47	38.13	4.51	20.45	3.52	0.2	30.85
Change after	Model 1	Model 2	Model 3	Model 4	Model 5	Model 6	Model 7	Model 8	Model 9	Model 10
Cohesion	54.55	15.19	30.44	45.45	44.77	18.52	11.52	21.57	31.58	37.7
FS	1.611	0.577	1.294	0.582	1.233	0.377	1.315	0.413	0.314	1.606
Unit weight	18.17	12.82	20.98	19.43	21.87	13.93	22.92	15.8	18.18	14.96
Internal friction angle	35.52	18.33	25.41	3.47	38.13	4.51	20.45	3.52	0.2	30.85

Figure 39 Comparison of FS as a function of cohesion

The FS increases after increasing the cohesion value, but Models 2, 4, 6, 8, 9 still fail. Models 4,6,8,9 fail because of their low angle of internal friction. Model 2 fails because of its low unit weight and relative small cohesion. Therefore, an individual key parameter can change the value of final FS, but it cannot determine whether the failure of the whole slope will occur or not.

Thirdly, there is a regular relationship between FS and the seven key parameters chosen (slope height, slope angle, angle of internal friction, unit weight, cohesion, loading applied on the slope surface and the distance between the slope edge and the crawler crane). Flatter, gentler the slope, higher strength of soil, smaller loading by the mobile crawler crane and longer distance away from the slope edge result a larger FS.

Finally, a statistical analysis should be carried out for discussion based on the results of Slide models created and analyzed. The following two tables shows key parameters, FS and x, y, R for global minimum slip surface for the 150 Slide models done.

Slope height	slope angle	ϕ	γ	c	Pmax	x
18.27	37.43	35.52	16.17	54.55	850.01	0.33
20.61	40.81	18.33	12.82	15.19	977.03	1.42
29.07	25.38	25.41	20.98	30.44	1186.08	1.12
23.33	41.91	3.47	19.43	45.45	693.78	2.82
13.96	59.73	38.13	21.87	44.77	580.25	1
12.19	39.11	14.51	13.93	18.52	622.57	0.5
16.25	16.68	20.45	22.92	31.52	673.20	5
28.84	33.03	13.52	15.8	21.57	570.33	8.3
10.77	42.55	0.2	18.18	31.58	862.34	16.5
17.71	31.85	30.85	14.96	37.7	637.37	1
14.58	15.26	25.76	22.72	37.6	961.06	16.37
7.81	61.28	21.57	17.38	35.1	1030.93	12.39
28	58.99	39.9	14.7	15.05	892.61	3.24
28.07	18.22	2.64	21.51	47.85	882.19	5.65
16.14	26.14	16.18	12.74	4.19	856.62	18.95
13.36	33.9	39.63	17.01	31.2	799.34	2.6
9.1	50.21	6.87	20.47	59.38	831.55	3.66
16.18	53.77	28.6	16.65	13.85	778.44	28.38

Table 10 Key parameters for 150 slide models

21.28	40.23	20.51	17.04	53.21	927.97	8.98
4.69	11.06	18.4	22.85	34.5	803.02	15.54
20.72	50.84	17.8	23.83	17.36	1113.90	23.18
27.23	12.54	7.4	22.08	28.36	1199.65	3.01
19.68	61.66	33.64	16.08	28.48	1187.34	19.95
9.39	64.79	17.58	21.19	15.2	1263.75	25.82
18.66	28.47	38.33	18.5	46.62	1095.78	14.69
10.38	31.04	20.57	11.81	11.93	1051.14	0.51
10.75	62.64	7.45	12.05	46.44	845.45	21.23
18.19	40.01	27.82	23.37	46.28	703.86	13.56
22.15	10.03	19.25	12.77	21.44	952.21	29.22
16.65	69.4	14.49	17.01	54.55	894.13	21.05
16.82	33.43	32.85	14.59	54.67	730.79	14.6
29.81	30.03	37.26	14.2	56.29	715.19	9.35
13.03	67	5.59	23.49	40.75	1253.89	25.87
23.74	49.65	11.19	22.87	52.41	561.09	19.68
19.62	30.77	9.42	14.96	51.59	684.67	7.36
19.51	41.34	35.91	12.17	53.3	711.89	26.32
20.38	36.3	14.38	17.3	14.14	709.69	12.24
19.35	47.17	32.64	12.61	50.35	602.16	15.38
14.18	52.96	15.89	20.86	42.53	822.51	16.98
11.42	38.68	27.97	14.39	23.87	1051.17	27.02
29.04	28.9	13.21	15.36	3.59	1266.37	20.61
27.65	68.96	3.66	11.77	45.9	648.26	22.86
24.52	65.26	14.59	16.51	45.08	1080.55	12.06
25.78	23.26	28.36	17.01	41.07	1009.42	15.73
22.92	34.09	37.92	21.67	48.9	903.70	20.01
9.93	49.68	40.7	15.3	16.65	948.13	22.75
19.18	14.2	27.12	13.33	24.62	690.93	24.98
25.97	43.2	19.69	15.33	17.72	874.69	22.53
23.27	30.73	27.67	12.01	22.53	976.38	16.73
6.85	18.16	21.52	12.3	17.07	1026.55	17.49
16.51	50.58	31.63	19.02	57.53	468.65	21.03
21.12	16.92	8.32	15.47	23.45	834.46	24.54
19.42	54.73	33.82	17.86	3.15	930.93	19.58
28.36	44.85	15.79	21.46	45.94	568.29	24.67
28.57	42.87	30.13	21.12	32.97	922.27	12.94
11.24	36.62	38.15	19.32	49.92	600.84	5.14
23.58	42.66	21.99	24.45	53.47	915.41	21.26

Table 11 Key parameters for 150 slide models, (continued)

21.35	29.89	11.33	19.03	20.67	940.14	14.75
27.71	18.7	27.66	16.82	32.51	744.40	14.9
12.25	33.9	23.68	22.8	11.23	875.62	26.13
20.59	24.67	9.9	12.92	59.82	1239.97	26.65
22.14	36.76	21.2	19.43	19.62	481.27	3.58
27.7	11.61	25.28	21.46	27.34	638.73	26.72
18.14	14.75	38.08	23.96	8.44	833.69	9.24
4.1	30.99	19.26	13.53	0.43	1035.00	6.61
7.54	60.63	31.86	20.48	12.78	1385.13	6.71
19.46	40.81	5.6	14.52	41.87	1121.68	28.48
29.11	37.4	30.33	23.98	20.32	696.75	25.34
19.16	12.75	11.03	21.88	37.19	586.38	12
4.99	15.94	10.61	13.2	10.03	1286.38	19.52
27.79	41	23.03	24.5	50.3	723.32	22.95
21.17	40.18	18.35	23.21	44.21	590.82	4.61
6.77	66.73	25.15	16.11	43.39	1128.92	20.84
19.29	16.91	15.91	18.33	27.73	1144.12	11.73
15.8	62.85	13.96	23.38	51.68	1130.32	6.67
24.21	11.13	8.91	12.58	7.71	1193.62	24.82
7.96	52.65	7.99	18.99	59.46	1143.93	12.45
18.01	14.21	27.74	13.47	19.22	710.57	10.12
28.36	64.63	19.82	15.25	38.17	832.05	0.41
20.17	55.11	20.38	17.07	49.62	1029.78	3.91
11.42	57.17	25.05	23.64	11.25	616.69	28.77
28.02	61.09	22.07	11.99	48.63	899.82	17.16
10	27.4	33.19	20.62	13.03	677.86	18.17
11.59	30.11	13.39	24.11	51.82	690.56	28.39
15.3	32.98	16.66	12.08	37.69	772.16	3.47
13.9	68.38	30.39	13.13	24.91	836.50	7.11
29.38	55.06	31.19	12.05	18.4	693.36	21.52
3.22	17.11	22.36	20.04	52.52	849.72	0.65
27.07	23.21	16.54	13.69	6.21	620.15	15.31
12	69.49	22.51	18.25	18.55	1167.88	6.88
17.33	48.7	29.74	22.34	26.88	590.00	1.28
11.56	49.42	8.96	12.3	25.46	1068.55	28.23
9.09	69.37	33.51	15.62	32.38	775.58	14.02
5.21	62.43	3.2	23.31	28.9	686.45	8.64
23.62	14.17	13.44	14.58	17.82	1020.30	17.45
26.46	65.63	22.97	12.92	44.46	532.05	8.95
7.09	12.07	6.7	19.19	8.11	721.46	20.69

Table 12 Key parameters for 150 slide models, (continued)

21.31	25.81	9.97	20.32	42.7	627.50	26.38
23.97	11.72	18.41	12.09	37.7	1008.12	23.65
11.1	27.91	19.05	16.34	36.57	685.58	6.67
26.19	18.69	24.26	17.89	48.79	1056.79	10.01
17.98	34.8	22.33	19.87	35.08	859.46	17.76
22.65	44.28	17.99	13.99	20.41	865.24	20.06
11.63	50.76	21.79	15.84	32.43	1063.84	21.26
24.19	58.1	12.09	15.44	34.68	685.24	8.49
17.52	40.53	34.19	13.98	29.41	666.44	8.57
14.04	38.65	13	16.7	49.02	759.73	19.95
25.37	44.19	24.99	21.56	44.51	858.33	8.76
19.52	34.83	10.08	16.32	25.67	774.98	9.89
20.24	24.36	38.93	22.95	45.97	1000.55	8.78
7.81	61.28	21.47	15.38	45.1	630.93	12.39
10.38	31.04	30.57	15.81	31.93	951.14	0.51
10.75	62.64	17.45	16.05	26.44	945.45	21.23
18.19	40.01	10.82	13.37	16.28	803.86	13.56
19.51	41.34	15.91	12.17	23.3	811.89	26.32
20.38	36.3	24.38	15.3	34.14	809.69	12.24
22.92	34.09	17.92	15.67	38.9	906.70	20.01
23.27	30.73	17.67	18.01	12.53	966.38	16.73
16.51	50.58	11.63	15.02	27.53	968.65	21.03
21.12	16.92	28.32	16.47	33.45	934.46	24.54
19.42	54.73	23.82	15.86	23.15	940.93	19.58
11.24	36.62	28.15	17.32	39.92	700.84	5.14
23.58	42.66	11.99	14.45	33.47	815.41	21.26
21.35	29.89	31.33	15.03	18.67	941.14	14.75
20.59	24.67	19.9	13.92	29.82	1200.97	26.65
22.14	36.76	20.2	17.43	18.62	581.27	3.58
18.14	14.75	8.08	13.96	10.44	1033.69	9.24
19.46	40.81	15.6	12.52	11.87	1021.68	28.48
18.01	14.21	7.74	12.47	29.22	910.57	10.12
21.17	40.18	38.35	21.21	54.21	570.82	4.61
20.81	28.2	2.6	19.6	55.13	622.98	14.08
28.83	23.5	25.59	24.36	59.84	679.93	13.86
11.53	44	11.69	16.68	13.71	566.81	29.47
9.3	27.47	39.38	15.03	26.34	706.69	12.69
11.44	34.68	19.69	17.51	29.76	552.33	29.03
18.91	30.34	40.71	15.49	24.98	676.82	12.09
28.99	32.75	19.75	20.25	46.74	1127.23	28.23

Table 13 Key parameters for 150 slide models, (continued)

14.24	48.7	32.08	16.6	49.55	754.88	19.21
8.14	34.14	38.83	16.44	11.23	526.81	15.78
10.18	47.04	20.05	11.63	6.82	644.59	8.96
10.6	42.24	37.62	19.78	21.44	853.26	11.16
25.87	60.42	13.9	18.58	30.36	642.85	12.94
9.39	41.55	18.8	13.63	18.11	896.33	25.53
11.31	49.24	30.11	15.9	14.46	956.23	26.31
11.45	20.74	6.19	14.5	25.33	1152.69	23.36
13.09	49.11	37.48	22.86	37.04	999.47	15.57
23.77	47.17	32.37	21.23	29.1	856.48	14.75
20.86	50.53	30.11	14.52	43.74	779.83	8.32
17.71	40.02	16.21	12.52	27.23	996.98	24.24
10.75	13.52	7.97	15.79	7.16	1078.99	18.47

Table 14 Key parameters for 150 slide models, (continued)

FS	x	y	R
1.611	28.007	38.892	21.622
0.577	28.911	41.648	22.218
1.294	52.447	71.896	46.303
0.582	22.338	40.022	30.144
1.233	11.052	33.441	22.949
0.619	25.048	29.977	15.185
1.9	51.248	52.928	40.705
0.781	25.524	67.836	57.727
0.54	23.197	36.358	31.822
1.606	32.863	39.663	22.882
2.794	44.955	71.913	67.368
1.574	18.954	27.432	22.328
0.873	2.424	53.608	43.245
0.714	52.668	72.932	72.513
0.905	18.607	54.911	44.9
1.728	26.927	35.364	21.87
0.77	20.173	25.003	15.033
1	11.954	30.495	21.285
1.262	21.098	51.344	41.249
3.074	33.471	37.21	36.345
0.663	12.437	36.679	27.026
1.01	67.126	113.382	111.231

Table 15 FS, x, y, R for global minimum slip surface

1.268	11.612	30.246	20.734
0.764	15.245	19.558	9.923
2.618	29.613	62.053	53.921
0.611	27.084	29.438	16.159
2.062	15.748	27.722	17.809
1.685	22.157	54.344	44.116
2.838	94.601	135.414	132.222
1.248	14.332	27.67	17.981
2.519	28.066	53.894	44.009
2.468	28.98	74.795	65.11
0.794	11.579	30.141	21.139
0.9	20.519	59.507	49.256
1.188	28.249	48.653	39.978
2.87	20.348	39.83	29.802
0.731	23.038	59.726	49.53
2.07	18.089	58.299	48.029
1.239	21.657	41.769	33.91
2.066	19.161	29.719	19.769
0.581	10.911	93.23	83.155
0.622	13.642	57.085	46.886
0.686	10.696	48.293	38.088
2.135	36.275	93.979	85.36
2.359	19.231	55.414	45.375
1.918	14.779	25.01	15.324
3.186	56.615	96.749	95.287
0.889	12.071	53.14	43.469
1.571	28.067	77.111	66.982
2.41	29.798	36.123	35.936
2.072	15.968	32.463	22.374
1.091	52.257	89.875	87.14
0.723	6.588	37.108	27.118
0.978	17.196	54.355	44.279
1.26	11.637	77.504	67.228
2.25	20.676	38.271	28.013
1.337	18.328	45.677	35.587
0.578	13.639	88.317	78.15
2.372	47.747	103.627	97.778
1.196	17.657	33.257	23.233
1.575	43.393	66.933	62.771
0.925	13.929	61.902	51.607

Table 16 FS, x, y, R for global minimum slip surface, (continued)

3.138	62.323	158.777	154.513
3.188	55.585	92.178	78.581
0.726	21.6	22.158	16.18
0.98	18.991	26.908	17.398
0.903	28.304	61.522	55.834
1.23	12.238	63.289	53.518
1.69	55.217	88.361	87.772
2.113	25.346	23.62	16.918
1.274	12.747	61.415	51.659
1.024	17.72	49.831	39.48
2.593	17.099	17.252	7.301
1.464	46.808	77.981	70.63
0.66	11.706	37.978	28.512
1.034	87.687	144.894	138.296
1.211	20.095	27.874	23.384
2.605	62.601	88.614	73.381
0.571	14.917	47.534	23.55
0.856	11.537	43.548	32.109
0.787	12.573	24.213	15.212
1.096	10.842	60.194	49.71
2.157	20.879	31.595	21.767
1.955	25.441	29.823	21.309
1.153	30.115	36.652	22.66
0.924	11.827	35.385	26.055
1.071	10.588	42.99	33.208
1.548	24.387	22.481	13.236
1.01	36.109	99.977	92.857
0.619	11.875	35.224	25.952
0.964	10.088	42.644	32.921
1.338	20.104	25.01	15.09
1.852	14.42	20.174	10.748
0.698	18.549	21.204	16.685
1.406	58.33	109.674	107.367
0.997	6.83	49.637	39.083
1.182	39.197	48.126	47.51
2.409	15.1	76.248	66.294
2.748	73.996	142.219	139.518
1.465	28.394	34.855	25.964
2.193	43.066	98.512	91.934
1.483	26.336	60.798	51.287

Table 17 FS, x, y, R for global minimum slip surface, (continued)

0.947	21.052	66.288	56.072
1.695	18.186	24.983	14.984
0.634	11.051	47.881	37.901
1.647	17.636	53.72	42.966
1.529	26.319	48.003	41.498
1.141	11.789	65.358	55.309
0.728	21.997	58.42	48.392
2.645	28.9	76.635	66.358
2.111	18.954	27.432	22.328
1.191	27.084	29.438	16.159
1.217	15.078	21.691	12.036
0.636	23.621	51.415	41.762
1.187	28.046	61.385	53.565
1.409	23.038	59.726	49.53
1.342	27.19	71.331	62.781
0.929	28.067	77.111	66.982
0.871	22.998	50.037	41.617
2.925	49.519	95.352	93.337
1.043	13.175	35.79	26.178
1.561	21.618	35.445	25.747
0.918	23.822	65.821	56.238
1.312	13.639	88.317	78.15
1.667	41.298	75.31	69.326
0.867	13.929	61.902	51.607
0.724	60.998	70.525	58.27
0.841	15.938	44.52	34.445
1.252	62.601	57.907	51.17
1.912	17.72	49.831	39.48
0.856	37.16	42.528	40.278
2.057	31.981	106.475	97.993
0.838	17.857	28.149	17.995
2.911	27.827	39.033	32.362
1.868	21.378	31.533	21.728
2.425	24.738	66.571	56.841
1.406	25.83	60.629	51.273
2.318	17.691	29.603	19.507
2.273	18.423	24.705	14.705
0.758	21.827	33.935	23.705
1.969	23.2	35.19	26.644
0.62	8.276	58.2	47.624

Table 18 FS, x, y, R for global minimum slip surface, (continued)

1.591	18.343	25.07	15.048
1.356	15.21	25.517	15.693
0.981	35.832	50.619	50.609
1.919	13.848	29.86	20.237
1.301	11.098	44.8	35.176
1.33	12.488	50.241	40.562
1.217	27.77	57.26	49.925
0.776	46.213	60.678	56.412

Table 19 FS, x, y, R for global minimum slip surface, (continued)

In summary, in these 150 Slide models the following observation can be made:

- The highest values for each key parameter are 29.81m (slope height), 69.49° (slope angle), 40.71° (angle of internal friction), 24.50kN/m³ (unit weight), 59.84kPa (cohesion), 1385.13kPa (Pmax) and 29.47m (x).
- The lowest values for each key parameter are 3.22m (slope height), 10.03° (slope angle), 0.20° (angle of internal friction), 11.63kN/m³ (unit weight), 0.43kPa (cohesion), 468.65kPa (Pmax) and 0.33m (x).
- The highest value for FS was 3.188, located at (x, y, R) of (94.601m, 158.777m, and 154.513m).
- The lowest value for FS was 0.540, located at (x, y, R) of (2.424m, 17.252m, and 7.301m).
- The average values for each key parameter are 18.00m (slope height), 38.53° (slope angle), 21.40° (angle of internal friction), 17.24kN/m³ (unit weight), 31.67kPa (cohesion), 855.83kPa (Pmax) and 15.19m (x).
- The average values for FS, x, y, R were 1.438, 25.910m, 53.764m and 44.762m, respectively.

Out of the 150 Slide models 35% have failed, and 65% were safe. In civil engineering, these statistic data are reasonable and applicable. Therefore, they can be used to simulate practical engineering situation and considered to be representative.

3.7 The Effect of Having No Crane on the Slope

To investigate the effect of no crane on the slope, 26 independent Slide slope stability models were built (16 safe and 10 failing) following *Figure 40* and *Figure 41*. First, the FS with the load applied will be obtained by the Slide software. Then, the FS of removing the load due to the crawler crane will be obtained as well.

1	Slope height	slope angle	φ	γ	c	Pmax	x	FS (with the load)	FS (without the load)
2	29.07	25.38	25.41	20.98	30.44	1186.08	1.12	1.294	1.706
3	23.33	41.91	3.47	19.43	45.45	693.78	2.82	0.582	0.755
4	7.81	61.28	21.57	17.38	35.1	1030.93	12.39	1.574	1.928
5	28	58.99	39.9	14.7	15.05	892.61	3.24	0.873	1.101
6	18.66	28.47	38.33	18.5	46.62	1095.78	14.69	2.618	3.068
7	10.38	31.04	20.57	11.81	11.93	1051.14	0.51	0.611	1.64
8	23.74	49.65	11.19	22.87	52.41	561.09	19.68	0.9	0.908
9	19.62	30.77	9.42	14.96	51.59	684.67	7.36	1.188	1.664
10	25.97	43.2	19.69	15.33	17.72	874.69	22.53	0.889	0.889
11	23.27	30.73	27.67	12.01	22.53	976.38	16.73	1.571	1.851
12	28.36	44.85	15.79	21.46	45.94	568.29	24.67	0.978	0.978
13	28.57	42.87	30.13	21.12	32.97	922.27	12.94	1.26	1.31
14	20.59	24.67	9.9	12.92	59.82	1239.97	26.65	1.575	2.179

Figure 40 26 independent slide models

15	22.14	36.76	21.2	19.43	19.62	481.27	3.58	0.925	1.079
16	19.29	16.91	15.91	18.33	27.73	1144.12	11.73	1.464	1.894
17	15.8	62.85	13.96	23.38	51.68	1130.32	6.67	0.66	1.058
18	11.42	57.17	25.05	23.64	11.25	616.69	28.77	0.787	0.787
19	28.02	61.09	22.07	11.99	48.63	899.82	17.16	1.096	1.319
20	17.33	48.7	29.74	22.34	26.88	590.00	1.28	0.964	1.272
21	11.56	49.42	8.96	12.3	25.46	1068.55	28.23	1.338	1.338
22	16.18	53.77	28.6	16.65	13.85	778.44	28.38	1	1
23	21.28	40.23	20.51	17.04	53.21	927.97	8.98	1.262	1.723
24	4.69	11.06	18.4	22.85	34.5	803.02	15.54	3.074	4.915
25	4.99	15.94	10.61	13.2	10.03	1286.38	19.52	2.113	2.113
26	27.79	41	23.03	24.5	50.3	723.32	22.95	1.274	1.274
27	21.17	40.18	18.35	23.21	44.21	590.82	4.61	1.024	1.24
28	16 safe + 10 fail = 26 (with the load)								

Figure 41 26 independent slide models, (continued)

To compare the difference, the following chart *Figure 42* was created. The horizontal axis is 26 samples, and the vertical axis is the FS values. The difference can be clearly displayed by the markers.

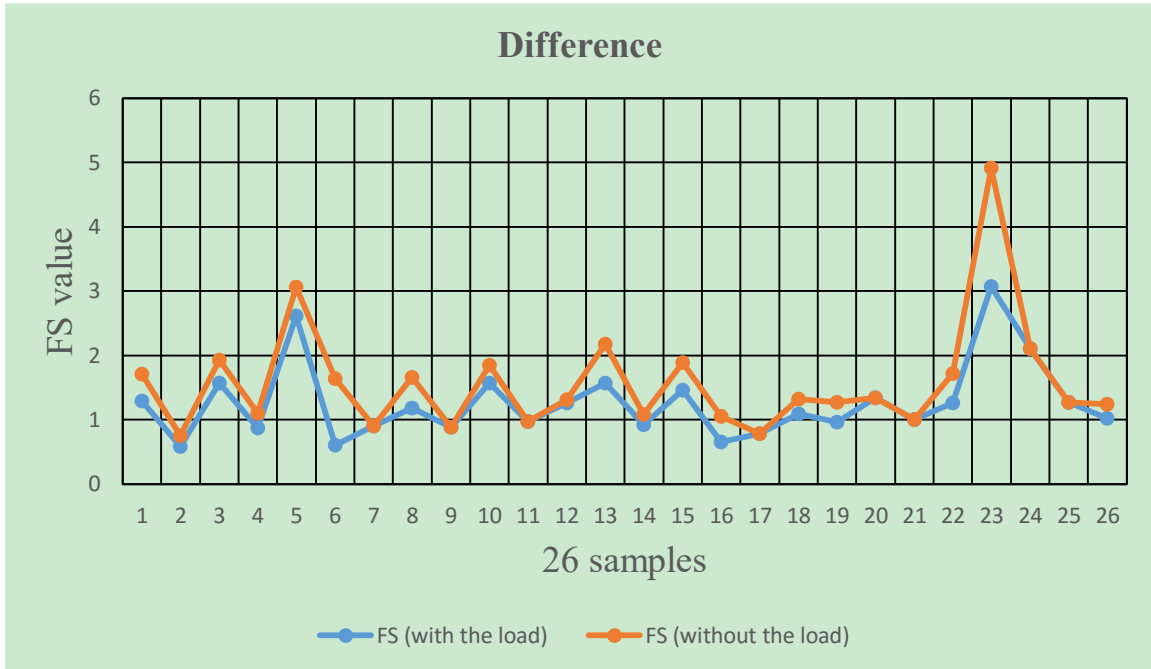


Figure 42 Table Difference between FS (with the load) and FS (without the load)

The chart shows that after removing the crawler crane load, the FS will increase or at least equal to the value with the load applied. The percent about how much the FS increases is also studied by using the following equation (3-17):

$$Difference (\%) = \frac{|FS_{with\ the\ load} - FS_{without\ the\ load}|}{FS_{with\ the\ load}} * 100\% \quad (3-17)$$

The results are summarized in *Table 20*. For mathematical statistics, the average difference is 25.8%, while the maximum difference is 168.4% and the minimum difference is 0.

FS (with the load)	FS (without the load)	Difference
1.294	1.706	0.318392581
0.582	0.755	0.297250859
1.574	1.928	0.224904701
0.873	1.101	0.261168385
2.618	3.068	0.171886937
0.611	1.64	1.684124386
0.9	0.908	0.008888889
1.188	1.664	0.400673401
0.889	0.889	0
1.571	1.851	0.178230426
0.978	0.978	0
1.26	1.31	0.03968254
1.575	2.179	0.383492063
0.925	1.079	0.166486486
1.464	1.894	0.293715847
0.66	1.058	0.603030303
0.787	0.787	0
1.096	1.319	0.203467153
0.964	1.272	0.319502075
1.338	1.338	0
1	1	0
1.262	1.723	0.365293185
3.074	4.915	0.598893949
2.113	2.113	0
1.274	1.274	0
1.024	1.24	0.2109375

Table 20 Difference statistics

Chapter 4 – Development, Training and Verification of the Artificial Neural Network

4.1 Training a Neural Network

After the credible ranges of key parameters were established, the Monte Carlo sampling was used to generate a set of Slide models. With all models built and analyzed, the resulting training dataset was ready to be used to develop the ANN in MATLAB.

4.2 Brief Introduction to ANN using MATLAB

MATLAB can be used in conjunction with a toolbox to develop an ANN using the results derived from the slope stability analyses. In MATLAB, the Neural Network Toolbox was used as a tool to create and aid the neural network to train the dataset. The Toolbox (*Figure 43*) has four primary applications, including input-output and curve fitting, pattern recognition and classification, clustering and dynamic time series. However, the only used applications were its input-output and curve fitting capabilities.

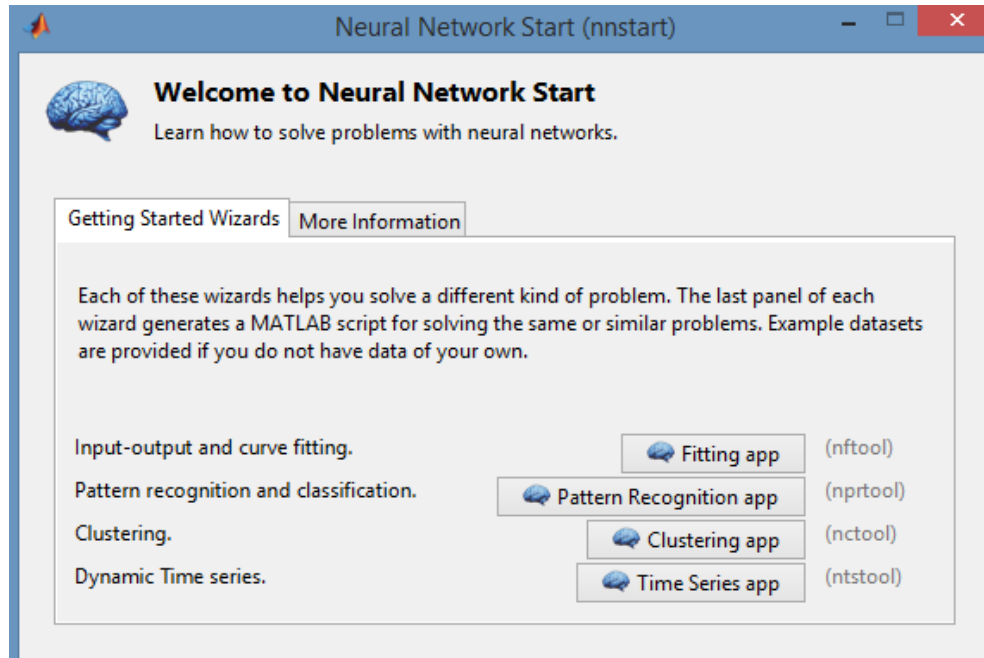


Figure 43 MATLAB - neural network toolbox

This toolbox can plot the *error histogram* and *regression curves* in order that users can estimate if the network has been trained with a good performance. If the performance is not adequate, the user can take action to improve it until the error (the difference between the target data and the output data) is minimum or the training performance satisfies the requirements.

The complete structure of the neural network is illustrated in *Figure 44*. In the setting of this example, the number 7 indicates how many items are contained in the input function. These items represents key parameters inputted in the Slide software, including the slope height, the slope angle, soil unit weight, angle of friction, cohesion, load distribution and so on. The number 10 indicates the number of the neurons in the hidden layer. The default of the hidden neurons is 10. If the performance of the network is poor, MATLAB recommends that user take measures to increase the neuron number. Ultimately, number 4 in the output indicates the number of the output results, which is FS in slope stability analysis.

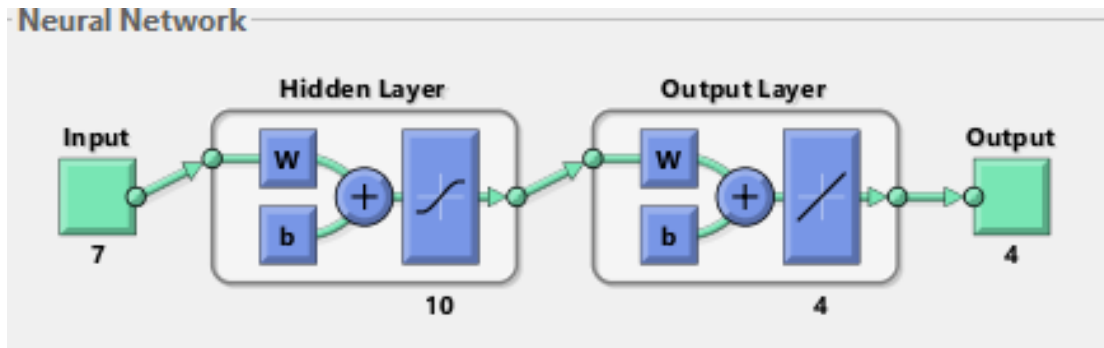


Figure 44 Neural network structure in MATLAB

MATLAB has provided users with three algorithms (Figure 39), which are Levenberg-Marquardt algorithm, Bayesian Regularization algorithm, and the Scaled Conjugate Gradient algorithm. Levenberg-Marquardt algorithm is recommended for most problems. However for some small dataset, Bayesian Regularization algorithm can take longer but obtains a better solution. For large problems, the Scaled Conjugate Gradient algorithm is recommend since it uses gradient calculations which take less memory and more efficient than the Jacobian calculation the other two algorithms use.

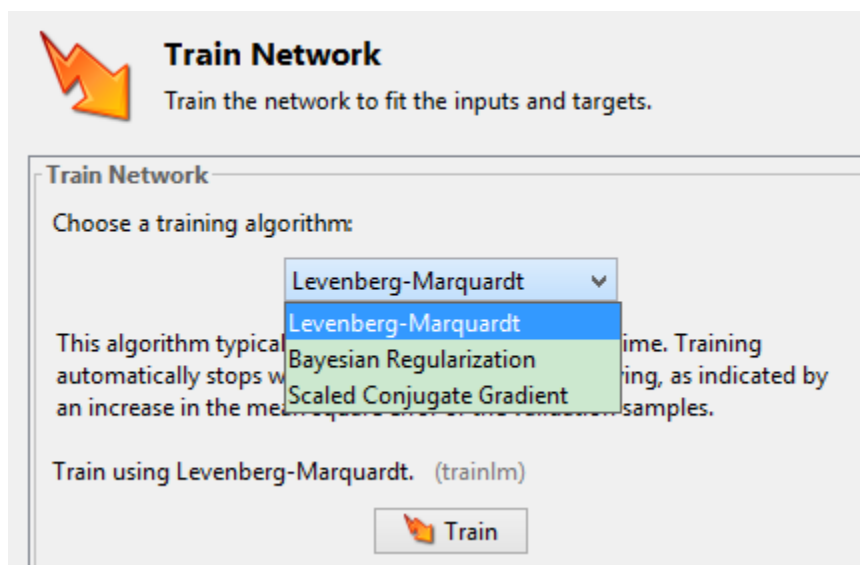


Figure 45 Selection on the training algorithm in MATLAB

The regression (*Figure 46*) and error histogram are the criteria to estimate whether the curve fitting is good and neural network has been trained successfully. All the data samples have been divided randomly into 70% for training, 15% for validation, and 15% for testing. In regression diagram, the R-values measure the correlation between outputs and targets. An R-value of 1 means a close relationship, and 0 means a random relationship. More points should fall down along the 45-degree inclined line, where the network output is equal to the targets. For this example, it shows that the fit is reasonably good, since the R-values in each case are 0.90 or above.

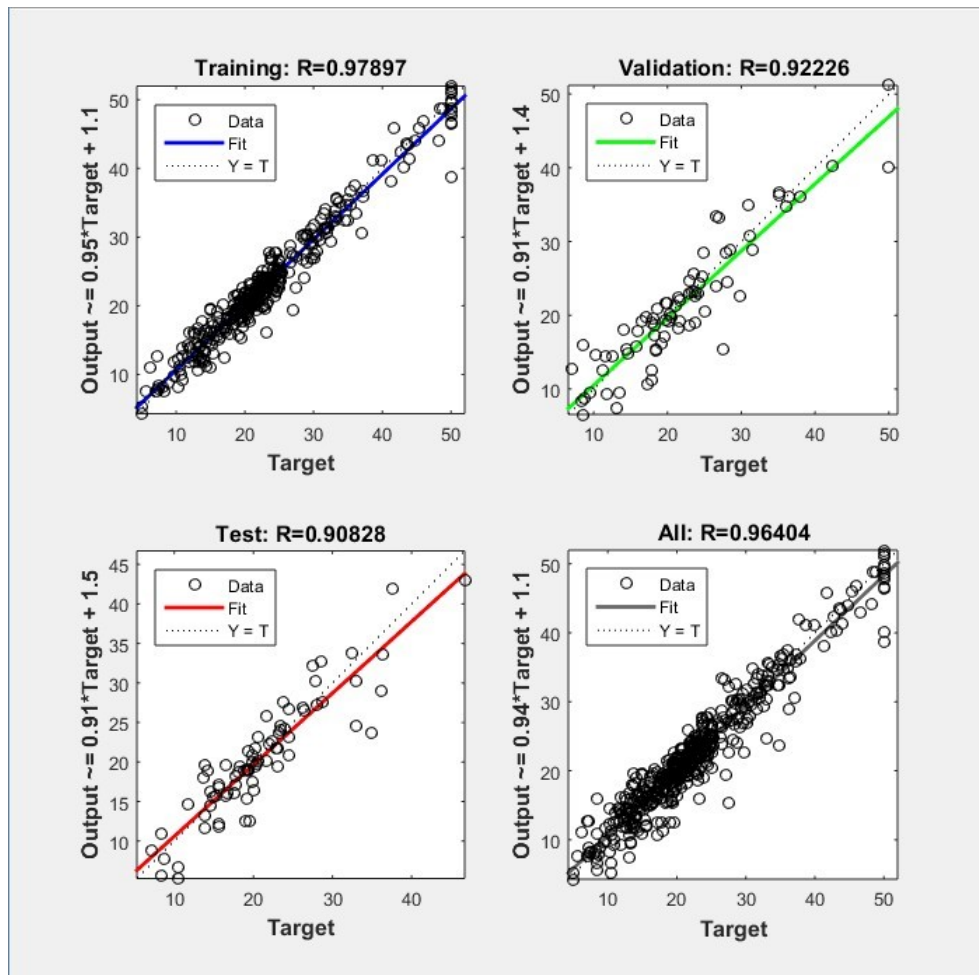


Figure 46 Regression

Similarly, the error histogram (*Figure 47*) shows the distribution of the errors caused by all the data samples. Three different colors are used to distinguish the training data samples, the

validation data samples and the test data samples. The tendency of the data sample converges toward the Zero Error line, and it demonstrates that the output results approximate the target data.

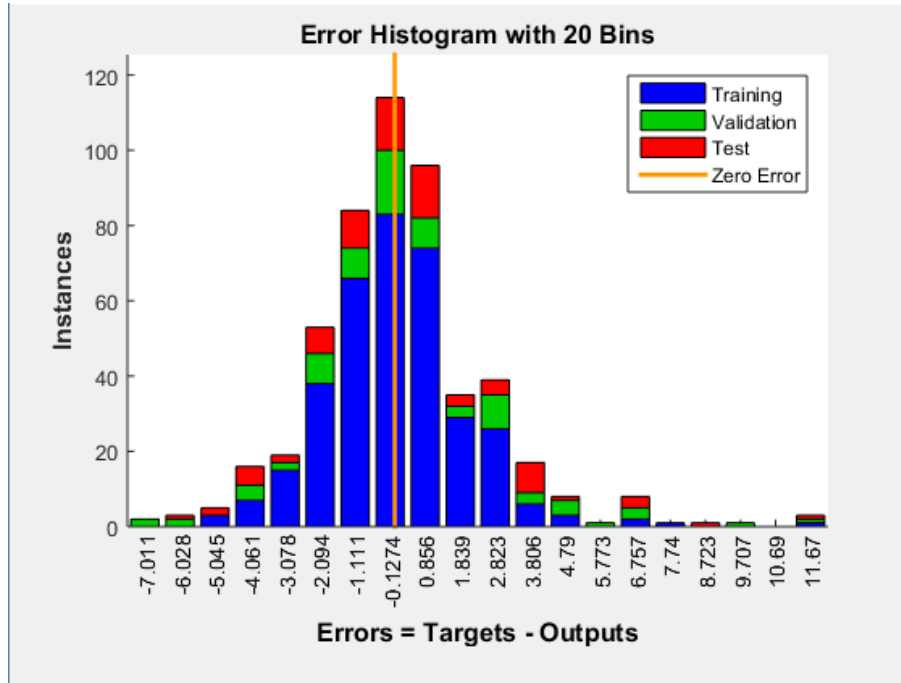


Figure 47 Error histogram in MATLAB

4.2 Data filtering

A quite necessary step before training a neural network is to remove inferior or non-physical data samples from the dataset. After establishing 150 models, the dataset must include as few as possible exceptional FS, which are too large or too small, because they were generated by the Monte Carlo sampling of the key input parameters. For the ANN training, data sample selection is the key factor to affect training performance. In these 150 models, 4 data samples were deemed to be too large, with FS of 5.323, 5.053, 6.297, and 5.638. For example the 31st data sample, as an example and its Slide model is illustrated in *Figure 48*. As evident from the figure, the computed critical failure surface is almost coincident with the slope face. It was deemed to be an outlier in the dataset.

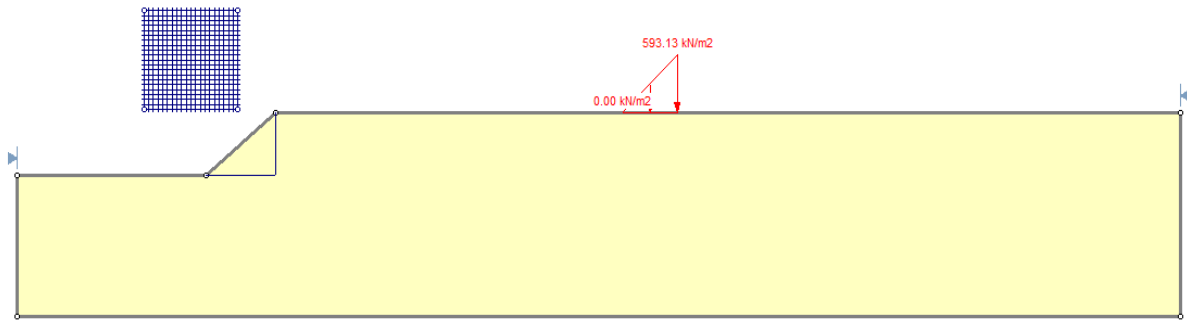


Figure 48 An example data sample that resulted in an inappropriate failure surface

This Slide model was generated with slope height of 5.13 m, slope horizontal length of 5.09 m, soil unit weight of 17.88 kN/m^3 , cohesion of 44.66 kPa, and friction angle 30.22 degrees, respectively. The slope height approximates minimum value of the credible range, and the soil properties reach the maximum. It is almost non-realistic for practical engineering situations, since it is quite stable that civil engineers will not be concerned by the failure of this slope setup.

Similarly, another example is 83th data sample, as shown in Figure 49.

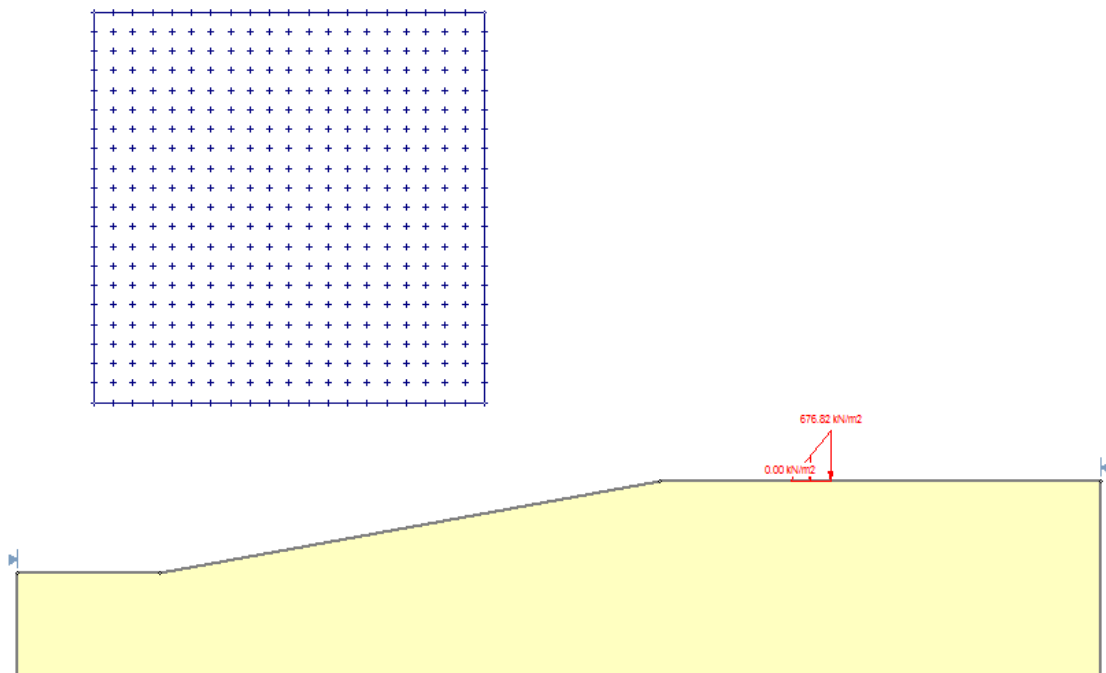


Figure 49 An example data sample that resulted in an inappropriate failure surface

The problem in this slope is slope angle 10.34 degrees (the valid slope angle credible range minimum value was 10 degrees). The slope is too gentle and flat that will never have a slide failure, and therefore it will not be considered in the practical dataset.

Similarly, two data samples resulted in a FS that are too small (0.227 and 0.125). For example, 55th data sample as an instance; its soil properties (unit weight 12.88 kN/m³, cohesion 10.23 kPa, and friction angle 9.76 degrees) demonstrate that it is the worst friable soil. Comprehensively, civil engineers will take measures to replace the worse soil with more high-strength soil without a doubt. It is explicit and simple for civil engineers' assignment, but it will obstruct MATLAB to obtain good training performance for the ANN.

Thus, these six outlier samples were replaced by six newly-generated samples. The quality of these new samples was checked. The following pictures show how the training performance improves after replacement.

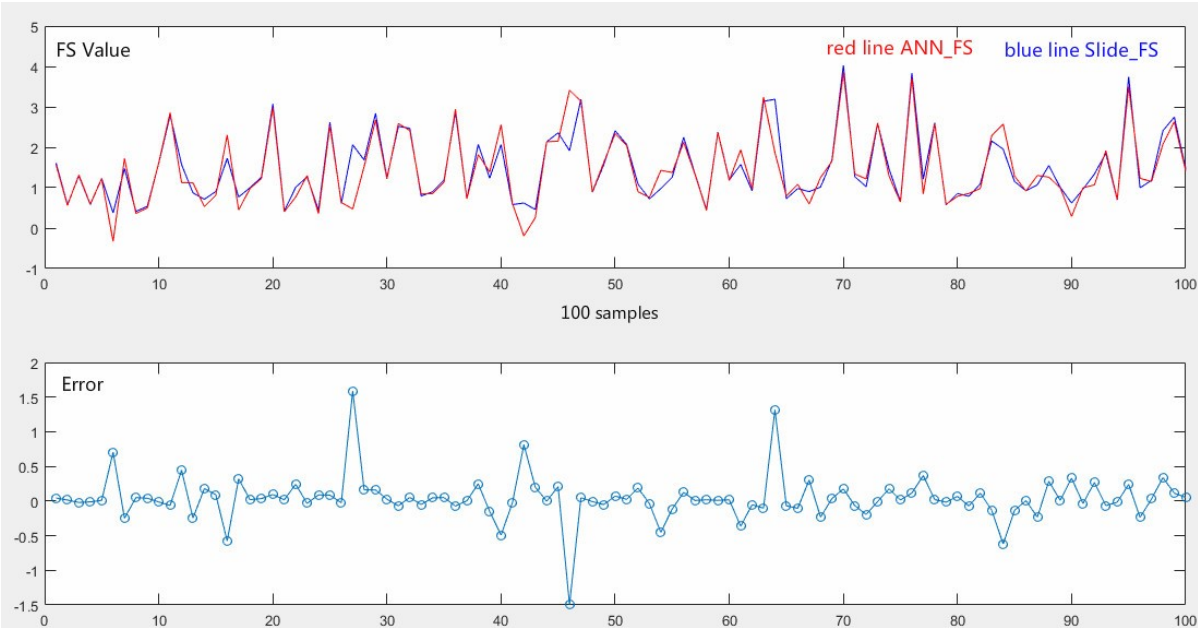


Figure 50 ANN predicting capabilities before replacement of outlier sample datasets

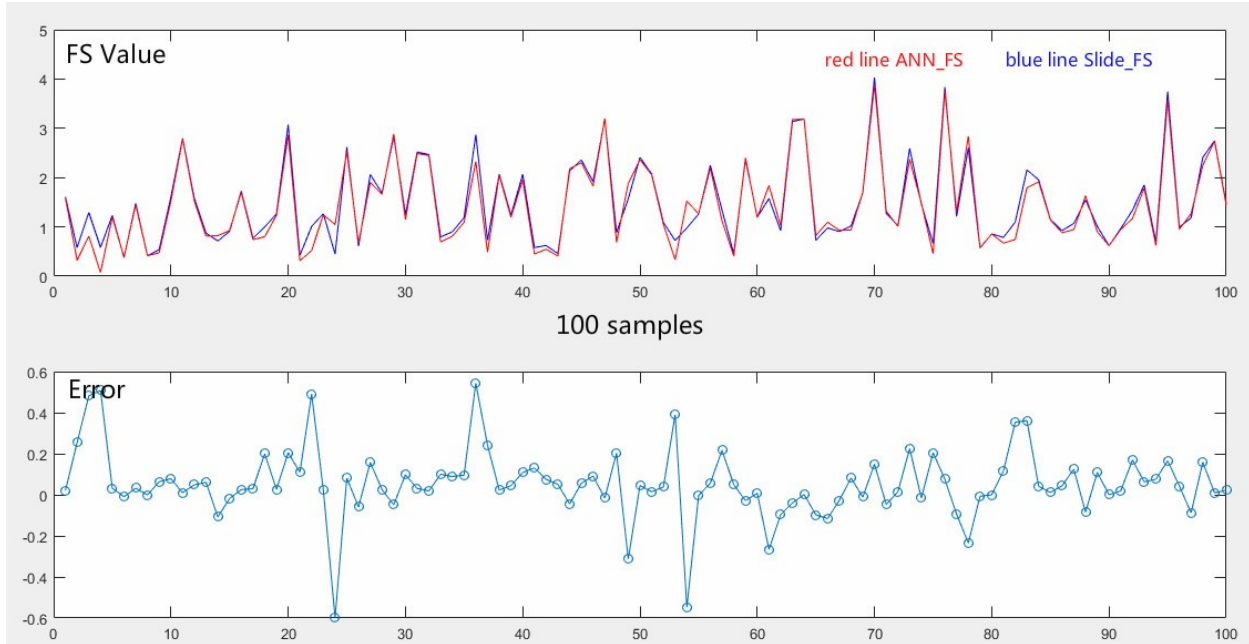


Figure 51 ANN predicting capabilities after replacement of outlier sample datasets

In *Figures 50 and 51*, the top diagram illustrates horizontal axis representing the 100 samples, and vertical axis represents the FS value. Blue color represents Slide calculation (output data), and red color represents MATLAB ANN prediction (output data from ANN). The bottom diagram illustrates horizontal axis represents 150 samples and vertical axis represents the difference or error between the Slide calculated output data and the ANN predicted output data.

From the comparison, the MATLAB prediction does not fit the Slide calculation polygonal line before replacement. The error (minimum and maximum) can be in the range of [-1.5, 1.5] before replacement, but the error was improved to be in the range of [-0.6, 0.5] after replacement. A considerable improvement.

4.3 MATLAB Script for the ANN

The whole process of ANN development and training can be divided into two main parts. Firstly, a simple $y=x^2$ case was studied to learn how the neural network works and master the MATLAB command usage. Then, by importing the input data and output data from the Slide analyses, a

FeedForwardnet network (newff) can be build. The results show that the error of training data is very small (maximum error 0.2), but new sample used in testing has a large difference with expectation (ANN value 0.3526, expectation 0.856). Therefore, one effective measure can be carried out to resolve with the problem. The improvement was to check if data entry mistakes existed, since training performance extremely depends on accuracy and selection of data samples. It was found that the originally entered data had two evident entry mistakes. After correcting, the training error was reduced after correction (ANN value 1.2434, expectation 0.856).

The details of the MATLAB script used in building the neural network and its corresponding interpretation are stated as follows:

```
inputdata=inputdata';%convert a 150*7 matrix (7 samples of 150 elements) to a
7*150 matrix (150 samples of 7 elements)

outputdata=outputdata';%convert a 150*1 matrix (1 sample of 150 elements) to
a 1*150 matrix (150 samples of 1 element)

figure(1);

subplot(2,1,1)

plot(outputdata,'b');%draw the top diagram, blue color

hold on;

net=newff(inputdata,outputdata,[20,20],{'tansig','purelin'},'trainlm');%build
ANN

net.trainparam.epochs=50;

net.trainparam.goal=0.001;

net=train(net,inputdata,outputdata);%train (R=0.86347)

net=train(net,inputdata,outputdata);%regression is not good, so retrain
(R=0.96256)

net=train(net,inputdata,outputdata);%regression is good, so stop training
(R=0.97193, R value=1 is best)

outputdata_net=sim(net,inputdata);%outputdata_net: ANN FS calculation

error=outputdata-outputdata_net;%calculate the differences between Slide
output FS and ANN output FS (150 samples)
```

```

plot(outputdata_net,'r');%draw the top diagram, red color

subplot(2,1,2)

plot(error,'o-');%draw the bottom diagram

X = [20.81,28.2,2.6,19.6,55.13,622.98,14.08]';%new test sample

Y = sim(net,X)

```

Firstly, *xlsread* function was used to import *inputdata* (model key parameters) and *outputdata* (Slide analysis results, FS, x, y, and R) in Excel format into the workspace and create *inputdata* and *outputdata* variables. Then through analyzing the $y=x^2$ example case, it was discovered that each row represents one element in the training neural network. So these two variables need to be transposed by converting a 150×7 matrix (7 samples of 150 elements) to a 7×150 matrix (150 samples of 7 elements), and similarly by converting a 150×1 matrix (1 sample of 150 elements) to a 1×150 matrix (150 samples of 1 element). In this script, the *newff* network was adopted. One validation method is to compare *outputdata* with *outputdata_net* and observe how much two polygonal lines fit as seen in *Figure 52*. Another validation method is to draw the error diagram and observe the error range.

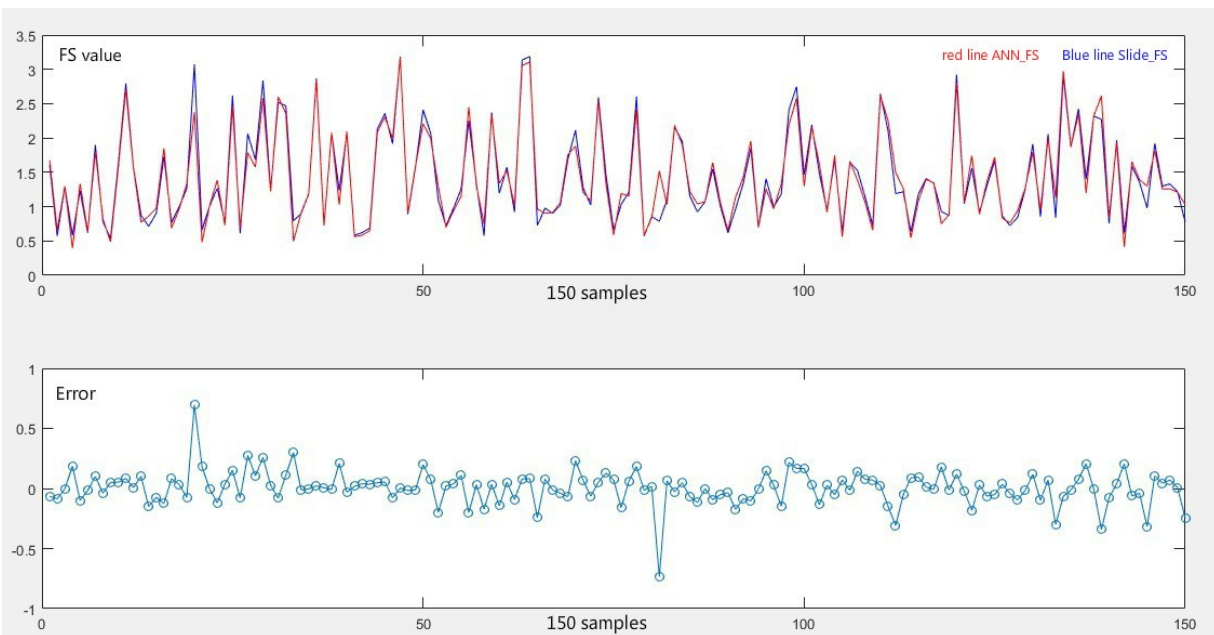


Figure 52 ANN training and error (difference in outputdata and outputdata_net)

4.4 FeedForwardnet Network Introduction

FeedForwardnet network is one prevalent type of BP (backpropagation) neural network, as mentioned above. A summary of its properties and limitations, as a general BP neural network, are as follows (Li, 2013):

- BP neural network can be applied to classification, clustering, prediction and so on. It needs a certain amount of historic data. Through training history data, a neural network can learn the systematic methodology and information.
- BP neural network is actually based on the practice, instead of Bionics. Therefore, the meaning of practicability is more significant than the biological neural network similarity.
- For certain algorithms, no definitive theory can be applied to determine the neuron number in the hidden layers, specific activation function, initial training data selection and so on. The only way is to retrain the neural network again and again.
- Even though BP neural network is effective, it is also well-known for its complicated calculation, low-speed calculation, and local optimization. So, programmers provide a large amount of solutions to reform the BP network, and various new-style neural networks also emerge at the same time.

In the MATLAB script, the FeedForwardnet network command used was:

```
net=newff(inputdata,outputdata,[20,20],{'tansig','purelin'},'trainlm');
```

Where: [20,20] represents two hidden layers, and each layer contained 20 neurons; *tansig* represents input layer function; *purelin* represents output layer function; *trainlm* represents training algorithm. For *trainlm* algorithm, it was a choice of non-linear optimization method between Newton's algorithm and the Gradient Descent algorithm. It owns much higher training velocity than *traingd* algorithm (generally in 6 epochs it can finish the training). And it can avoid the possibility for falling into a local optimum and missing the global one. For *tansig* input layer function, it is actually the Hyperbolic Tangent method from mathematics. In 18th century, the definition was given by $\tanh(x)=\sinh(x)/\cosh(x)$, which can be derived by Euler's formula. Using

tansig as the activation function, convergence capability of neural network is much better than using a Logistic function.

4.5 Training and Testing

As previously stated, the neural network used in this thesis to train was the FeedForwardnet network (*newff*). The following *Figure 53* illustrates ANN structure used:

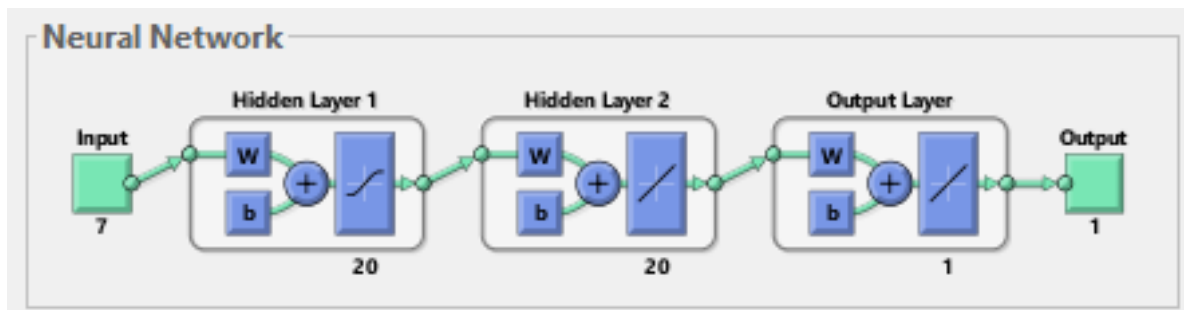


Figure 53 ANN structure

Generally for an ANN there are three ways that can be used to improve training and predictive performance:

- One way is to increase the amount of data samples used. If the number of imported data samples is not sufficient, no good neural network can be obtained. Initially, the number of imported data samples was 100. For improving the training performance, another 50 newly generated data samples were added into training neural network. It was found that the quality and selection of 150 imported data samples was one of the most important ingredients in improving the predicting capability of the ANN. Data samples should be uniformly distributed and reflect the systematic characteristic of neural network. Furthermore, the entry mistakes of imported data samples must be checked to ensure the network precision.
- Another way is to re-train your network until the R-value approximates 1. Observing R-value can be used to evaluate neural network performance at preliminary stage. Regression or R-value measures the correlation between *outputdata* and *outputdata_net*.

- Alternative way is to increase neurons and add hidden layers to the ANN. At first, *newff* function was using 10 hidden layers contains 10 neurons. It performs inadequately and its best performance was $R=0.89$. Then, the *newff* function was changed to 20 hidden layers containing 20 neurons. After several repetition and attempts, the [20,20] case was determined as prime selection that two hidden layers are included, and each layer contains 20 neurons. However the networks with more than 40 neurons and 2 hidden layers are also tested, and they performed worse than the [20, 20] case.

In the training process, the MATLAB system distributed the 150 samples into 15% for validation, 15% for testing, and 70% for training as shown in *Figure 54*. Training samples were presented to the network during training, and the network was adjusted according to its error. Validation samples were used to measure network generalization, and to halt training when generalization stops improving. Test samples have no effect on training and so provide an independent measure of network performance during and after training.

A FeedForwardnet network with sigmoid hidden neurons and linear output neurons, can fit multi-dimensional mapping problems arbitrarily well, given consistent data and enough neurons in its hidden layer. The network was trained with Levenberg-Marquardt backpropagation algorithm (*trainlm*), unless there was not enough memory, in which case scaled Conjugate Gradient backpropagation (*trainscg*) would have been used. In our case the memory was never exhausted.

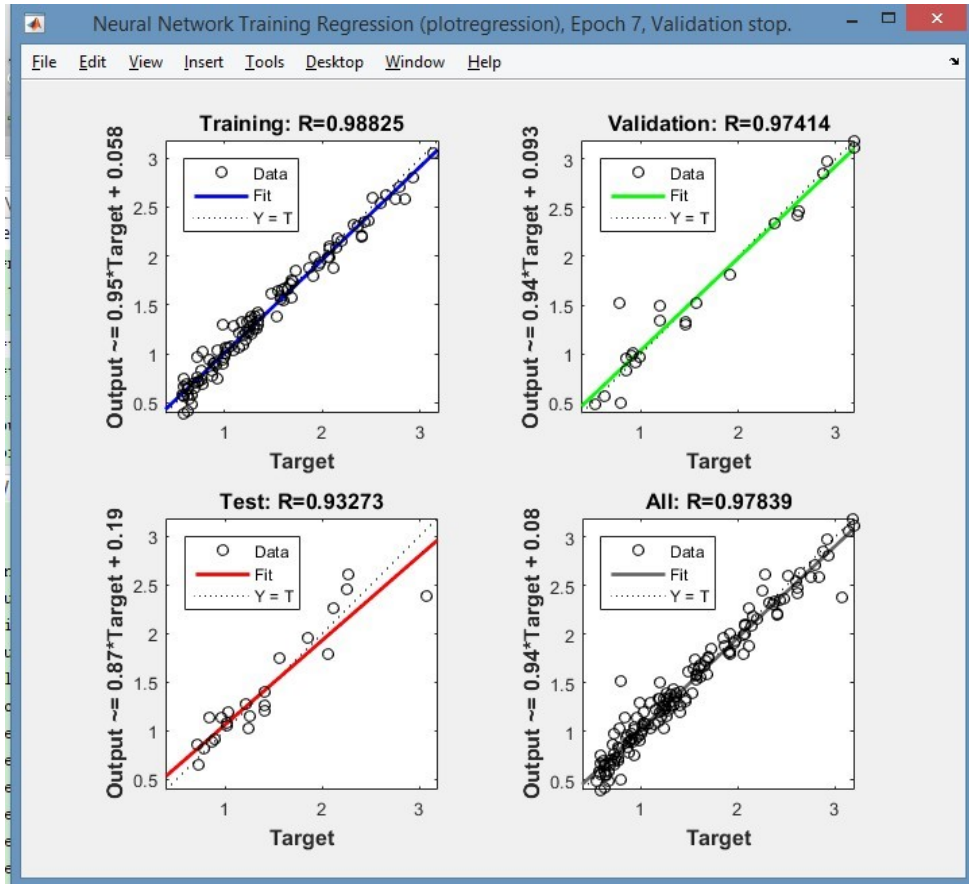


Figure 54 MATLAB ANN regression results

4.6 Interpretation of ANN Predictions Using an Average Error Value

To further qualitatively assess the predicting capabilities of the developed ANN, the following equation was used to estimate error:

$$error (\%) = \frac{|Slide_FS - ANN_FS|}{Slide_FS} * 100\% \quad (4-1)$$

After retraining and improving the neural network several times, the ultimate average error with 20 newly-generated independent test samples (not part of the 150 samples used in ANN development) was 0.67 percent as recorded in *Figure 55*, where the maximum error is 1.7% and the minimum error is 0.06%.

	A	B	C	D	E	F	G	H	I	J	K	L
7	Slope and Soil Properties			Triangular Load								
8	Slope Height H	Slope Angle θ (angle)	Angle of Internal Friction ϕ (angle)	unit weight γ (kN/m ³)	Cohesion c (kPa)	Magnitude (Pmax)	length (3k)	x	Slide Fs	ANN Fs	error	
9	Model 1	16.54	40.52	20.15	12.33	16.88	652.14	4.065	20.53	1.253	1.2322	0.01660016
10	Model 2	20.63	33.26	15.32	16.28	25.66	764.59	4.065	12.59	0.978	0.9655	0.012781186
11	Model 3	10.03	25.26	9.85	15.98	18.88	1035.22	4.065	22.36	1.421	1.4228	0.001266714
12	Model 4	15.23	30.99	26.77	12.16	36.22	862.85	4.065	17.74	2.04	2.0342	0.002843137
13	Model 5	22.59	40.36	30.12	13.22	8.99	1275.36	4.065	24.53	1.15	1.1527	0.002347826
14	Model 6	25.31	46.02	19.06	15.55	23.09	870.09	4.065	10.95	0.788	0.7848	0.004060914
15	Model 7	10.25	36.97	23.69	20.88	11.64	615.93	4.065	18.32	1.242	1.2437	0.00136876
16	Model 8	18.02	38.53	21.4	17.24	31.67	855.83	4.065	15.19	1.29	1.3038	0.010697674
17	Model 9	26.31	50.22	13.59	15.39	28.33	803.95	4.065	11.96	0.661	0.6568	0.006354009
18	Model 10	18.22	33.26	20.03	18.02	13.63	876.08	4.065	14.13	1.034	1.0346	0.000580271
19	Model 11	17.56	37.23	20.94	12.25	23.63	716.34	4.065	19.36	1.401	1.4055	0.003211991
20	Model 12	13.96	29.36	14.28	15.69	13.99	699.78	4.065	17.51	1.029	1.0198	0.008940719
21	Model 13	21.99	37.2	24.05	22.39	52.07	1147.30	4.065	21.08	1.626	1.6118	0.008733087
22	Model 14	8.96	25.53	30.26	21.22	10.33	851.89	4.065	15.89	2.016	2.0055	0.005208333
23	Model 15	20.18	49.17	16.81	18.45	24.71	665.37	4.065	9.56	0.756	0.7675	0.01521164
24	Model 16	24.06	56.83	7.85	14.08	53.85	1151.99	4.065	13.06	0.699	0.7057	0.009585122
25	Model 17	27.04	38.23	27.96	13.46	46.56	877.84	4.065	17.23	1.69	1.7127	0.013431953
26	Model 18	15.26	23.01	25.52	22.32	30.86	874.77	4.065	23.59	2.238	2.2263	0.005227882
27	Model 19	9.04	50.78	11.26	16.45	20.21	633.19	4.065	7.83	0.666	0.6644	0.002402402
28	Model 20	17.16	32.04	22.56	14.72	41.96	1025.45	4.065	23.07	1.889	1.8976	0.004552673
29	Signature: Xin Ai										Average error value	0.006770323

Figure 55 Errors between Slide results and ANN prediction for the 20 independent test cases

The average error indicates that neural network can be competent to accomplish Slide software’s task with a relatively high precision. It also demonstrate this research project was conducted successfully, since it is convenient and beneficial for other users to import key parameters and obtain the FS directly without using a slope stability analysis software.

Chapter 5 – Summary and Conclusions

5.1 General Remarks

The purpose of this thesis research was to assess the stability of homogeneous slopes subjected to loads from crawler cranes and to develop an ANN to be able to predict the critical FS and the location of the associated failure surface. Based on the review of fundamental knowledge of soil mechanics and slope stability, all slope stability analysis models in this thesis were based on Bishop simplified method, with no underground water, without weak or stratified layers.

Artificial neural networks, due to their large amount of neurons interconnected into a vast network, can be used to estimate or approximate functions that can depend on a large number of inputs and are generally unknown. In this thesis, the *backpropagation* neural network was adopted and the training algorithm selected was the Levenberg-Marquardt algorithm. This algorithm typically requires more memory but less time. The use of this method in the ANN training automatically stopped when the generalization stopped improving. Generally speaking, it was effective and suitable for solving the problem formulated in this thesis.

Using the developed and trained ANN, the average error in the predicting capabilities of the ANN with 20 independent test dataset samples was found to be 0.677 percent. It was sufficiently precise and capable of estimating the FS of slopes in the context of the data-limited nature of geomechanics problems. For practical engineering, the maximum error, which was 1.6 percent, in the test sample set can also be accepted and applied as well.

It was found that for training the ANN, the key factor and the basic requirement of the whole process is the *quality* and *amount* of dataset used for training. After meeting the basic requirements, the methods to improve the training performance, such as changing neural network function or type, or changing the training algorithm, and re-training the neural network several times (until R value is close to or equal to 1), can be very effective, as demonstrated.

5.2 Limitation

5.2.1 Limitation of Thesis

- The main limitation of the thesis is slope condition limitation as mentioned in Chapter 1. The type of slopes which can be solved by thesis method should be constructed homogenous slopes without the presence of groundwater or weak layers, the method of analysis was Bishop simplified method.
- The secondary limitation of the thesis is crawler crane load calculation simplification. In this thesis, only two primary loads, hoisting load and crawler crane self-weight, are considered to calculate the magnitude of the load applied on the slope surface. However, in the practical engineering, the stability of the crawler crane will consider more than two loads when the driver is operating. For example, the braking force and wind load will apply horizontal forces on the crawler crane. On the other hand, this research only considers the basic boom length's credible range. It does not take account extended boom and retracted boom situations. Therefore, the simulation for crawler crane operation in the research is a simplification of practical engineering considerations.

5.2.2 Limitation of Applicability of ANN

- One defect of neural networks, particularly in their automated learning mechanisms, is that they need sufficient representative training data originating from real-world operation or analysis. It is typical, because any learning machine requires a large amount of input data to learn the underlying structure of the system, which permits it to generalize its knowledge to new cases. Consequently in this research, prior to creating a neural network, at least 150 slope stability analysis models were generated. It cost one whole month of preparation and analysis work to create this dataset.
- Another evident defect is the ANN's invariance property. For example, the neural network created in this research can only be applied to slopes on the limited condition of homogeneous slopes, Bishop simplified method, no groundwater, no weak layer and no stratified layers. If any new key parameter (such as groundwater) needs to be added, the neural network in this research cannot be competent. It needs to be re-created, re-trained and ultimately re-verified. Considered in practical engineering, the slope condition varies with different location and cannot be as theoretical as thesis assumption without

underground water and weak layer. Conclusively, in applied engineering field, the function of neural network cannot totally replace the traditional slope stability analysis methods or software at the current time

- Ultimate defect of an ANN is entry mistakes from its creator and their effect. Without any doubt, the quality and amount of dataset is the critical factor for training a neural network. A large amount of data of 150 slope stability analysis models needed to be generated and analyzed. Practically, the possibility of making tiny data entry mistakes is so high for researchers that they require extra time to check the correctness of imported data. If the number of imported slide models is greater than 150 models, it may need at least one week to check before training to ensure quality.

References

1. Abdalla, A. J., Attom, M., and Hawileh, R. (2012). Artificial Neural Network Prediction of Factor of Safety of Slope Stability of Soils. *14th International Conference on Computing in Civil and Building Engineering* (p. 7). Moscow, Russia: ISCCBE.
2. Abramson, L. W., Lee, T. S., Sharma, S., and Boyce, G. M. (2002). *Slope Stability and Stabilization Methods*. New York: John Wiley & Sons.
3. Bowles, J. E. (1997). *Foundation Analysis and Design*. The McGraw-Hill Companies, Inc.
4. *Canadian Foundation Engineering Manual 4th edition*. (2006). The Canadian Geotechnical Society.
5. Code for investigation of geotechnical engineering GB50021-2003. (2003).
6. Coduto, D. (2011). *Geotechnical Engineering Principles and Practices*. New Jersey: Pearson Higher Education.
7. Duncan, C. W., and Christopher, W. M. (2005). *Rock Slope Engineering (4th Edition)*. Spon Press.
8. Eberhardt, E. (2003). Rock Slope Stability Analysis - Utilization of Advanced Numerical Techniques. *Earth and Ocean Sciences at UBC*, 41. Retrieved from Wikipedia: http://en.wikipedia.org/wiki/Slope_stability_analysis
9. Engineering and Design - Slope Stability. (2003). *US Army Corps of Engineers*.
10. Farhang, R., and Frédéric, D. (2011). Discrete-element Modeling of Granular Materials. Montpellier: Wiley. Retrieved from Wikipedia: https://en.wikipedia.org/wiki/Discrete_element_method
11. *Foundation & Earth Structures*. (1986). Alexandria: Naval Facilities Engineering Command.

12. Geological Engineering Manual, 4th Edition. (2006). Beijing: China Construction and Industry Press.
13. Geological Investigation Manual for Hydraulic Projects. (1982). Beijing: Hydraulic and Electric Press.
14. Gilat, A. (2004). MATLAB: An Introduction with Applications 2nd Edition.
15. Gurney, K. (1997). *An introduction to Neural Networks*. London.
16. Hammah, R. E., Yacoub, T., Corkum, B., Wibowo, F., & Curran, J. H. (2007). Analysis of Blocky Rock Slopes with Finite Element Shear Strength. Toronto: Rocscience Inc. & Toronto University, 6.
17. Hao, J. L. (2015, 02). *Hydraulic Crawler Crane*. Retrieved from Construction Process.
18. Haycraft, W. R. (October 2011). History of Construction Equipment. *journal of construction engineering and management* © ASCE, 4.
19. Holtz, R., and Kovacs, W. (1981). *Introduction to Geotechnical Engineering*.
20. Kliche, C. A. (1999). *Rock Slope Stability*. Colorado.
21. Kusakabe, O., Kimura, T., and Yamaguchi, H. (Dec. 1981). Bearing Capacity Of Slopes Under Strip Loads On The Top Surface. *Japanese Society of Soil Mechanics and Foundation Engineering*, 12.
22. Lawrence, J. (1994). Introduction to Neural Networks.
23. Lei, H. (2011). Three Dimensional Numerical Manifold Method and Rock Engineering Applications. *Nanyang Technological University*, 52.
24. Lei, L. (2014). *Quantitative analyses and methods of slope stability*. Retrieved from Construction engineering education web:
<http://www.jianshe99.com/lunwen/gongchengjishu/ma2014041714273214235716.shtml>
25. Li, Z. (2013). The Backpropagation Algorithm of Neural Networks. 23.
26. Linderburg, M. R. (n.d.). *civil engineering reference manual for the PE exam, 14 Edition*.

27. Liu, X. T. (2005). Soil Bearing Capacity for crawler crane. 182.
28. LiuH. (2003). Discussion on the Relationship between Standard Penetration Blow Counts and Physical Mechanical Parameters of Foundation Soil.
29. LuH.T. (2005). Soil Mechanics. Nanjing, China: Press of Hohai University.
30. McCaffrey, J. (2012). Neural Network Back-Propagation for Programmers.
31. Mehryar, M., Afshin, R., and Ameet, T. (2012). *Foundations of Machine Learning*. Cambridge, Massachusetts: The MIT Press.
32. Meyerhof. (1956). *Foundation Engineering Handbook*.
33. NAVFAC. (1986). *Design Manual 7.01, Soil Mechanics*. US Government Printing Office.
34. NAVFAC. (1986). *Design Manual 7.02, Foundations and Earth Structures*. US Government Printing Office.
35. Peck. (1974). *Foundation Engineering Handbook*.
36. *Product Introduction (Matlab)*. (2015). Retrieved from Mathworks:
<http://www.mathworks.com/>
37. *Product Introduction (Slide)*. (2015). Retrieved from Rocscience:
<https://www.rocscience.com/>
38. Robertson, P. K. (n.d.). Soil behaviour type from the CPT: an update. 8.
39. Robertson, P. K., and Cabal, K. L. (n.d.). Estimating soil unit weight from CPT. 8.
40. Sathyanarayana, S. (2014). A Gentle Introduction to Backpropagation. 15.
41. Saxe, A. (2012). *The backpropagation algorithm*. Retrieved from Stanford University:
<http://web.stanford.edu/~asaxe/papers/backpropagation.pdf>
42. *SCX500 Hydraulic Crawler Crane Specifications*. (n.d.). Retrieved from Hitachi Sumitomo Heavy Industries Construction Crane Co.,Ltd.: <http://www.hsc-crane.com/e/>

43. Shields, D., Chandler, N., and Garnier, J. (1990). *Bearing Capacity of Foundations in Slopes*. 10.
44. *Soil Cohesion and Soil Friction Angle* . (2014, 10 31). Retrieved from Geotechdata. Info: [:http://www.geotechdata.info/parameter](http://www.geotechdata.info/parameter)
45. Soil Corrolation. (2014). In *Caltrans Geotechnical Manual* (p. 5). California, USA: Department of California Transportation.
46. Teng, W. (2005). *Crawler Crane Stability Calculation*. Retrieved from Baidu Wenku: http://wenku.baidu.com/link?url=oZVZYGy5un4_Lqq2hhcqS_4cE5xMG9B7VZZH1hDzfWaQnWkITec-oWF-VUDWIOQyjNIME9oLB_C3MAFMbF8HpXNAI_lyXvHGD9XcswXkPqS
47. Terzaghi, K., Peck, R.B., and Mesri, G. (1996). *Soil Mechanics in Engineering Practice 3rd Ed.* John Wiley & Sons.
48. Wang, T. L., and Shen, G.L. (2002). Deduction of Error Backpropagation Algorithm and Procedure to carry out. *China Academic Journal Electronic Publishing House*.
49. Zheng, Y. R., and Zhao, S. Y. (2004, 10). Appllication of Strength Reduction FEM in Soil and Rock Slope. *Chinese Journal of Rock Mechanics and Engineering*, 23(19)(3381~3388), 8.
50. Zhu, D.Y., Lee, C.F., and Jiang, H.D. (2003). Generalised framework of limit equilibrium methods for slope stability analysis.
51. ZhuH. (2004). Correlation Analysis of Internal Friction Angle and Standard Penetration Blow Number for Fine-grained Soil. Pearl River, 2.
52. Zsaki, A. M. (n.d.). *SlopeStabilityNotes*. Retrieved from <https://moodle.concordia.ca/moodle/course/view.php?id=69620>

Appendix

Credible Range Relative Documents Collection

N63.5 (blows)	1	2	3	4	5	6	7	8	9	10
Unit weight (clay)	1.60-1.75	1.70-1.80	1.75-1.85	1.80-1.87	1.84-1.89	1.86-1.90	1.88-1.93	1.90-1.95	1.90-2.00	1.95-2.04

Table 1 Unit weights as a function of blows (Geology Manual for Hydraulic Projects, 1982)

N63.5 Blows	Angle of internal friction (degrees)	
	Silty sand	Sand
4	16	20
5	18	22
6	20	24
7	22	26
8	24	28

Table 2 the relationship between the angle of internal friction ϕ and the SPT Penetration N63.5 Blows (Geology Manual for Hydraulic Projects, 1982)

Unit weight, Angle of internal friction for cohesionless soil			
SPT Penetration (blows/foot)	ϕ (sands)	Density of Sand	Unit weight (T/m ³)
<4	<29	very loose	1.1-1.8
4 to 10	29-30	loose	1.4-2.0
10 to 30	30-36	medium	1.7-2.2
30 to 50	36-41	dense	1.7-2.3
>50	>41	very dense	2.0-2.3
Cohesion for cohesive soils			
SPT value (N)	soil compactness	c (kPa)	
0 to 4	Very soft to soft	12.5	
4 to 8	Soft to medium	25	
8 to 16	Medium to stiff	50	
16 to 32	Stiff to very stiff	100	
>32	Vert stiff to hard	200	

Table 3 unit weight, angle of internal friction for cohesionless soil, and cohesion for cohesive soils (Foundation Engineering Handbook, Peck 1974)

Soil Type		Density (g/cm ³)	c (kPa)	φ (degrees)
Sand	Coarse sand	2.05	2	42
		1.95	1	40
		1.9	0	38
	Medium sand	2.05	3	40
		1.95	2	38
		1.9	1	35
	Fine sand	2.05	6	38
		1.95	4	36
		1.9	2	32
	Silty sand	2.05	8	36
		1.95	6	34
		1.9	4	28
Silt		2.1	10	30
		2	7	28
		1.95	5	27
Clay	Silty clay	2	50	22
		1.95	25	21
		1.9	19	20
		1.85	11	19
		1.8	8	18
	Clay	1.9	82	18
		1.85	41	17
		1.75	36	16

Table 4 unit weight, cohesion, and angle of internal friction (Geological Engineering Manual, 4th Edition, Published in 2006)

SPT Penetration, N-value (blows/foot)	φ sands (degrees)
<4	<30
4 to 10	30-35
10 to 30	35-40
30 to 50	40-45
>50	>45

Table 5 angle of internal friction (Meyerhof 1956, Foundation Engineering Handbook)

Soil Type	γ (lb/ft³)
Sand, loose and uniform	90
Sand, dense and uniform	109
Sand, loose and well graded	99
Sand, dense and well graded	116
Glacial clay, soft	76
Glacial clay, stiff	106
USCS Soil Group	c, as compacted (lb/ft²)
GW	0
GP	0
GM	-
GC	-
SW	-
SP	-
SM	1050
SM-SC	1050
SC	1550
ML	1400
ML-CL	1350
CL	1800
OL	-
MH	1500
CH	2150

Table 6 unit weight and cohesion (Civil engineering reference manual for the PE exam, 14 Edition, Michael R. Linderburg)

N, SPT blows	15	17	19	21	25	29	31
c(kPa)	78	82	87	92	98	103	110
Angle of internal friction(degree)	24.3	24.8	25.3	26.4	27	27.3	

Table 7 cohesion and angle of internal friction for clay (Code for investigation of geotechnical engineering GB50021-2003)

Physical Parameters	Sandy loam	Loam	Clay loam
Bulk unit weight(kN/m ³)	15	15	14
Cohesion(kPa)	10	20	30
Angle of internal friction(degree)	35	20	10

Table 8 unit weight, cohesion and angle of internal friction (Canadian Geotechnical Manual, Published by the Canadian Geotechnical Society)

Unit weight		
SPT Penetration (blows/ foot)	γ (lb/ft³) (granular soils)	
0 - 4	70 - 100	
4 to 10	90 - 115	
10 to 30	110 - 130	
30 to 50	110 - 140	
>50	130 - 150	
Angle of internal friction		
SPT Penetration (blows/foot)	ϕ (degrees) (granular soils)	Density of Sand
0	25-30	very loose
4	27-32	loose
10	30-35	medium
30	35-40	dense
50	38-43	very dense
Cohesion		
SPT Penetration (blows/ foot)	Estimated Consistency (cohesive soil)	c (kPa)
0 - 2	Very Soft	0 - 0.25
2 to 4	Soft	0.25 - 0.5
4 to 8	Medium	0.5-1.0
8 to 16	Stiff	1.0-2.0
16 - 32	Very Stiff	2.0-4.0
>32	Hard	>4

Table 9 unit weight, cohesion, and angle of internal friction (Foundation Analysis, Bowels)

Proposed common SBT description	Approximate unit weight (kN/m³)
Sensitive fine-grained	17.5
Clay - organic soil	12.5
Clays: clay to silty clay	17.5
Silt mixtures: clayey silt & silty clay	18
Sand mixtures: silty sand to sandy silt	18-18.5
Sands: clean sands to silty sands	19
Dense sand to gravelly sand	19.5-20
Stiff sand to clayey sand	19
Stiff fine-grained	20.5

Table 10 unit weight (Soil behaviour type from the CPT: an update, P.K. Robertson, Gregg Drilling & Testing Inc., Signal Hill, California, USA)

Unit weight		
Soil Type	γ (lb/ft³)	
Sand; clean, uniform, fine or medium	84 - 136	
Silt; uniform, inorganic	81 - 136	
Silty Sand	88 - 142	
Sand; Well-graded	86 - 148	
Silty Sand and Gravel	90 - 155	
Sandy or Silty Clay	100 - 147	
Silty Clay with Gravel; uniform	115 - 151	
Well-graded Gravel, Sand, Silt and Clay	125 - 156	
Clay	94 - 133	
Colloidal Clay	71 - 128	
Organic Silt	87 - 131	
Organic Clay	81 - 125	
Cohesion		
SPT Penetration (blows/ foot)	Estimated Consistency (fine-grained soil)	c (kPa)
<2	Very Soft	<0.125
2 to 4	Soft	0.125 - 0.25
4 to 8	Medium	0.25 - 0.5
8 to 15	Stiff	0.5-1.0
15 - 30	Very Stiff	1.0 - 4.0
>30	Hard	>2

Table 11 unit weight and cohesion (NAVFAC 7.02)

When $N < 5$	$\phi = 8.5 * \ln N + 5.0$
When $5 \leq N \leq 15$	$\phi = 6.5 * \ln N + 9.5$
When $N > 15$	$\phi = 7.1 * \ln N + 9.6$

N (SPT penetration blow counts)	1	2	3	4	5	6	7	8	9	10
Angle of internal friction (degree)	5	11	14.5	17	20	21	22	23	23.5	24
N (SPT penetration blow counts)	11	12	13	14	15	16	17	18	19	20
Angle of internal friction (degree)	25	25.5	26	26.5	27	29	29.5	30	30.5	31

Table 12 the relationship between SPT penetration N blow counts and angle of internal friction for fine-grained soils (Correlation Analysis of Internal Friction Angle and Standard Penetration Blow Number for Fine-grained Soil, Hai Zhu)

Description	USCS	Soil friction angle [°]		
		min	max	Specific value
Well graded gravel, sandy gravel, with little or no fines	GW	33	40	
Poorly graded gravel, sandy gravel, with little or no fines	GP	32	44	
Sandy gravels - Loose	(GW, GP)			35
Sandy gravels - Dense	(GW, GP)			50
Silty gravels, silty sandy gravels	GM	30	40	
Clayey gravels, clayey sandy gravels	GC	28	35	
Well graded sands, gravelly sands, with little or no fines	SW	33	43	
Well-graded clean sand, gravelly sands - Compacted	SW	-	-	38
Well-graded sand, angular grains - Loose	(SW)			33
Well-graded sand, angular grains - Dense	(SW)			45
Poorly graded sands, gravelly sands, with little or no fines	SP	30	39	
Poorly-graded clean sand - Compacted	SP	-	-	37
Uniform sand, round grains - Loose	(SP)			27
Uniform sand, round grains - Dense	(SP)			34
Sand	SW, SP	37	38	
Loose sand	(SW, SP)	29	30	
Medium sand	(SW, SP)	30	36	
Dense sand	(SW, SP)	36	41	
Silty sands	SM	32	35	
Silty clays, sand-silt mix - Compacted	SM	-	-	34
Silty sand - Loose	SM	27	33	
Silty sand - Dense	SM	30	34	

Clayey sands	SC	30	40	
Clayey sands, sandy-clay mix - compacted	SC			31
Loamy sand, sandy clay Loam	SM, SC	31	34	
Inorganic silts, silty or clayey fine sands, with slight plasticity	ML	27	41	
Inorganic silt - Loose	ML	27	30	
Inorganic silt - Dense	ML	30	35	
Inorganic clays, silty clays, sandy clays of low plasticity	CL	27	35	
Clays of low plasticity - compacted	CL			28
Organic silts and organic silty clays of low plasticity	OL	22	32	
Inorganic silts of high plasticity	MH	23	33	
Clayey silts - compacted	MH			25
Silts and clayey silts - compacted	ML			32
Inorganic clays of high plasticity	CH	17	31	
Clays of high plasticity - compacted	CH			19
Organic clays of high plasticity	OH	17	35	
Loam	ML, OL, MH, OH	28	32	
Silt Loam	ML, OL, MH, OH	25	32	
Clay Loam, Silty Clay Loam	ML, OL, CL, MH, OH, CH	18	32	
Silty clay	OL, CL, OH, CH	18	32	
Clay	CL, CH, OH, OL	18	28	
Peat and other highly organic soils	Pt	0	10	

Table 13 angle of internal friction (Geotechdata.info - Updated 31.10.2014, Website: <http://www.geotechdata.info/parameter>)

Description	USCS	Cohesion (kPa)		
		min	max	Specific value
Well graded gravel, sandy gravel, with little or no fines	GW	-	-	0
Poorly graded gravel, sandy gravel, with little or no fines	GP	-	-	0
Silty gravels, silty sandy gravels	GM	-	-	0
Clayey gravels, clayey sandy gravels	GC	-	-	20
Well graded sands, gravelly sands, with little or no fines	SW	-	-	0
Poorly graded sands, gravelly sands, with little or no fines	SP	-	-	0
Silty sands	SM	-	-	22
Silty sands - Saturated compacted	SM	-	-	50
Silty sands - Compacted	SM	-	-	20
Clayey sands	SC	-	-	5
Clayey sands - Compacted	SC	-	-	74
Clayey sands -Saturated compacted	SC	-	-	11
Loamy sand, sandy clay Loam - compacted	SM, SC	50	75	
Loamy sand, sandy clay Loam - saturated	SM, SC	10	20	
Sand silt clay with slightly plastic fines - compacted	SM, SC	-	-	50
Sand silt clay with slightly plastic fines - saturated compacted	SM, SC	-	-	14
Inorganic silts, silty or clayey fine sands, with slight plasticity	ML	-	-	7
Inorganic silts and clayey silts - compacted	ML	-	-	67

Inorganic silts and clayey silts - saturated compacted	ML	-	-	9
Inorganic clays, silty clays, sandy clays of low plasticity	CL	-	-	4
Inorganic clays, silty clays, sandy clays of low plasticity - compacted	CL	-	-	86
Inorganic clays, silty clays, sandy clays of low plasticity - saturated compacted	CL	-	-	13
Mixture if inorganic silt and clay - compacted	ML-CL	-	-	65
Mixture if inorganic silt and clay - saturated compacted	ML-CL	-	-	22
Organic silts and organic silty clays of low plasticity	OL	-	-	5
Inorganic silts of high plasticity - compacted	MH	-	-	10
Inorganic silts of high plasticity - saturated compacted	MH	-	-	72
Inorganic silts of high plasticity	MH	-	-	20
Inorganic clays of high plasticity	CH	-	-	25
Inorganic clays of high plasticity - compacted	CH	-	-	103
Inorganic clays of high plasticity - saturated compacted	CH	-	-	11
Organic clays of high plasticity	OH	-	-	10
Loam - Compacted	ML, OL, MH, OH	60	90	
Loam - Saturated	ML, OL, MH, OH	10	20	
Silt Loam - Compacted	ML, OL, MH, OH	60	90	
Silt Loam - Saturated	ML, OL, MH, OH	10	20	

Clay Loam, Silty Clay Loam - Compacted	ML, OL, CL, MH, OH, CH	60	105	
Clay Loam, Silty Clay Loam - Saturated	ML, OL, CL, MH, OH, CH	10	20	
Silty clay, clay - compacted	OL, CL, OH, CH	90	105	
Silty clay, clay - saturated	OL, CL, OH, CH	10	20	
Peat and other highly organic soils	Pt	-	-	

Table 14 cohesion (Geotechdata.info - Updated 31.10.2014, Website:
<http://www.geotechdata.info/parameter>)

Unit weight, Angle of internal friction for cohesionless soil			
SPT Penetration (blows/foot)	ϕ (degrees) (sands)	Density of Sand	unit weight (t/m³)
<4	<29	very loose	1.1-1.8
4 to 10	29-30	loose	1.4-2.0
10 to 30	30-36	medium	1.7-2.2
30 to 50	36-41	dense	1.7-2.3
>50	>41	very dense	2.0-2.3
Cohesion for cohesive soils			
SPT value (N)	Soil compactness	c (kPa)	
0 to 4	Very soft to soft	12.5	
4 to 8	Soft to medium	25	
8 to 16	Medium to stiff	50	
16 to 32	Stiff to very stiff	100	
>32	Vert stiff to hard	200	

Table 15 unit weight, angle of internal friction for cohesionless soil, and cohesion for cohesive
soils (Foundation Engineering Handbook, Peck 1974)

N SPT blow counts	Cohesion (kPa)	Angle of internal friction (degrees)
3.8	23.3	2.8
4.5	23.1	5.8
13.7	95.1	12.1
5.8	31	4.1
5.1	43	6.8
4.6	29.2	4.2
11.5	75.7	11.1
14.2	84.7	15.7
10.5	54.5	11.1
14.9	84.1	15.6
11.8	57.6	13.1
3.7	24.8	3.9
6.1	45	6.2
15	99	14.6
13.1	65.2	11.7
9.5	56.3	8.7
14.4	66.3	12.5
15.7	73	14.2
5.6	22.7	7.4
6.7	29.3	7.1
9.6	44.1	9
13.2	66.1	12.5
5.6	26	5.4
6.5	33	8.5
10.6	58	12.8
3.8	19	5
5	23	5.8
6.2	31	7.3
8.5	49	10.3
9.7	42	8
13	75	12.2
5	27.1	7.7
4.9	30	6.6
5.7	30	8
11.3	75	12.9

Table 16 angle of internal friction for clay (Discussion on the Relationship between Standard Penetration Blow Counts and Physical Mechanical Parameters of Foundation Soil, Liu Hui, Xuzhou Institute of Architectural Technology, Xuzhou, Jiangsu, China)

N SPT blow counts	Cohesion (kPa)	Angle of internal friction (degrees)
10.4	53.9	13.5
11.4	58.9	13.4
5.8	19	6.5
9.3	51	13.1
13.7	71.2	12.8
12.5	84	15.3
8.8	49	10.5
1.9	16	4.7
12.5	56.5	16
6.8	42.6	9.8
13.7	67	13.4
5	30.3	5.4
5.9	24	9.2
5.2	20	7.3
15.9	64.9	14.4
8	39.5	10.2
4.3	18	7.1

Table 17 cohesion for silty clay (Discussion on the Relationship between Standard Penetration Blow Counts and Physical Mechanical Parameters of Foundation Soil, Liu Hui, Xuzhou Institute of Architectural Technology, Xuzhou, Jiangsu, China)

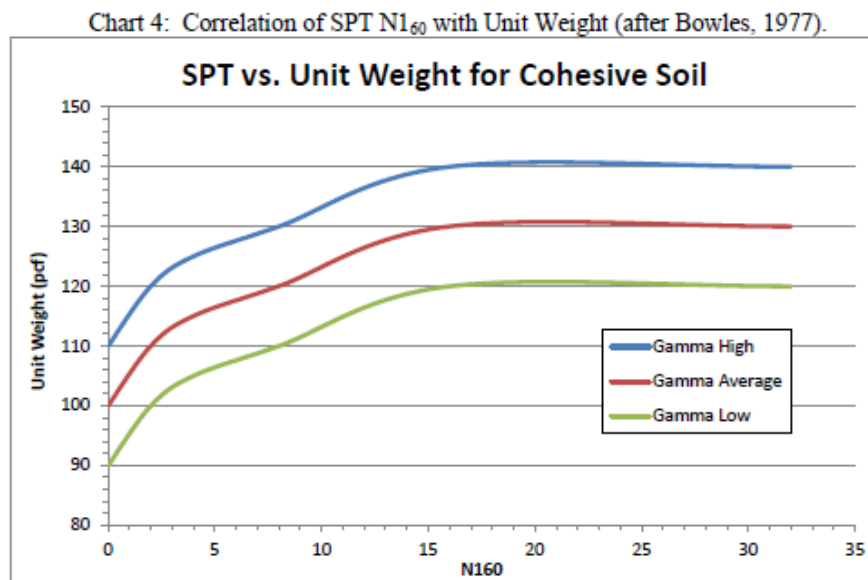


Figure 1 correlation of SPT N_{160} with unit weight (Soil correlation, Caltrans Geotechnical Manual, Caltrans: California Department of Transportation)